THE EVALUATION OF A STALL-FLUTTER SPRING-DAMPER PUSHROD IN THE ROTATING CONTROL SYSTEM OF A CH-54B HELICOPTER

David O. Adams

United Aircraft Corporation

Prepared for:

Army Air Mobility Research and Development Laboratory

August 1973

DISCLAIMERS

The findings in this report are not to be construed as an official Department of the Army position unless so designated by other authorized documents.

When Government drawings, specifications, or other data are used for any purpose other than in connection with a definitely related Government procurement operation, the United States Government thereby incurs no responsibility nor any obligation whatsoever; and the fact that the Government may have formulated, furnished, or in any way supplied the said drawings, specifications, or other data is not to be regarded by implication or otherwise as in any manner licensing the holder or any other person or corporation, or conveying any rights or permission, to manufacture, use, or sell any patented invention that may in any way be related thereto.

Trade names cited in this report do not constitute an official endorsement or approval of the use of such commercial hardware or software.

DISPOSITION INSTRUCTIONS

Destroy this report when no longer needed. Do not return it to the originator.

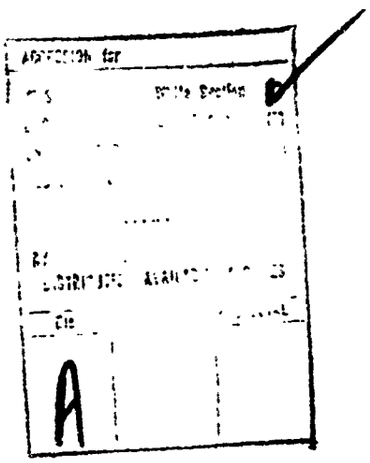

UNCLASSIFIED

Security Classification

AD 771962

DOCUMENT CONTROL DATA - R & D

(Security classification of title, body of abstract and indexing annotation must be entered when the overall report is classified)

1 ORIGINATING ACTIVITY (Corporate author)
Sikorsky Aircraft Division
United Aircraft Corporation
Stratford, Connecticut

2a. REPORT SECURITY CLASSIFICATION
Unclassified

2b. GROUP

3 REPORT TITLE
THE EVALUATION OF A STALL-FLUTTER SPRING-DAMPER PUSHROD IN THE ROTATING CONTROL SYSTEM OF A CH-54B HELICOPTER

4 DESCRIPTIVE NOTES (Type of report and inclusive dates)
Final Report

5 AUTHOR(S) (First name, middle initial, last name)
David O. Adams

6 REPORT DATE	7a. TOTAL NO. OF PAGES	7b. NO OF REFS
August 1973	~~100~~ 105	13

8a. CONTRACT OR GRANT NO	9a. ORIGINATOR'S REPORT NUMBER(S)
DAAJ02-71-C-0058	USAAMRDL Technical Report 73-55
b. PROJECT NO. Task 1F162204AA4301	
c.	9b. OTHER REPORT NO(S) (Any other numbers that may be assigned this report)
d.	SER-64372

10 DISTRIBUTION STATEMENT
Approved for public release; distribution unlimited.

11 SUPPLEMENTARY NOTES	12. SPONSORING MILITARY ACTIVITY
	Eustis Directorate U.S. Army Air Mobility R&D Laboratory Fort Eustis, Virginia

13 ABSTRACT

This program was conducted to evaluate the effect of rotating control system damping on stall-induced control loads and on aircraft handling qualities in stall. Such damping was introduced in the CH-54B control system by replacing the standard pushrods by a spring-damper assembly. The CH-54B helicopter was chosen as the test vehicle because it exhibits stall-induced loads.

Dynamic analyses defined pushrod stiffness and damping characteristics required to reduce the high-frequency torsional response of the main rotor blades. Spring-damper pushrods exhibiting the desired characteristics were designed, fabricated, and laboratory tested to assure that design requirements were met. The spring-damper pushrods were installed on a test rotor head and tested on the Sikorsky main rotor whirl tower.

Flight tests in stalled conditions were conducted at 48,000 pounds gross weight with standard pushrods and with spring-damper pushrods. The results showed that the spring-damper pushrods reduced high-frequency, stall-induced rotating control loads by almost 50%. Fixed system control loads were reduced by 40% peak to peak. Handling qualities in stall remained acceptable.

The program proved that rotating pushrod damping can significantly reduce stall-induced control loads.

DD FORM 1 NOV 68 1473 REPLACES DD FORM 1473, 1 JAN 64, WHICH IS OBSOLETE FOR ARMY USE.

UNCLASSIFIED

Security Classification

14 KEY WORDS	LINK A		LINK B		LINK C	
	ROLE	WT	ROLE	WT	ROLE	WT
Helicopter Rotor Stall						
Spring-Damper						
Helicop.er Rotor Control System						
CH-54B Helicopter						

DEPARTMENT OF THE ARMY
U S ARMY AIR MOBILITY RESEARCH & DEVELOPMENT LABORATORY
EUSTIS DIRECTORATE
FORT EUSTIS VIRGINIA 23604

This report has been reviewed by the Eustis Directorate, U.S. Army Air Mobility Research and Development Laboratory and is considered to be technically sound.

The purpose of this investigation was to determine the feasibility of reducing stall-induced dynamic control loads by replacing the conventional helicopter pitch links with a spring damper system. This purpose was accomplished by building specially designed spring damper units and, after thoroughly evaluating these units in ground and bench tests, evaluating them in actual flight. The flight tests were successful, and the concept did effectively attenuate the stall-induced control loading. The results of this total program are thoroughly and accurately documented in this report.

This report is published for the dissemination of the results of this research and to encourage further study in this particular area. The program was conducted under the technical management of Mr. W. E. Nettles of the Technology Applications Division of this Directorate.

Task 1F162204AA4301
Contract DAAJ02-71-C-0058 (Mod. P00003)
USAAMRDL Technical Report 73-55
August 1973

THE EVALUATION OF A STALL-FLUTTER SPRING-DAMPER PUSHROD IN THE ROTATING CONTROL SYSTEM OF A CH-54B HELICOPTER

Final Report

Sikorsky Engineering Report No. SER-64372

By

David O. Adams

Prepared By

Sikorsky Aircraft Division
United Aircraft Corporation
Stratford, Connecticut

for

EUSTIS DIRECTORATE
U.S. ARMY AIR MOBILITY RESEARCH AND DEVELOPMENT LABORATORY
FORT EUSTIS, VIRGINIA

ABSTRACT

This program was conducted to evaluate the effect of rotating control system damping on stall-induced control loads and on aircraft handling qualities in stall. Such damping was introduced in the CH-54B control system by replacing the standard pushrods by a spring-damper assembly. The CH-54B helicopter was chosen as the test vehicle because it exhibits stall-induced loads.

Dynamic analyses defined pushrod stiffness and damping characteristics required to reduce the high-frequency torsional response of the main rotor blades. Spring-damper pushrods exhibiting the desired characteristics were designed, fabricated, and laboratory tested to assure that design requirements were met. The spring-damper pushrods were installed on a test rotor head and tested on the Sikorsky main rotor whirl tower.

Flight tests in stalled conditions were conducted at 48,000 pounds gross weight with standard pushrods and with spring-damper pushrods. The results showed that the spring-damper pushrods reduced high-frequency, stall-induced rotating control loads by almost 50%. Fixed system control loads were reduced by 40% peak to peak. Handling qualities in stall remained acceptable.

The program proved that rotating pushrod damping can significantly reduce stall-induced control loads. Further studies are recommended to evaluate potential benefits of the spring-damper pushrod concept for higher speed helicopters and to develop practical production designs.

FOREWORD

The design, fabrication and tests of the CH-54B pushrod spring-dampers were performed under Contract DAAJ02-71-C-0058, Task 1F162204AA4301, with the Eustis Directorate, U. S. Army Air Mobility Research and Development Laboratory, Fort Eustis, Virginia. This work is part of the Eustis Directorate program to understand the mechanism of, and methods of, alleviating stall-induced rotor dynamic problems.

The work was performed under the general direction of Mr. William Nettles, Technology Applications Division of the Eustis Directorate. Principal participants at Sikorsky Aircraft were Walter Gerstenberger and David Adams, Project Managers; and Robert Faiz, Charles Niebanck, Robert Blackwell, and Harlow Smith, who participated in the design and evaluation of the concept. The program was flown by engineering test pilots Charles Reine and John Peterson and was under the general supervision of Robert Zincone, Rotor Design Section Supervisor and William Paul, Chief of Aircraft Design & Development.

TABLE OF CONTENTS

	Page
ABSTRACT	iii
FOREWORD	v
LIST OF ILLUSTRATIONS	viii
LIST OF TABLES	ix
LIST OF SYMBOLS	x
INTRODUCTION	1
DISCUSSION	4
Analytical Design	4
Functional Design	17
Ground Tests	29
Flight Tests	44
Analysis of Performance	57
CONCLUSIONS	76
RECOMMENDATIONS	77
LITERATURE CITED	78
APPENDIX, Structural Analysis	80
DISTRIBUTION	90

LIST OF ILLUSTRATIONS

Figure		Page
1	Stall-Flutter Spring-Damper Pushrod Assembly	2
2	Schematic of the Spring-Damper Free Vibration Problem	5
3	Effect of Spring-Damper Properties on First Torsional Mode Frequency and Damping	7
4	Measured CH-54B Pushrod Load Time-Histories, Structural Substantiation Flight Tests . . .	9
5	Comparison of Test and Analytical Pushrod Load	10
6	Effect of Spring-Damper Parameters on the Amplitude of Vibratory Control Loads	11
7	Comparison of Pushrod Loads With Spring-Dampers and With Rigid Pushrods, CH-54B 110 Knots, 100% N_R, 47,000 Lb GW, Banked Right Turn	13
8	Typical Calculated Spring-Damper Loads, CH-54B, 110 Knots, 100% N_R, 47,000 Lb GW, Banked Right Turn	14
9	Stall-Flutter Spring-Damper Pushrod, Final Configuration	18
10	Inner Bushing, Fatigue Test Item	19
11	Outer Bushing, Fatigue Test Item	20
12	Main Housing, Fatigue Test Item	22
13	Orifice Plate and End Cap, Interior, Fatigue Test Item	23
14	Orifice Plate and End Cap, Exterior, Fatigue Test Item	24
15	Rotor Head Installation Schematic	25

LIST OF ILLUSTRATIONS

Figure		Page
16	Spring-Damper Dynamic Test Setup in the Sikorsky 200K Universal Rotor Blade Fatigue Test Machine	30
17	Spring-Damper Centrifugal Load Dynamic Test Setup	31
18	Flight and Fatigue Test Loading Spectrums	33
19	End Cap Weldment Fatigue Test Setup in an IV-20 Fatigue Test Machine	35
20	End Cap Weldment Fatigue Test Results	37
21	Spring-Damper System Installed on the Sikorsky 10,000 HP Whirl Test Tower	40
22	Spring-Damper Installed on Whirl Test Rotor Head	41
23	Spring-Damper System Flight Aircraft Installation	53
24	Spring-Damper System Flight Aircraft Installation	54
25	First Flight of the Spring-Damper System, February 6, 1973	56
26	Rotating Pushrod Load Comparison, 110 Kt	58
27	Rotating Pushrod Load Comparison, 115 Kt	59
28	Spectral Analysis, Rigid Pushrod Load	60
29	Spectral Analysis, Spring-Damper Load	61
30	Rotating Control Load Harmonics Reduction	62
31	Pushrod Load Against ERITS	63
32	Comparison of Stationary Control Loads	64
33	Spectral Analysis, Stationary Control Load With Rigid Pushrods	65

LIST OF ILLUSTRATIONS

Figure		Page
34	Spectral Analysis, Stationary Control Load With Spring-Damper Pushrods	66
35	Stationary Control Load Against ERITS	67
36	Spring-Damper Displacement and Load	68
37	Comparison of Cockpit Vibration Levels	70
38	Longitudinal and Lateral Control Positions	71
39	Comparison of Actual and Derived Conventional Pushrod Loads	73
40	Comparison of Actual and Derived Spring-Damper Pushrod Loads, C = 70	74
41	Comparison of Actual and Derived Spring-Damper Pushrod Loads, C = 40	75
42	Rod End Structural Analysis	81
43	Inner Shaft Structural Analysis	82
44	Middle Cylinder Structural Analysis	83
45	Main Housing Structural Analysis	84
46	Cone/Flange Attachment Bolts Structural Analysis	85
47	Cone Analysis Geometry	87
48	Cone Analysis Axial Stress Summary	88
49	Determination of Cone Stress Concentration Factor	89

LIST OF TABLES

Table		Page
I	Natural Frequency and Damping Values for Normal Modes Cases	8
II	Normal Modes Spring-Damper Cases, CH-54B, 110 Knots	15
III	Spring-Damper Fatigue Strength Summary . . .	27
IV	Flight Test Conditions	47
V	Flight Test Data Summary	51

LIST OF SYMBOLS

AOB	angle of bank
CAS	calibrated airspeed, kt
C_D	damping rate, lb-sec/in.
C/C_C	damping ratio
ERITS	equivalent retreating indicated tip speed
GW	aircraft gross weight
I	torsional moment of inertia
K	spring constant
K_D	damper spring rate, lb/in.
N_R	rotor speed
θ_{75}	blade angle at 75% rotor radius
ω_θ	torsional natural frequency, cycles/sec
ω/Ω	ratio of natural frequency to rotor frequency

INTRODUCTION

Control system loads generate one of the major limits to forward speed and maneuvering capability of helicopters. The slope of the control load buildup is often so steep that it represents a fundamental aeroelastic limit of the rotor system which cannot be removed by strengthening the entire control system without incurring unacceptable weight penalties. Studies of the problems reported in References 1-7 indicate that the abrupt rise in control loads is caused by a rapid buildup in the high-frequency blade torsional moments. Stall-flutter is a contributing factor to these high-frequency moments. In forward flight, the angles of attack on the retreating side of the rotor exceed steady-state stall values and under these conditions the unsteady aerodynamics can induce negative damping, which, in turn, produces pitch oscillation of the rotor blade. Low or negative torsional aerodynamic damping on the retreating side also makes the blade more responsive to rotor loading harmonics which are close to the blade torsional frequency. The end result is rapid buildup of higher harmonic control loads during maneuvers and high-speed flights.

The response of the rotor system is usually not unstable, because the blades are moving into and out of the negative damping region once per revolution. However, during maneuvers in which a significant portion of the rotor disc is deeply stalled, very large oscillations can exist (Reference 7).

Efforts to understand the problem have centered on defining unsteady aerodynamic characteristics of the blades in stall (References 6 and 4) and on incorporating these data into blade aeroelastic computer analyses (References 6 and 9). Results of these studies are encouraging. The buildup of control loads and high-frequency stall-induced loads is predicted with reasonable accuracy.

Recognizing that the basic cause of the problem was insufficient pitch damping, the Eustis Directorate complemented their analytical programs by contraction with Sikorsky Aircraft to evaluate the effects of pushrod dampers on control loads of the CH-54B helicopter. The CH-54B helicopter was well suited for the study since it exhibits high-frequency stall-induced control loads during maneuvers and maximum speeds at 48,000 pounds gross weight. Rotating pushrod dampers were used instead of fixed system damping because they provided damping directly at the blade attachment. The basic pushrod damper concept is shown in Figure 1. It consists of a piston that is restrained and sealed in a cylinder by two elastomeric bushings. As the spring-damper operates, all changes in damper length are the result

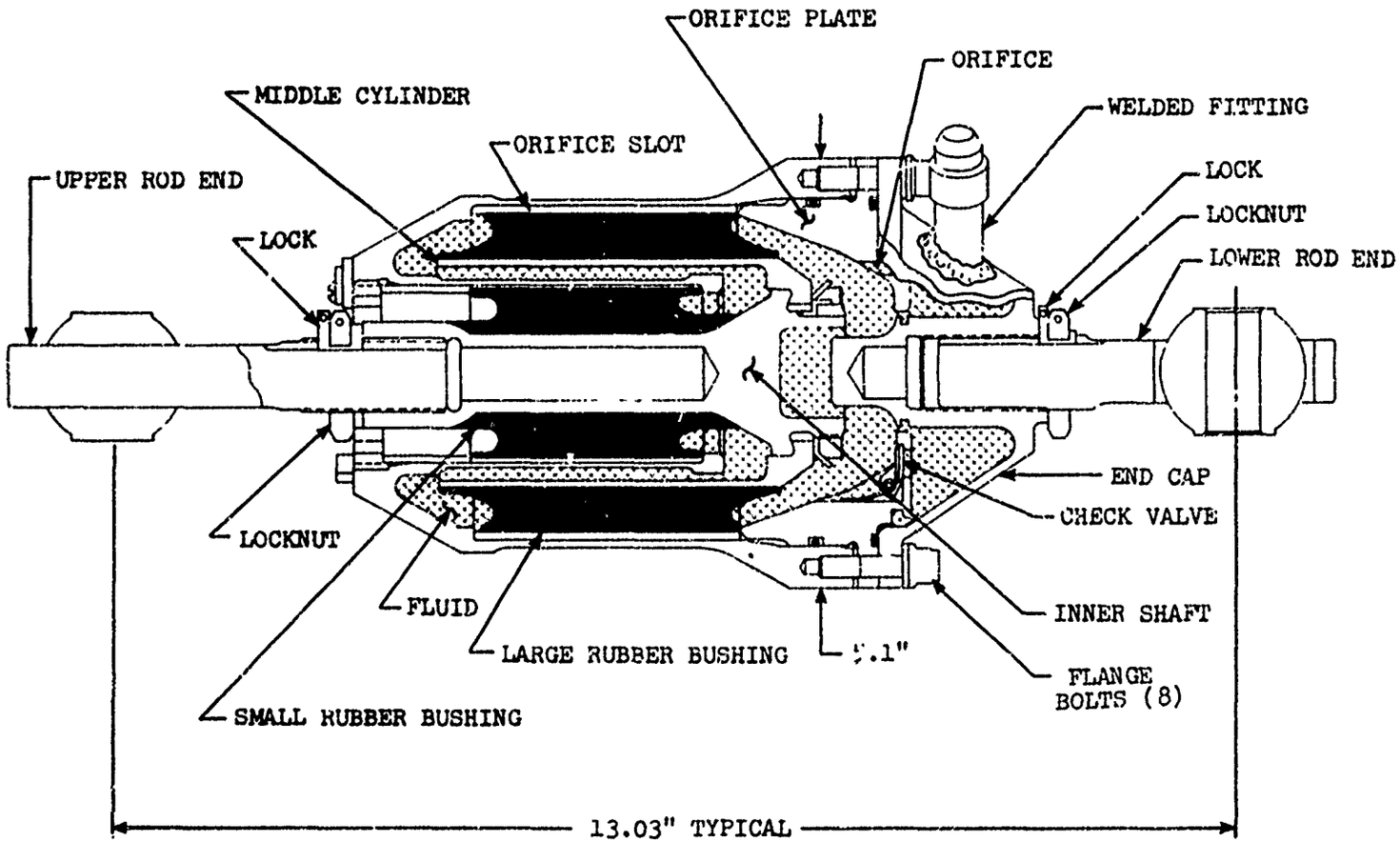

Figure 1. Stall-Flutter Spring-Damper Pushrod Assembly.

of longitudinal shear deflections of the elastomeric bushings. The piston contains passages that restrict the flow of fluid and generate differential pressure on the piston. An air-fluid accumulator system allows for expansion and contraction and prevents cavitation.

The study to evaluate this concept was in five phases:

Phase I	Analytical Design
Phase II	Functional Design
Phase III	Ground Tests
Phase IV	Flight Tests
Phase V	Analysis of Performance

DISCUSSION

ANALYTICAL DESIGN

Part 1 - Description of Analytical Procedure

An aeroelastic analysis of the CH-54B rotor was performed to evaluate the effectiveness of spring-dampers in reducing the control loads associated with retreating blade stall-flutter and to evolve design criteria. The primary mathematical tool used was the Normal Modes Aeroelastic Blade Analysis. This analysis, which is described in detail in Reference 8, represents blade flatwise, edgewise, and torsional elastic deformation by a summation of normal mode responses and performs a time-wise integration of the modal equations of motion. In the analysis of a steady-state condition, the equations of motion of a single blade are integrated through several rotor revolutions until the predicted motion becomes cyclic within a specified tolerance. This analysis can also be used to study blade transient response following a control input or disturbance. Aerodynamic blade loading is determined from airfoil data tabulated as a function of blade section angle of attack, Mach number, and first and second time derivatives of angle of attack. As demonstrated in Reference 9 (prepared under USAAVLABS Contract DAAJ02-71-C-0003), this aeroelastic analysis is capable of predicting the control loads caused by stall flutter when unsteady aerodynamic effects and nonuniform rotor inflow are taken into account. Accordingly, unsteady aerodynamics and a nondistorted helical wake inflow were used throughout this investigation.

The version of the Normal Modes Program used for this study is a single-blade, fixed-hub analysis. The assumptions are made that all blades are identical and encounter the same loads at given azimuthal and radial positions and that blade forces and moments do not cause hub motion. Any phenomena which are related to nonuniformity between blades or to the effect of hub motion on blade response are not described by this analysis. Consideration of these phenomena was beyond the scope of this effort.

For a blade restrained at the root by a pushrod, the first step in the aeroelastic analysis is the calculation of the undamped natural frequencies and modes for a blade rotating in a vacuum. In order to analyze the spring-damper/blade system using the normal modes procedure, the damped free vibration modes and frequencies were calculated based on the model shown in Figure 2. The torsional system was represented by fifteen elastically connected lumped inertias restrained in torsion by a spring-damper at the blade root. The eigenvalues and eigenvectors of the system response were calculated using a Lagrangian formulation of the damped free vibration equations. A radial mode shape, natural frequency and modal damping were calculated and used in the forced response aeroelastic solution.

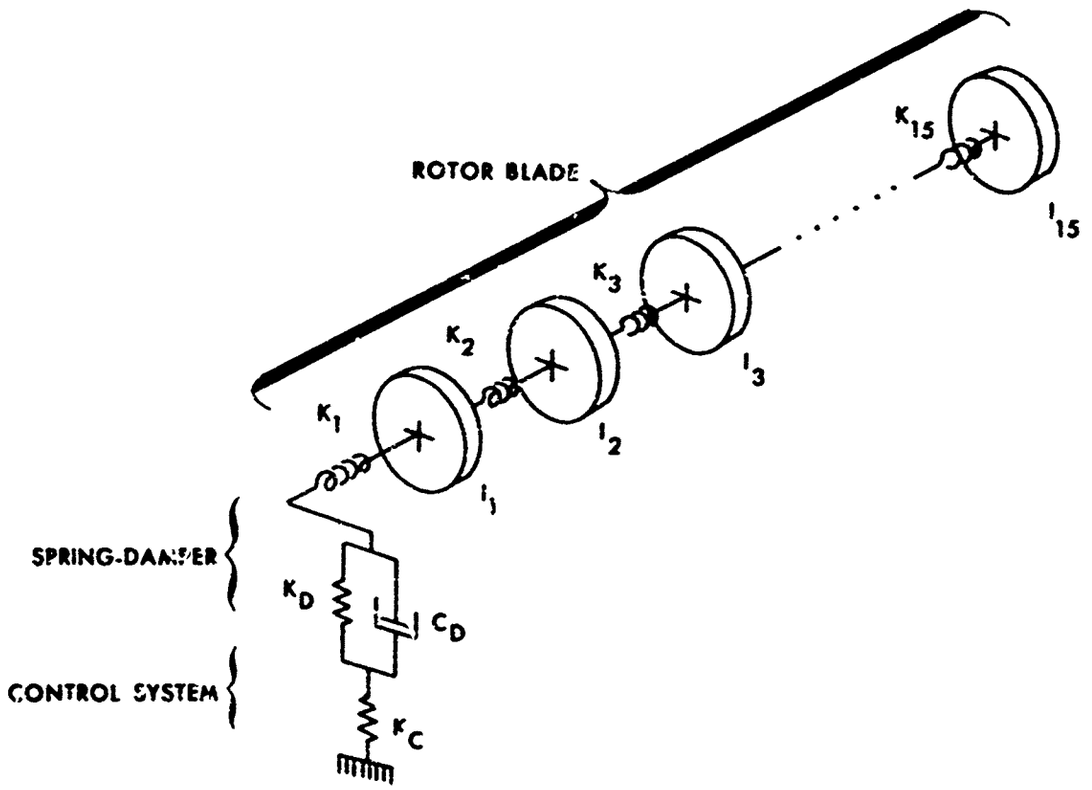

Figure 2. Schematic of the Spring-Damper Free Vibration Problem.

Part 2 - Calculation of the CH-54B Spring Damper Behavior

The first step in analyzing the behavior of the CH-54B spring-damper was to employ the free vibration analysis to determine the general relationship between the properties of the damper itself and those of the blade first torsional mode. Figure 3 shows the variation of blade first torsional natural frequency and percent critical damping with changes in the spring and damping constants of the spring damper. (For reference, the selected damper configuration, which has an elastic stiffness, K_D, of 5000 lb/in. and a damping constant, C_D, of 90 lb-sec/in., is denoted by a solid symbol.) Three trends are evident from this figure:

1. For a given damper spring constant, K_D, high levels of damping can increase the root dynamic stiffness enough to result in torsional natural frequencies which are close to those obtained with a rigid pushrod. It is clear from Figure 2 that as the damping constant, C_D, is increased, the damper spring is effectively bridged so that the torsional natural frequency approaches the standard pushrod value (7.4 per rev.)

2. For each spring constant, K_D, a specified value of the damping constant, C_D, maximizes the model damping. Increasing or decreasing the damping constant decreases the percent critical damping ratio of the torsional vibration.

3. The variation in the percent critical damping parameter with damping constant is relatively gradual, so small manufacturing differences between the six production dampers will not cause great differences in first torsional mode damping.

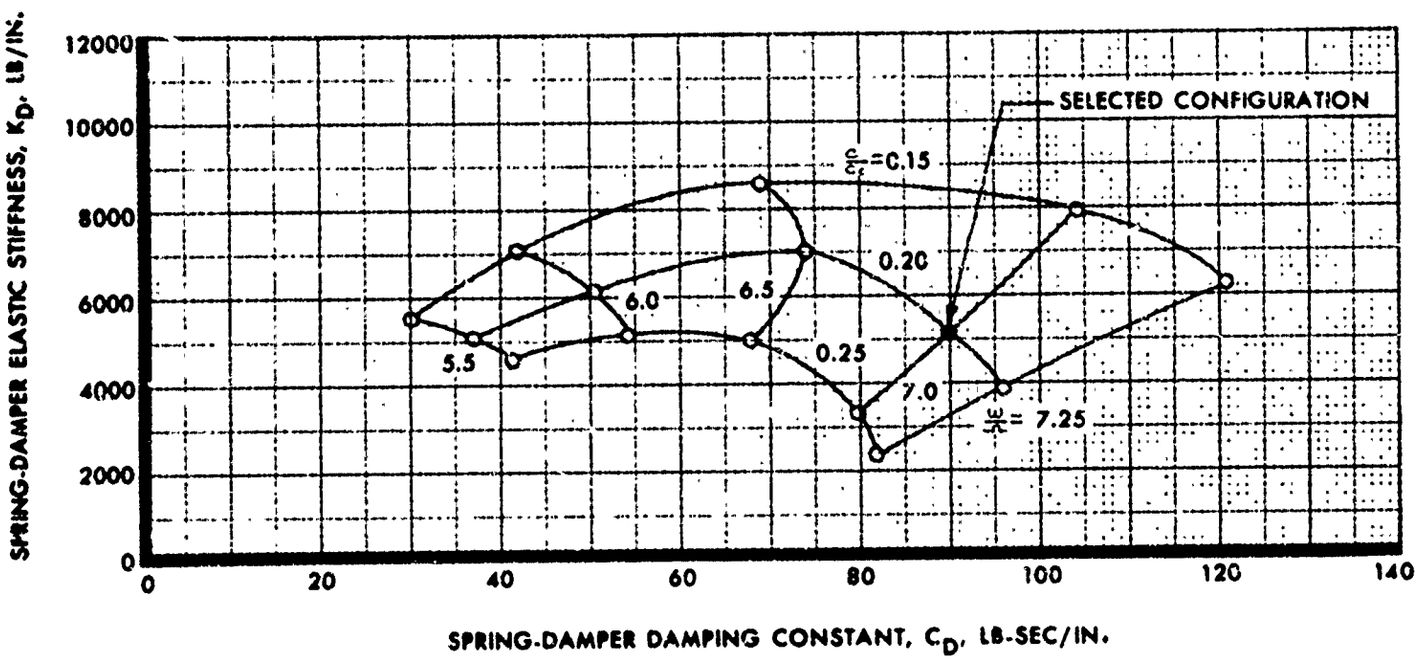

Figure 3. Effect of Spring-Damper Properties on First Torsional Mode Frequency and Damping.

Table I shows the natural frequencies and damping ratios for ten possible damper configurations which were analyzed using the Normal Modes Aeroelastic Blade Analysis.

TABLE I. NATURAL FREQUENCY AND DAMPING VALUES FOR NORMAL MODES CASES

		Spring-Damper Spring Rate, K_D, lb/in.			
		4000	5000	8500	∞ (Standard Pushrod)
Spring-Damper Damping Constant, C_D, lb-sec/in.	0	$C/C_C = 0$ $\omega/\Omega = 4.84$	$C/C_C = 0$ $\omega/\Omega = 5.15$	$C/C_C = 0$ $\omega/\Omega = 5.90$	$C/C_C = 0$ $\omega/\Omega = 7.4$
	35	—	$C/C_C = 0.194$ $\omega/\Omega = 5.43$	$C/C_C = 0.096$ $\omega/\Omega = 6.05$	—
	55	—	$C/C_C = 0.264$ $\omega/\Omega = 6.05$	$C/C_C = 0.137$ $\omega/\Omega = 6.25$	—
	90	—	$C/C_C = 0.203$ $\omega/\Omega = 7.01$	$C/C_C = 0.154$ $\omega/\Omega = 6.81$	—

Figure 4 shows the pushrod loads measured for a CH-54B with a gross weight of 47,000 lb at 110 knots, 100% N_R at sea level.

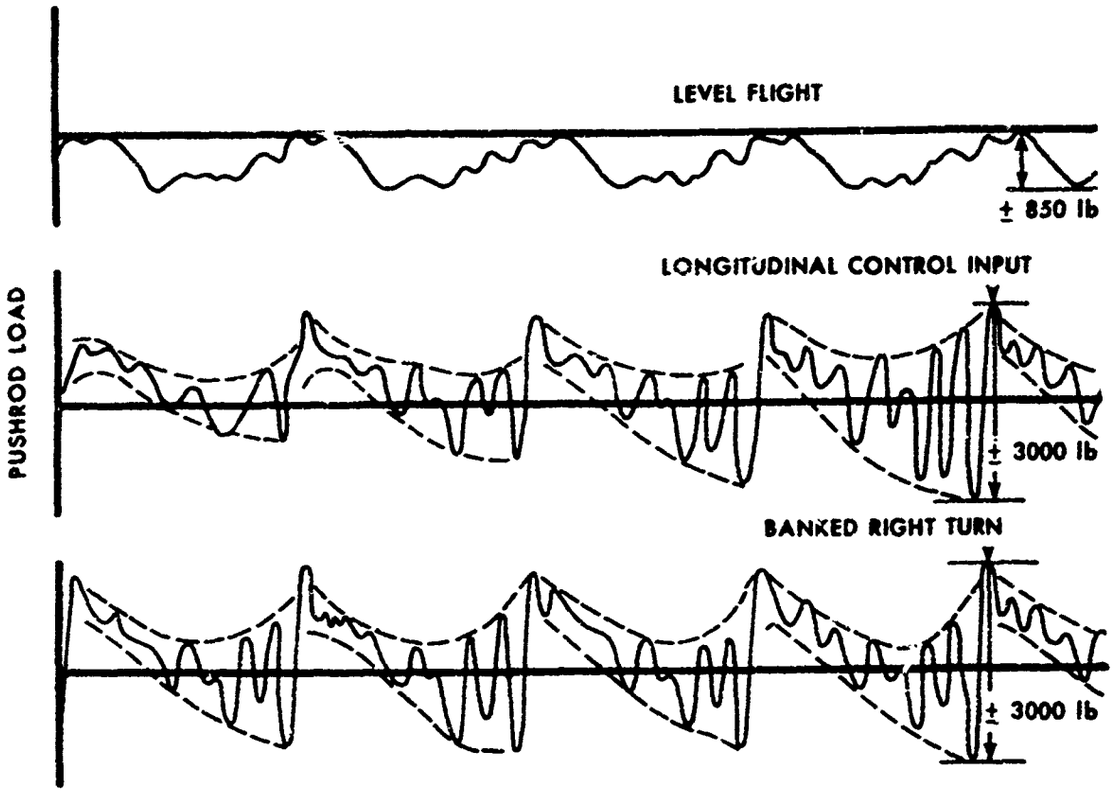

Figure 4. Measured CH-54B Pushrod Load Time-Histories, Structural Substantiation Flight Tests

For steady level flight there are no high-frequency retreating blade moments, but when rotor lift is increased either following a longitudinal stick pulse or in the execution of a turn, vibratory pushrod loads grow to ±3000 lb. Prior to the prediction of the effects of the spring-damper, the steady-state right turn was simulated with the standard CH-54B blade properties, mode shapes and natural frequencies. To model the increase in rotor lift experienced in the turn, a quasi-steady condition with collective pitch of 15 deg and shaft angle of -1.8 deg was used. This led to a calculated lift of about 60,000 lb and propulsive force of 3300 lb. The flow field induced in the rotor disc by the helical pattern of trailing tip vortices was calculated using the Non-Distorted Wake Geometry Analysis. The pushrod load which results from the normal modes calculation is compared with flight test results in Figure 5. Although the

calculated pushrod load shows a significantly greater steady nose-down load, the vibratory amplitude and frequency content of the analytical result match the test quite closely.

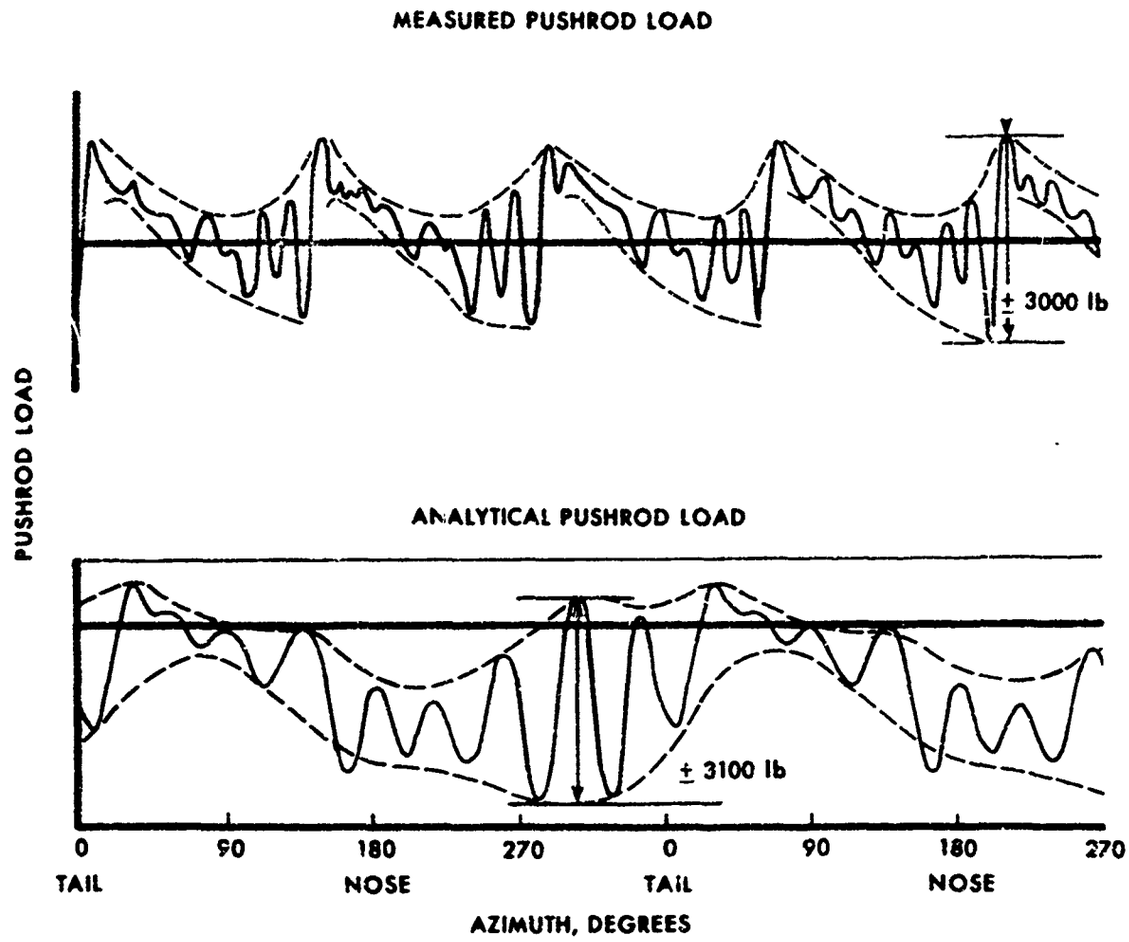

Figure 5. Comparison of Test and Analytical Pushrod Load.

To study the effectiveness of the spring-damper in reducing vibratory control loads, the flight condition described above was simulated using each of the spring-damper configurations listed in Table I. Each of these cases was run with the same control settings as the standard case. Also, the calculation procedure was simplified by assuming that the induced velocity field calculated from the standard flight condition was a good approximation of the flow fields of each of the spring-damper conditions.

Figure 6 summarizes the variation of stall-flutter control load amplitude computed for each of the damper configurations studied.

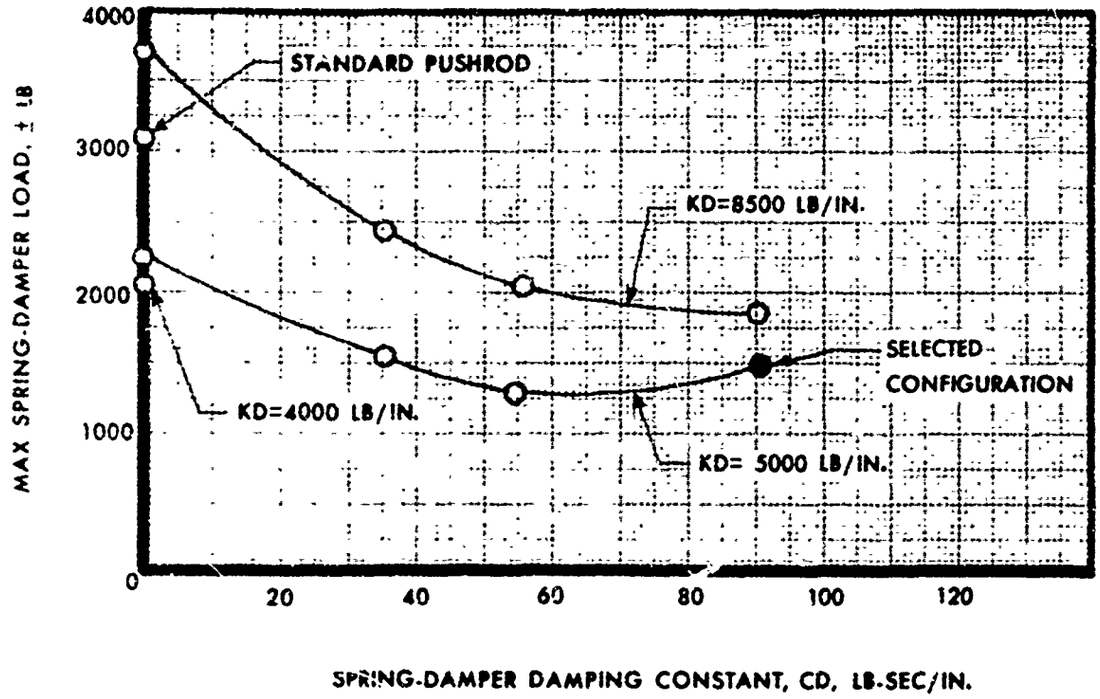

Figure 6. Effect of Spring-Damper Parameters on the Amplitude of Vibratory Control Loads.

It is clear that (1) damping at the blade root is effective in reducing control loads for a given root stiffness and (2) reducing root stiffness tends to decrease the loads for a given damping constant (at least for the ranges investigated). On the basis of these results and mechanical design considerations, a damper configuration was selected which had an elastic stiffness of 5000 lb/in. and a damping constant of 90 lb-sec/in. It should also be noted that this configuration produced a torsional frequency close to that of the standard blade.

Figure 7 compares the control loads calculated for the standard pushrod and for the selected spring damper. For the selected configuration, the free vibration analysis gives a torsional frequency of 7 per rev and 0.20 critical damping ratio. Figure 7 shows approximately equal amounts of 1 per rev variation occuring in the two control load time histories since the pushrod spring-dampers do not affect the low-frequency torsional motion. As a result, the overall peak-to-peak control load is reduced by only about 25%, while the high-frequency (7-8 per rev) retreating blade control loads which the dampers are designed to attenuate are reduced by more than 50%. It is the high-frequency loads that cause the 6 per rev control system loads in the fixed system.

Calculated time histories of damper load for two of the other possible damper configurations are shown in Figure 8. The first condition (K_D = 5000 lb/in., C_D = 0 lb-sec/in.) would result if the damper fluid were lost. The main effects to be noted are a decrease in torsional frequency from 7 per rev to about 5 per rev and an increase in the vibratory retreating blade control load from ±1475 lb to ± 2250 lb - a value which is still less than that obtained with the standard pushrod.

The second condition (K_D = 8500 lb/in., C_D - 90 lb-sec/in.) represents an increased spring rate which could result from the "Mullins Effect" in the rubber elastomer. This effect is an increase in spring rate with increasing frequency, and is presently not well defined. The torsional frequency in this case is reduced to 6.9 rev and the load is ±1850 lb - still a substantial reduction over rigid pushrods.

Part 3 - Summary

Table II summarizes the spring-damper configurations which were simulated using the Normal Modes Program. The amplitudes of both the overall blade root torsional moment and the stall-flutter moment are shown for these cases.

In summary, the analytical results discussed above indicated that the stall-flutter pushrod spring-damper would be effective in reducing control loads and would not be susceptible to instability due to loss of fluid.

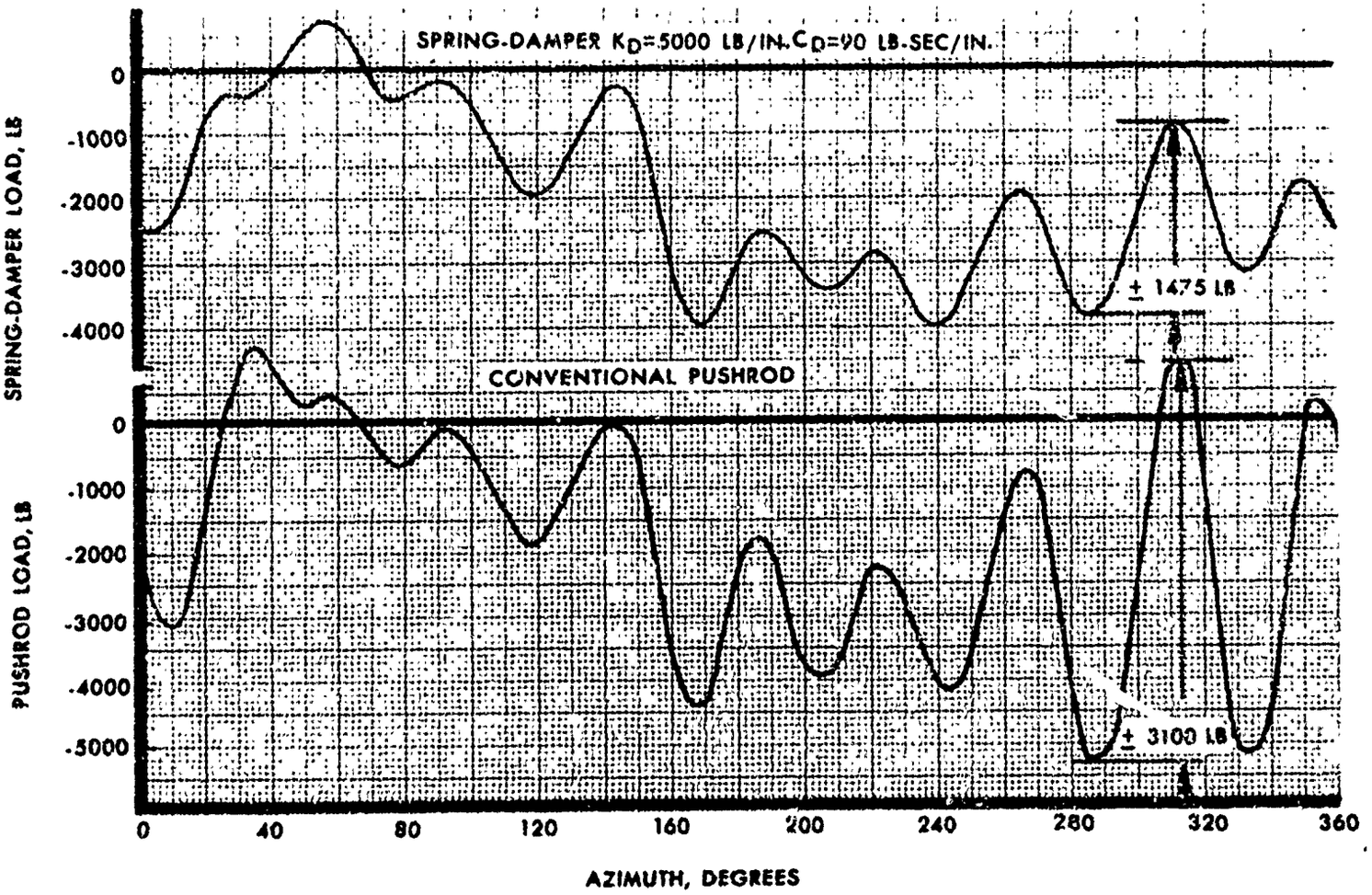

Figure 7. Comparison of Pushrod Loads With Spring-Dampers and With Rigid Pushrods, CH-54B, 110 Knots, 100% N_R, 47,000 Lb GW, Banked Right Turn.

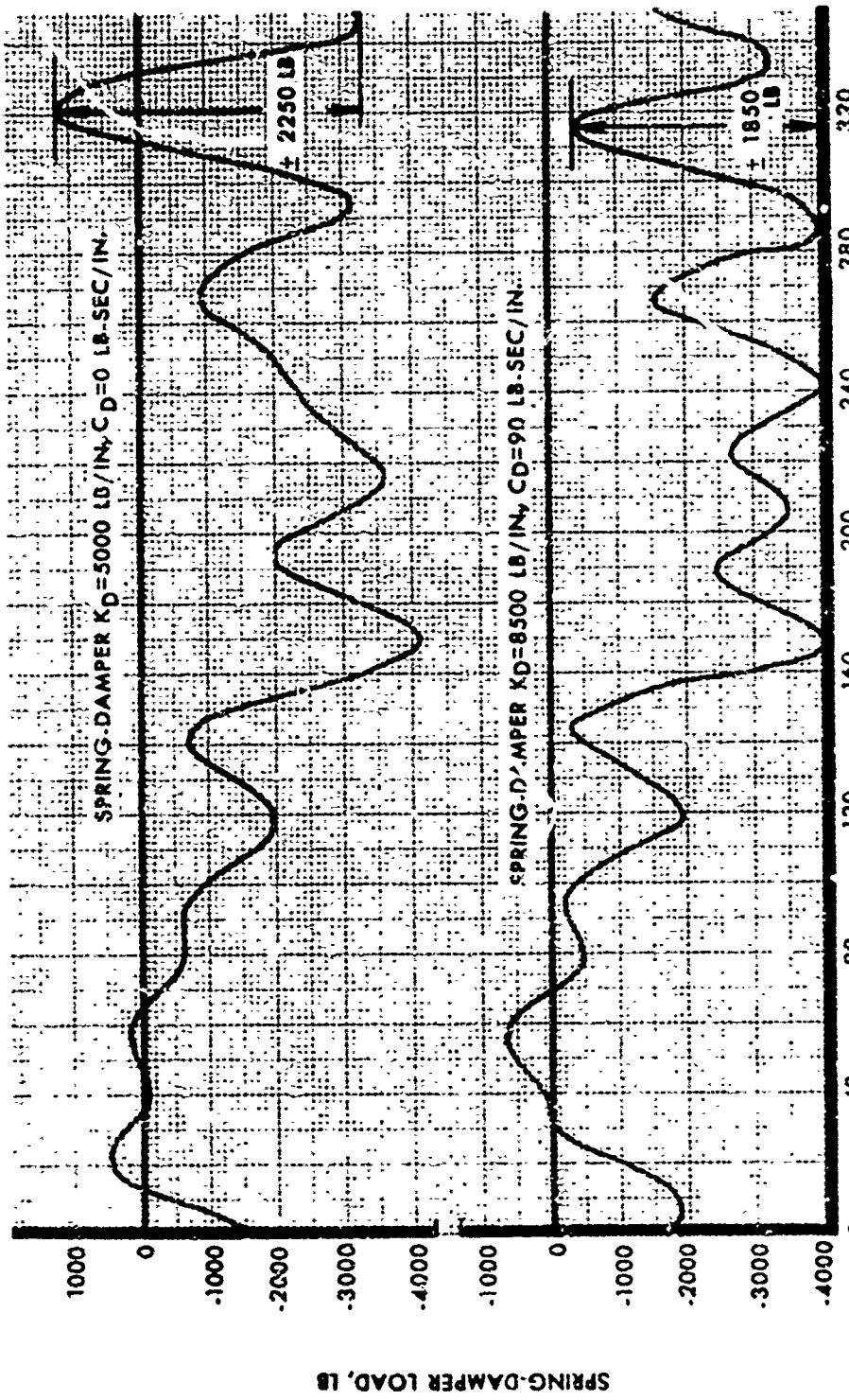

Figure 8. Typical Calculated Spring-Damper Loads, C-54B, 110 Knots, 100% N_R, 47,000 Lb GW, Banked Right Turn.

TABLE II. NORMAL MODES SPRING DAMPER CASES, CH-5

Case No.	K_D (lb/in.)	C_D (lb/sec/in.)	ω/Ω	C/C_c	Inflow	θ_{75} (deg)	Stall-Flutter Root Hom. (±in.-lb)	Ov Root Momen
1	Standard Pushrod		7.44	0	Constant	12.5	9,500	-7,8
2	Standard Pushrod		7.44	0	Constant	15.0	13,832	-15,5
3	6000	55	6.05	.214	Constant	15.0	4,800	-15,1
4	8500	55	6.25	.137	Constant	15.0	7,330	-13,5
5	8500	35	6.05	.096	Constant	15.0	8,000	-19,4
6	Standard Pushrod		7.44	0	Nondistorted Wake	15.0	26,500	-15,9
7	5000	0	5.15	0	Nondistorted Wake	15.0	18,850	-12,8
8	5000	35	5.43	.194	Nondistorted Wake	15.0	13,000	-13,2
9	5000	55	6.05	.264	Nondistorted Wake	15.0	11,000	-14,4
10	5000	90	7.01	.203	Nondistorted Wake	15.0	13,900	-15,8
11	8500	0	5.90	0	Nondistorted Wake	15.0	31,500	-15,0
12	8500	35	6.05	096	Nondistorted Wake	15.0	20,750	-14,7
13	8500	55	6.25	.137	Nondistorted Wake	15.0	17,400	-14,5
14	8500	90	6.81	.154	Nondistorted Wake	15.0	15,400	-15,8
15	4000	0	4.84	0	Nondistorted Wake	15.0	17,500	-12,0

TABLE II. NORMAL MODES SPRING DAMPER CASES, CH-54B, 110 KNOTS

ω/Ω	c/c_c	Inflow	Θ_{75} (deg)	Stall-Flutter Root Mom. (±in.-lb)	Overall Root Torsional Moment (in.-lb)	Lift (lb)	Prop. Force (lb)	Power (hp)
7.44	0	Constant	12.5	9,500	-7,870 ±10,786	56,709	5169	6914
7.44	0	Constant	15.0	13,832	-15,530 ±22,892	63,962	2404	9136
6.05	.214	Constant	15.0	4,800	-15,100 ±16,100	62,531	3109	9087
6.25	.137	Constant	15.0	7,330	-13,550 ±16,450	62,772	2820	8807
6.05	.096	Constant	15.0	8,000	-19,491 ±21,569	63,475	3185	8820
7.44	0	Nondistorted Wake	15.0	26,500	-15,911 ±27,854	60,616	3255	8543
5.15	0	Nondistorted Wake	15.0	18,850	-12,800 ±23,200	56,538	4281	6890
5.43	.194	Nondistorted Wake	15.0	13,000	-13,228 ±17,976	59,012	3742	7391
6.05	.264	Nondistorted Wake	15.0	11,000	-14,450 ±18,560	60,316	3435	8271
7.01	.203	Nondistorted Wake	15.0	13,000	-15,880 ±19,430	60,806	3091	8720
5.90	0	Nondistorted Wake	15.0	31,500	-15,050 ±31,500	58,516	3957	7557
6.05	.096	Nondistorted Wake	15.0	20,750	-14,787 ±17,447	59,929	3681	7635
6.25	.137	Nondistorted Wake	15.0	17,400	-14,500 ±19,170	60,891	3541	8029
5.81	.154	Nondistorted Wake	15.0	15,400	-15,800 ±20,350	61,098	3338	8588
5.84	0	Nondistorted Wake	15.0	17,500	-12,078 ±21,351	54,782	4252	6542

FUNCTIONAL DESIGN

Design Requirements

The aeroelastic analysis indicated that spring and damping introduced at the blade root in the rotating system could significantly reduce stall-induced loads. The most favorable location for a blade root spring-damper is at the pushrod connecting the rotating swashplate to the blade horn, since the existing pushrod may be replaced easily with the spring-damper. It was determined that a spring-damper device could be fabricated to replace the conventional pushrod, provided that the restrictive size limitations could be met. The use of an elastomer as the primary structural member met the size and spring rate requirements.

The design requirements, based on the aeroelastic analysis and the planned test programs, are summarized as follows:

- Replace Conventional Pushrod
- Life - 50 hr
- Load - ±5000 lb
- Spring Rate - 5000 lb/in.
- Damping Rate - 90 lb-sec/in.
- Maximum Elastic Deflection - ± 1/2 in.
- Adjustable for Rotor Tracking
- Fail-Safe Design

Principles of Operation

The final configuration of the stall-flutter spring-damper pushrod designed to meet the above requirements is shown in Figures 1 and 9.

The concept consists basically of a piston restrained in a cylinder by two natural rubber elastomeric bushings which provide the required spring rate. The bushings, shown in Figures 10 and 11, are mounted in parallel, thereby providing a fail-safe design. In addition, physical stops are incorporated to limit spring-damper deflection to ± 1/2 inch in the event of overload or complete rubber failure. No sliding action takes place as the spring-damper is deflected. Elastomeric elements were chosen because of their high allowable strains, integral hydraulic sealing, and compactness.

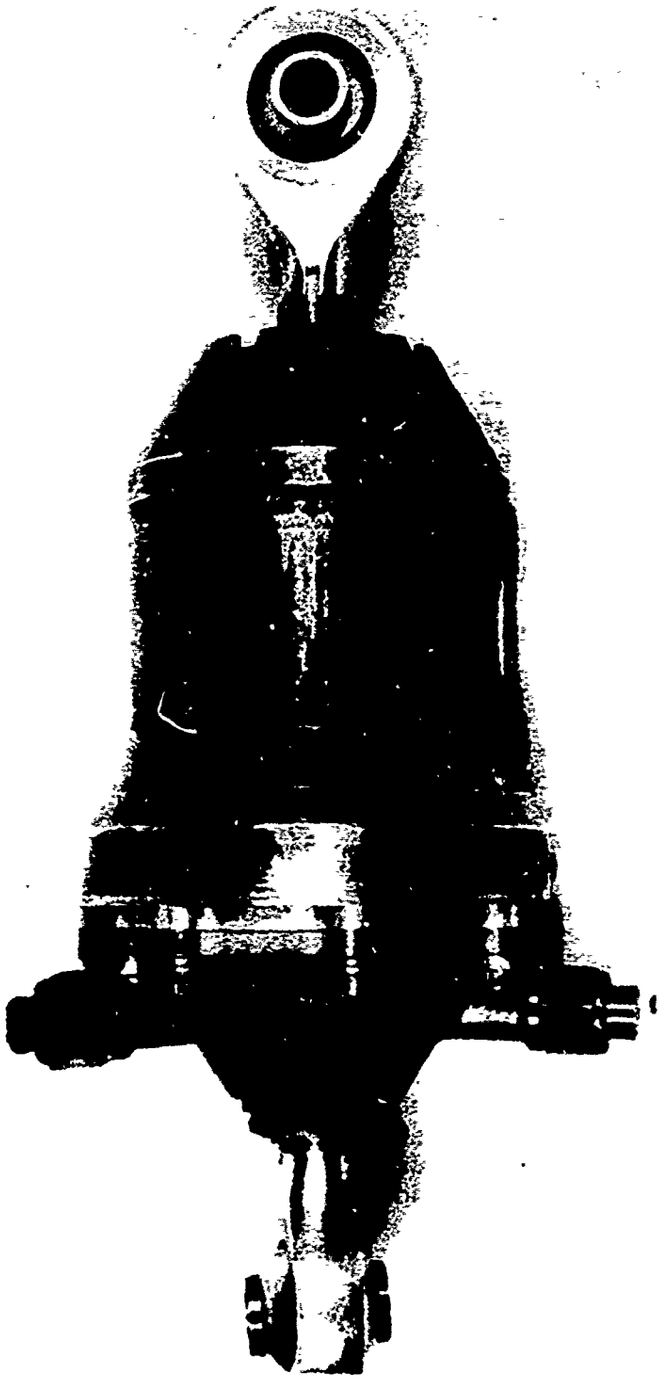

Figure 9. Stall-Flutter Spring-Damper Pushrod, Final Configuration.

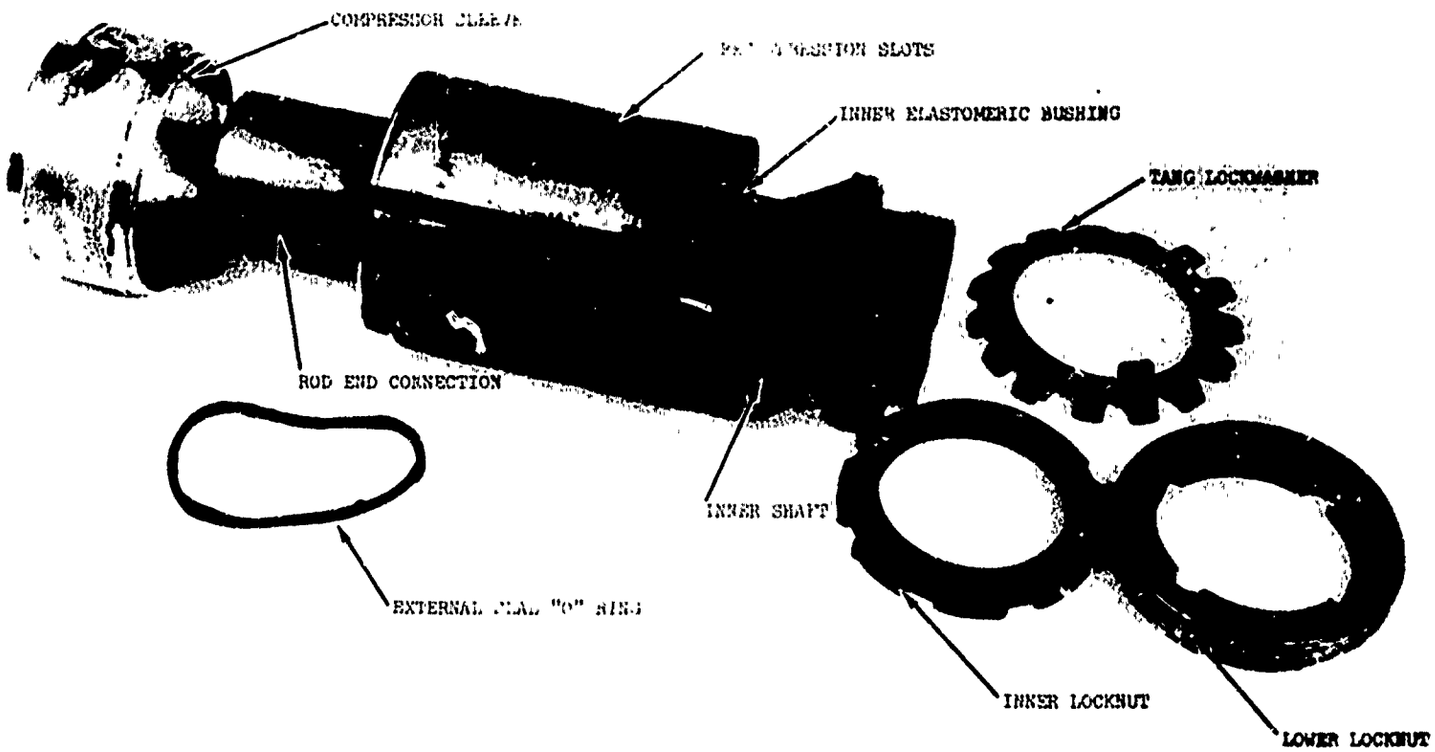

Figure 10. Inner Bushing, Fatigue Test Item.

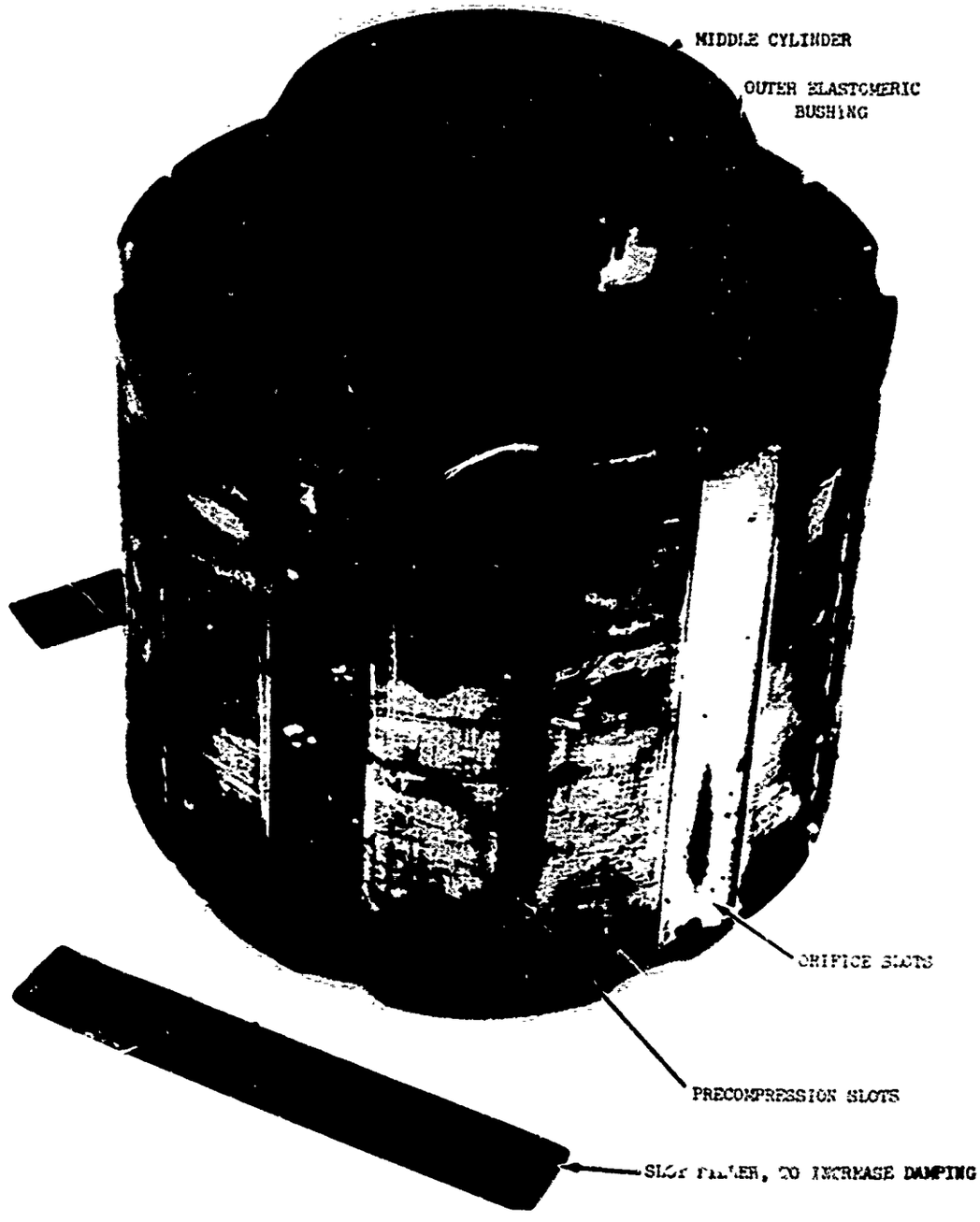

Figure 11. Outer Bushing, Fatigue Test Item.

Damping is obtained by displacement of fluid through orifices. The "orifice" passageways, shown in Figure 1, connect three chambers together. The small area side of the spring-damper cylinder is hydraulically connected to the large area side by means of slots cut across the "piston head", or large bushing. These slots are shown in Figure 11. The large area side is connected in turn to a "plenum chamber" by orifice holes and two check valves. These can be seen in Figures 13 and 14.

The plenum chamber was originally designed to house an integral air-oil accumulator to accept the fluid displaced by motion of the spring-damper, which is basically an unequal area cylinder. When the integral accumulator was found to be inadequate, provision was made to have all dampers connected to three accumulators by means of hoses (Figure 15). Each of the three accumulators can accept a 3-cubic-inch fluid volume change, which would not normally be sufficient, since each of the six spring-dampers can displace 3 cubic inches of fluid. However, the combination of all six plenum chambers into one ring of hoses and accumulators allows each damper to exchange fluid with the others. The plenum pressure is therefore maintained at a relatively constant, low value, governed by the amount of precharge on the air side of the accumulator system.

When the damper is being extended, fluid pressure increases on the small area side and decreases on the large area side. The resulting pressure difference across the large bushing forces fluid through the slot orifices, producing damping; i.e., the spring-damper force (resulting from the differential pressure) is proportional to piston velocity (which is proportional to the orifice flow rate). Since the fluid displaced across the large bushing during extension is not sufficient to fill the large area side, additional fluid from the plenum chamber is introduced to prevent cavitation. The check valves are oriented to open in response to the differential pressure generated during spring-damper extension, thereby providing an ample flow path. This flow is assisted by a positive plenum pressure maintained by precharging the accumulator system air side to 55 psig.

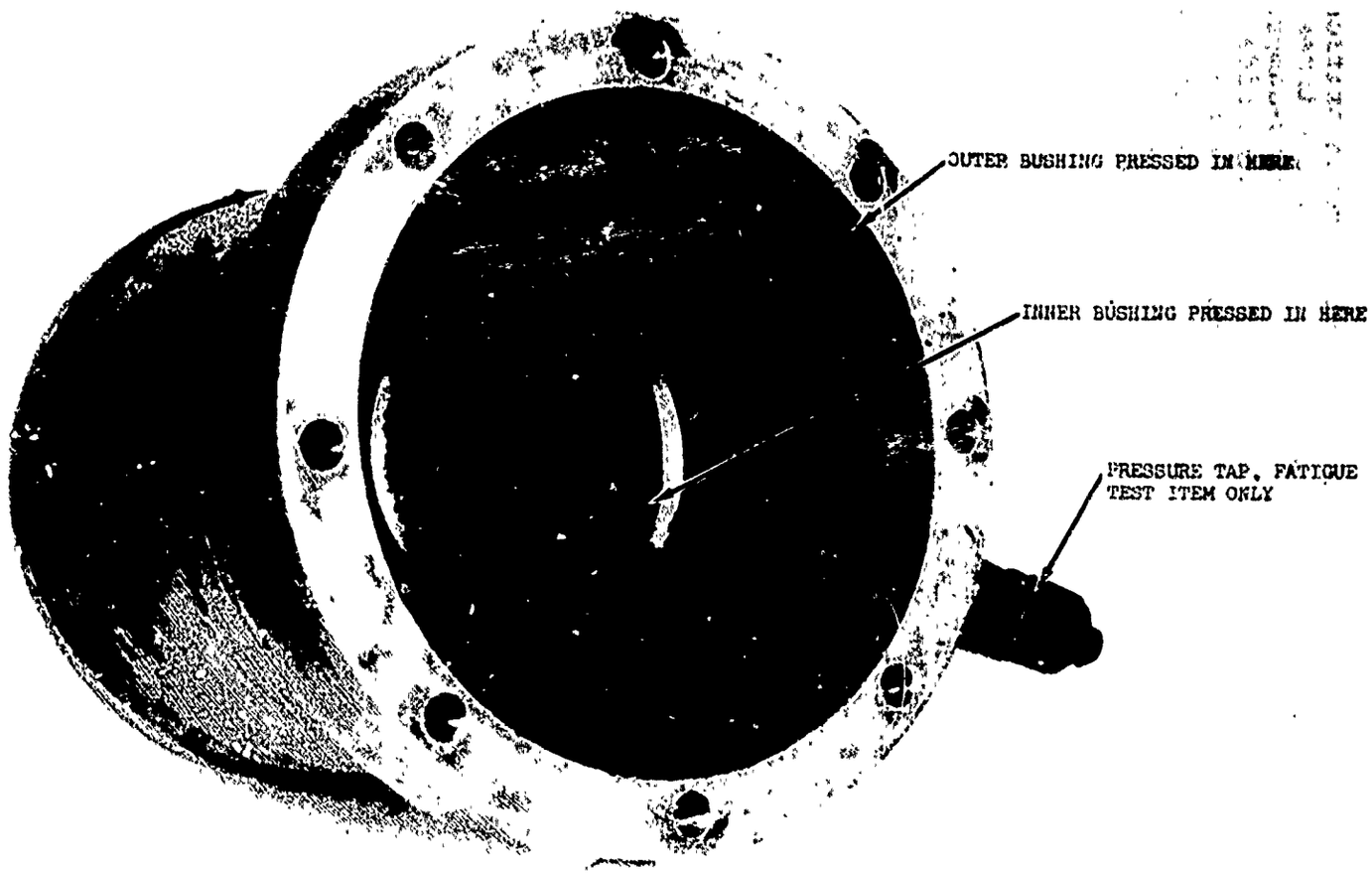

Figure 12. Main Housing, Fatigue Test Item.

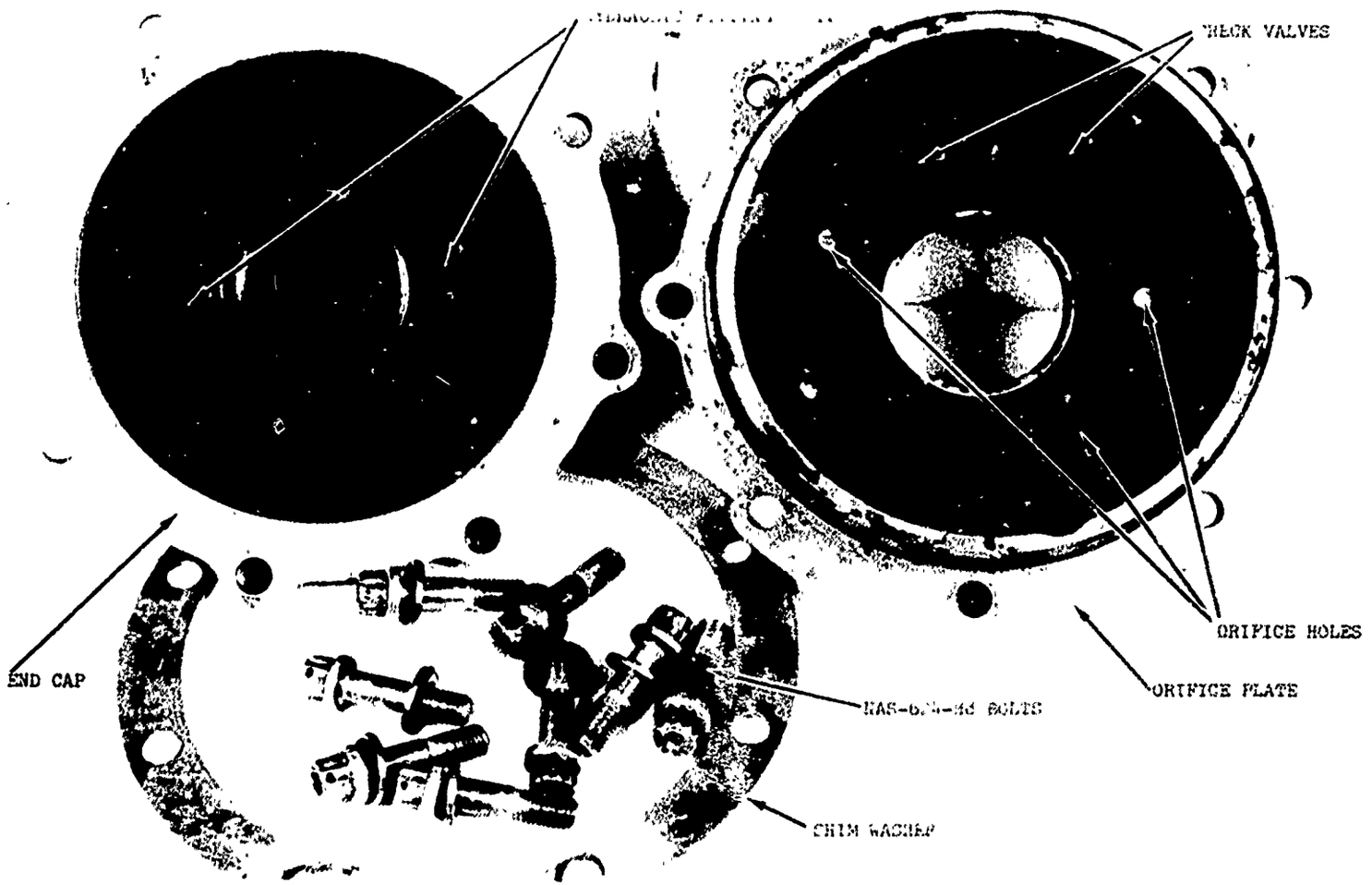

Figure 13. Orifice Plate and End Cap, Interior, Fatigue Test Item.

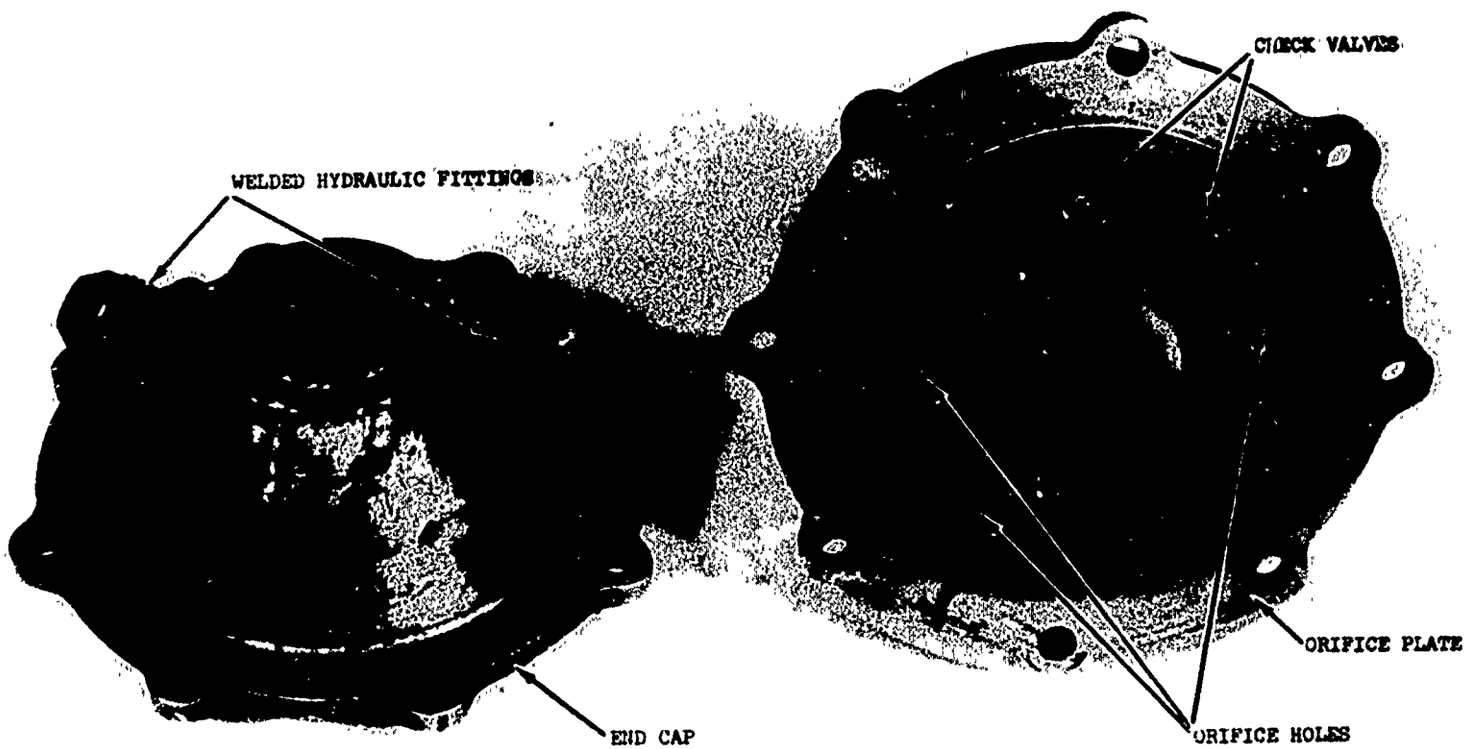

Figure 14. Orifice Plate and End Cap, Exterior, Fatigue Test Item.

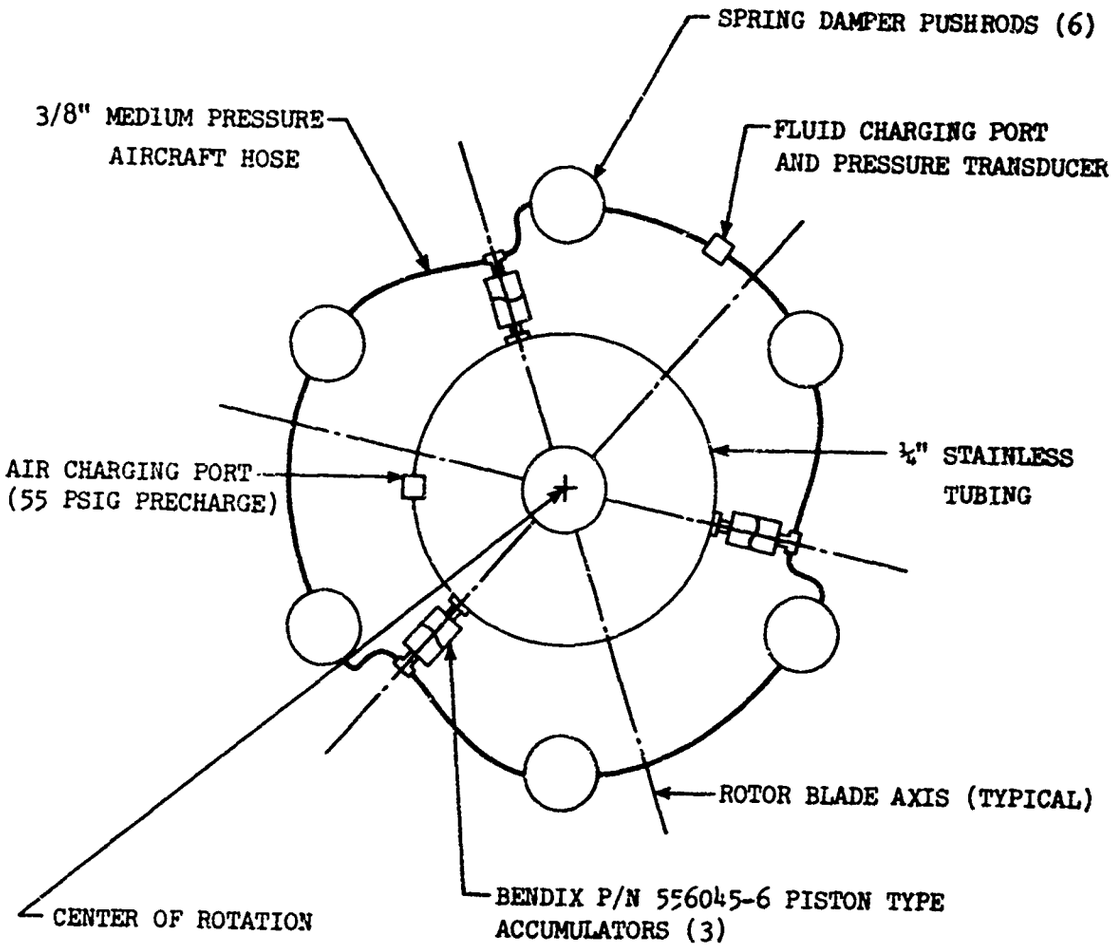

Figure 15. Rotor Head Installation Schematic.

When the spring-damper is being compressed, fluid pressure decreases on the small area side and increases on the large area side. The check valves are held closed by the pressure, and metering of fluid occurs through both sets of orifices - across the large bushing and through the orifice plate. These orifices are sized so that flow to the small area side is restricted less than flow into the plenum chamber, thereby preventing cavitation on the small area side.

Structural Design

The basic objective of the structural design effort was to produce a pushrod spring-damper that is at least as strong in fatigue as the conventional CH-54B rigid pushrod. This objective was attained and later substantiated in laboratory fatigue tests.

The basic structural analysis is presented in the appendix and is summarized below and in Table III.

Metal Components

Except for the elastomeric bushings, all structural components are machined from 4340 steel, heat treated to 150,000 psi ultimate strength. The orifice plate (aluminum) is not considered structural, since failure will only result in some loss of damping, without reducing the structural integrity of the spring-damper. The analysis of this component is therefore not included.

The fatigue mode of failure of the existing CH-54B rotating control rod is at the root of the 7/8 - 32 rod end threads. The structurally similar spring-damper rod end has an increased diameter at the critical area and has a strength increase of 80% over the production rod ends. Different thread pitches are used on each of the spring-damper rod ends in order to allow fine adjustments of blade track.

The spring-damper end cap, originally intended to house an integral air-oil accumulator, now incorporates two welded hydraulic fittings, as shown in Figure 9. An earlier version of the welded fittings installation is shown in Figures 13 and 14. This design change resulted when it was found that the integral accumulator was of insufficient volume to adequately handle the mechanical and thermal volume changes of the damper.

TABLE III. SPRING-DAMPER PUSHROD FATIGUE STRENGTH SUMMARY

Component	Part Number	Figure Number	Endurance Limit "Three Sigma" (± lb)	Fatigue Margin Over Production Pushrod
Production CH-54B Pushrod	64107-11006	-	2200	1.00
Rod Ends	EWR 33111-043,-044	9	3950	1.80
Inner Shaft	EWR 31449-101	10	3910	1.78
Middle Cylinder	EWR 31449-104	11	3220	1.46
Main Housing	EWR 33111-111	9,12	24250	11.0
Cone Flange Bolts (8)	NAS 624H8	13	3000	1.36
End Cap With Welded Fittings	EWR 30306-041,-042	9, 13, 14	2200	1.00

The welded end cap design was subjected to a "cone analysis" to determine the loss in fatigue strength over the original component. This analysis, outlined in the appendix, indicates that the fatigue strength of the welded end cap is at least equal to that of the production pushrod. The analysis is necessarily conservative, due to the statistical nature of welded structural joints in fatigue.

Elastomeric Bushings

The elastomeric bushings are sized primarily to produce the required spring rate within allowable strains. Adequate information on the fatigue properties of rubber under these conditions was not available, and substantiation of the required strength was left to the laboratory fatigue tests. The elastomeric material chosen initially was Buna-N rubber and was molded into the metal sleeves by Nichols Engineering Co., Shelton, Conn. This rubber failed in fatigue during initial testing, and a change to natural rubber was made. This elastomer was found to have adequate fatigue strength.

The spring-damper elastomeric installation is designed to maximize fatigue life through the use of precompression; that is, the rubber bushing assemblies are compressed radially when they are pressed into the housing. The metal outer sleeves of each bushing assembly are slotted (Figures 10 and 11) to allow this radial compression. The cylinders in the main housing which accept the bushing assemblies are shown in Figure 12.

Precompression improves the fatigue strength in two ways. First, the rubber-to-metal bond is improved, simply because a large amount of friction is generated to assist the bond. Second, areas of tensile stress in the elastomer are minimized and it is known that fatigue cracks in elastomeric structural members originate in areas of surface tensile stress.

Hydraulic Fluid

The change from Buna-N to natural rubber also necessitated a change from conventional MIL-H-5606 hydraulic oil as the damper fluid, since it is not compatible with natural rubber. A water/ethylene glycol solution was chosen as a test fluid because it is compatible with natural rubber and has adequate properties as a hydraulic fluid. The solution was mixed to provide a -10°F freezing level.

GROUND TESTS

The structural adequacy and performance characteristics of the stall-flutter spring-damper design were determined in a ground test program consisting of: (1) single unit qualification/fatigue/performance tests, (2) a simulated centrifugal load performance test, (3) a welded end cap fatigue test, (4) flight unit proof and acceptance tests, and (5) an installed system whirl test. The successful completion of all phases of this program provided the necessary confidence to proceed with the flight test program.

Part 1 - Single Unit Qualification Tests

The purposes of the qualification tests were to:

- Develop the performance characteristics of the spring-damper pushrod to the required levels.
- Obtain operating and structural data.
- Demonstrate structural adequacy of the spring-damper pushrod design for the planned flight tests by an accelerated fatigue test.

Test Facility

The test was conducted using a test fixture installed in the Sikorsky 200K universal rotor blade fatigue test machine (Figures 16 and 17). Axial loading of the spring-damper was accomplished by a hydraulically driven eccentric working through a series spring. The eccentric throw was varied to obtain the required loads, and eccentric speed was varied from 0 to 1200 rpm (20 Hz). Measurements were made of spring-damper load, displacement, temperature, and fluid pressure.

Development Tests

The test conditions selected for the first runs on the first qualification test item were: loads up to $\pm$5000 lb, displacements up to $\pm$1/2 in. (damper limits), and frequencies up to 20 Hz.

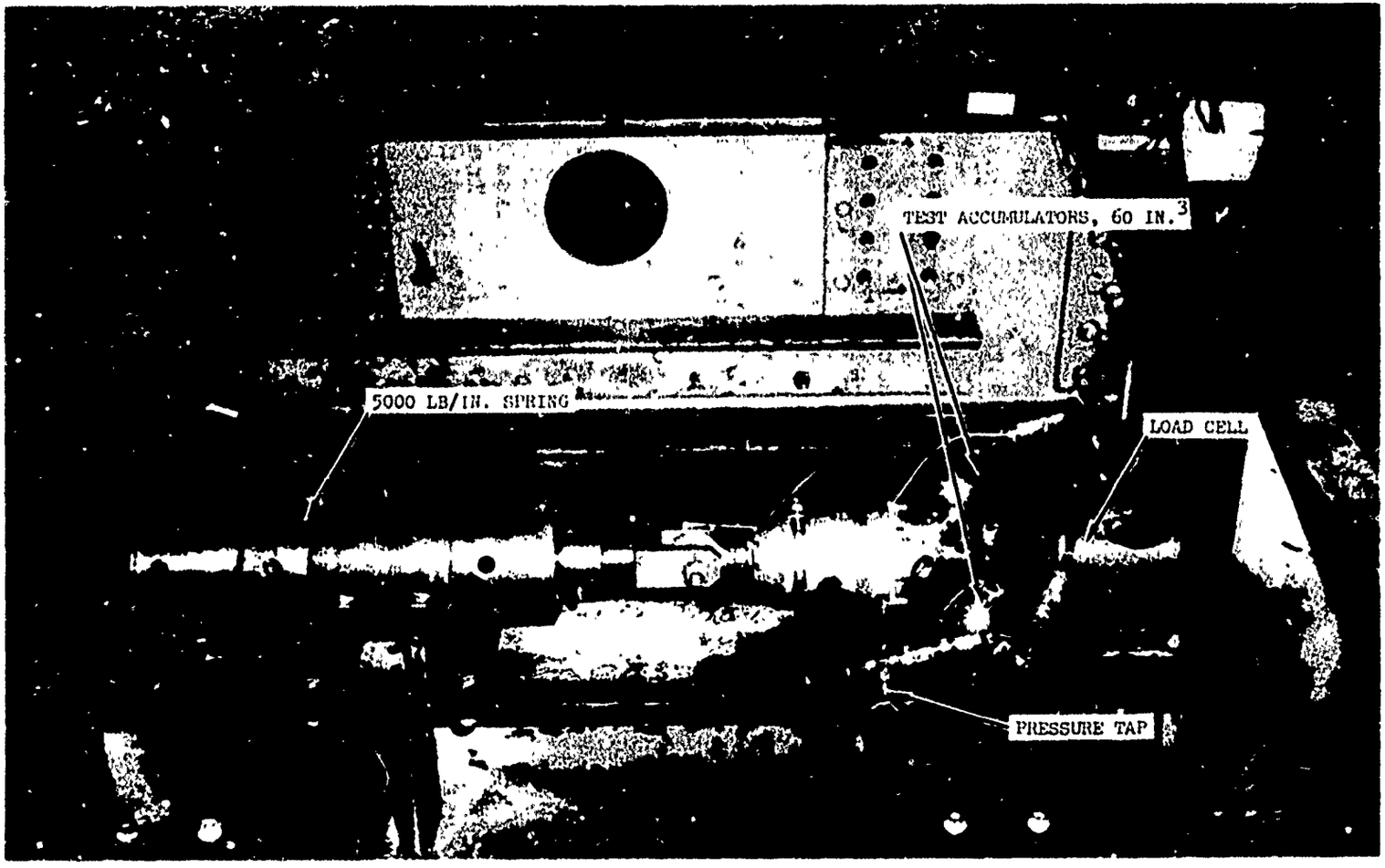

Figure 16. Spring-Damper Dynamic Test Setup in the Sikorsky "200K" Universal Rotor Blade Fatigue Test Machine.

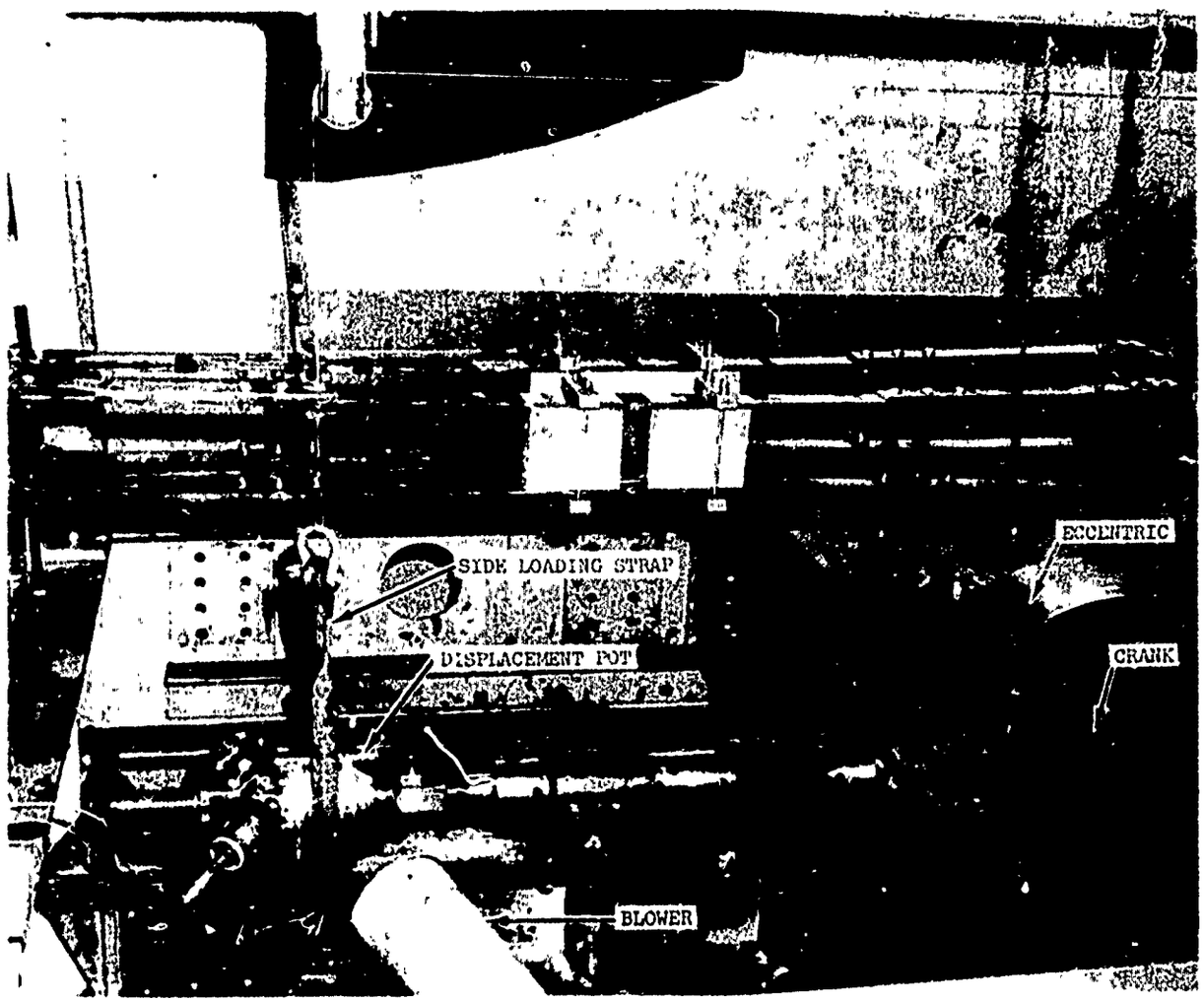

Figure 17. Spring-Damper Centrifugal Load Dynamic Test Setup.

Several design problems were uncovered during these runs, including external leaks, high dynamic spring rate, inconsistent damping rate, loss of precharge, and partial rubber failure. To correct these problems, improved sealing provisions were made and the internal accumulator concept was abandoned in favor of an external accumulator plumbed through hydraulic fittings welded on the end cap. The implementation of these changes produced the required damping characteristics when the redesigned damper was retested but a rubber fatigue failure was encountered after several minutes running at the maximum dynamic condition. To solve this problem, the Buna-N rubber was changed to natural rubber which has superior fatigue properties. The incompatibility of natural rubber with hydraulic oil, however, necessitated a change in the damper fluid to a water plus ethlene glycol (Prestone) mix. The freezing point of the mix was chosen to be -10°F.

At that point the damper configuration was fixed as follows:

Test fluid - water and Prestone, -10°F
Rubber - natural
Accumulators - external, 60 $in.^3$ bladder type
Precharge - 55 psig

Fatigue Endurance Tests

An estimate of the flight test loading spectrum was made, based on the flight test plan, and is shown in Figure 18. The endurance test spectrum is also shown in Figure 18. This spectrum is accelerated in both load and life. Loads of up to + 6000 lb were applied, and 38 times the expected flight cycles were applied at stall-flutter load levels. The total test cycles exceeded the flight cycles by a factor of 6.

The frequency used in all testing was 17 to 20 cps. Test runs were limited, at the high loads, by the damper temperature rise. Temperatures as high as 235°F were encountered after a few minutes running. (the rubber is known to deteriorate at 300°F). High temperatures were not expected in flight due to the brevity of the stall-flutter phenomenon, the lower loads and displacement, and better cooling due to airflow and lower ambient temperatures.

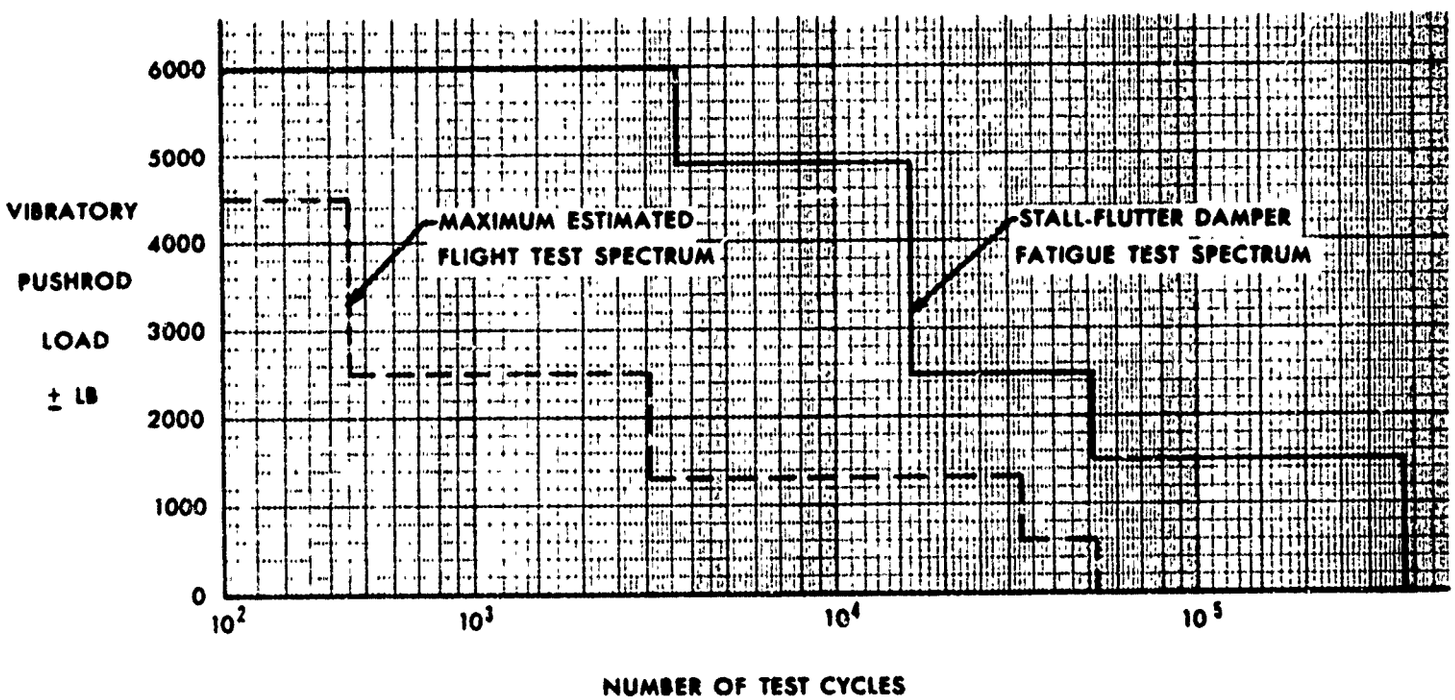

Figure 18. Flight and Fatigue Test Loading Spectrums.

At the completion of all testing, teardown and magnaflux inspections showed no evidence of structural failure, excessive deterioration, or wear. Posttest condition of the damper parts is shown in Figures 10, 11, 12, 13, and 14.

Part 2 - Simulated Centrifugal Load Performance Test

The purpose of this test was to determine if the centrifugal field in which the spring-damper operates had any effect on its performance. The test was accomplished using the reassembled fatigue test damper mounted in the endurance test machine.

The calculated side load was 300 lb, but a 400-lb load was actually used in the test. The loading strap and cable is shown in Figure 17. A short run at maximum load and frequency was made and the performance of the damper was measured.

No evidence of any change in damper characteristics was noted due to the application of the side load. Disassembly of the test damper showed no evidence of interference, wear, or abnormal deflection.

Part 3 - Welded End Cap Fatigue Test

Although a welded-port end cap had been substantiated as part of the single unit qualification test, it was not of "production" design or quality. The flight version of the welded end cap is far superior in fatigue strength to the earlier test version, but since some weld porosity was indicated by X-Ray inspection of these welds, another test was indicated. Of the seven welded end caps available, the one with the most porosity was selected for the fatigue test.

Test Program

The test was set up in an IV-20 fatigue test machine, as shown in Figure 19. Loading was accomplished axially at 1200 cpm with an initial level of $\pm$4000 lb. After 2.3 million cycles with no failure, the load was increased to $\pm$4700 lb. After an additional 108,000 cycles with no failure, the load was increased to +5900 lb. After an additional 8400 cycles at this level, the test rod end cracked at the spherical joint.

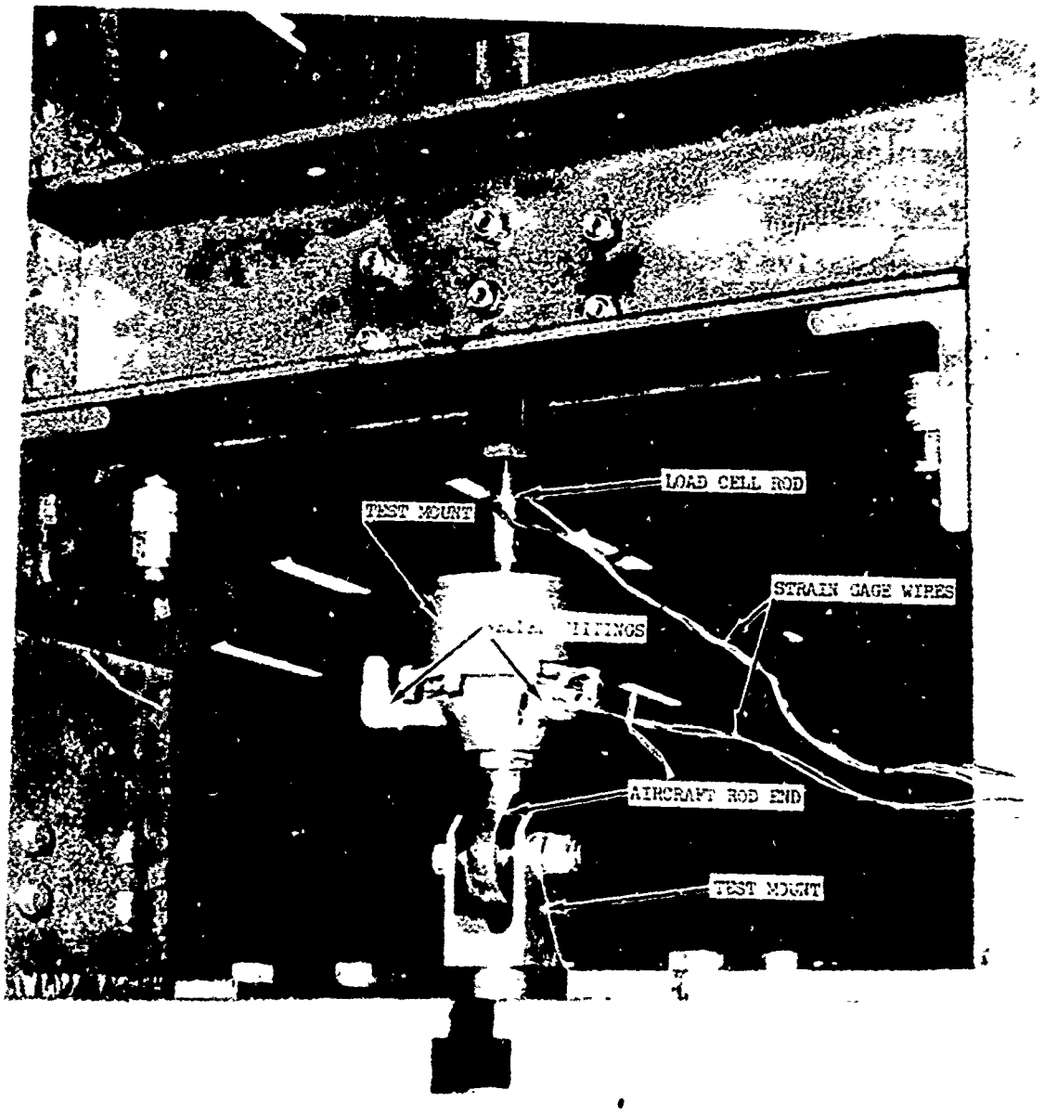

Figure 19. End Cap Weldment Fatigue Test Setup in an IV-20 Fatigue Test Machine.

At that point, the entire test article had been substantiated and the rod end failure had occurred at levels known to be well in excess of the required endurance limit. In order to obtain crack initiation and propagation data on the welded ports, the test was continued with a new rod end. However, after an additional 600,000 cycles at ±6000 lb load, a failure of the test machine hardware occurred and the test was terminated.

Test Results

A cumulative damage calculation was performed on the test data, and the results are shown in Figure 20. A mean endurance limit of ±5600 lb and a working endurance limit of ±3800 lb were verified in these tests for the welded port end cap.

In conclusion, this fatigue test demonstrated that the welded end cap and the rod end have fatigue strengths far in excess of that required to complete the 5-hour flight test.

Part IV - Flight Units Proof and Acceptance Tests

Test Program

The six spring-damper units to be used for the flight test program were assembled in a configuration identical to that of the qualification test item, with complete inspection by Sikorsky Quality Control. Each unit was then subjected to static proof loads of ±5000 lb and their spring rates were measured. The average spring rate was found to be 5158 lb/in. with an average deviation of ±4%.

A dynamic performance test was then performed on each of the flight units using the same test fixture as was used for qualification testing. A short run to ±4500 lb load at 18 cps was accomplished, with load and deflection being recorded for each unit. The average damping rate was found to be 90.3 lb-sec/in. with an average deviation of ±11%. The average dynamic spring rate was found to be 10,573 lb/in. with an average variation of ±9.3%.

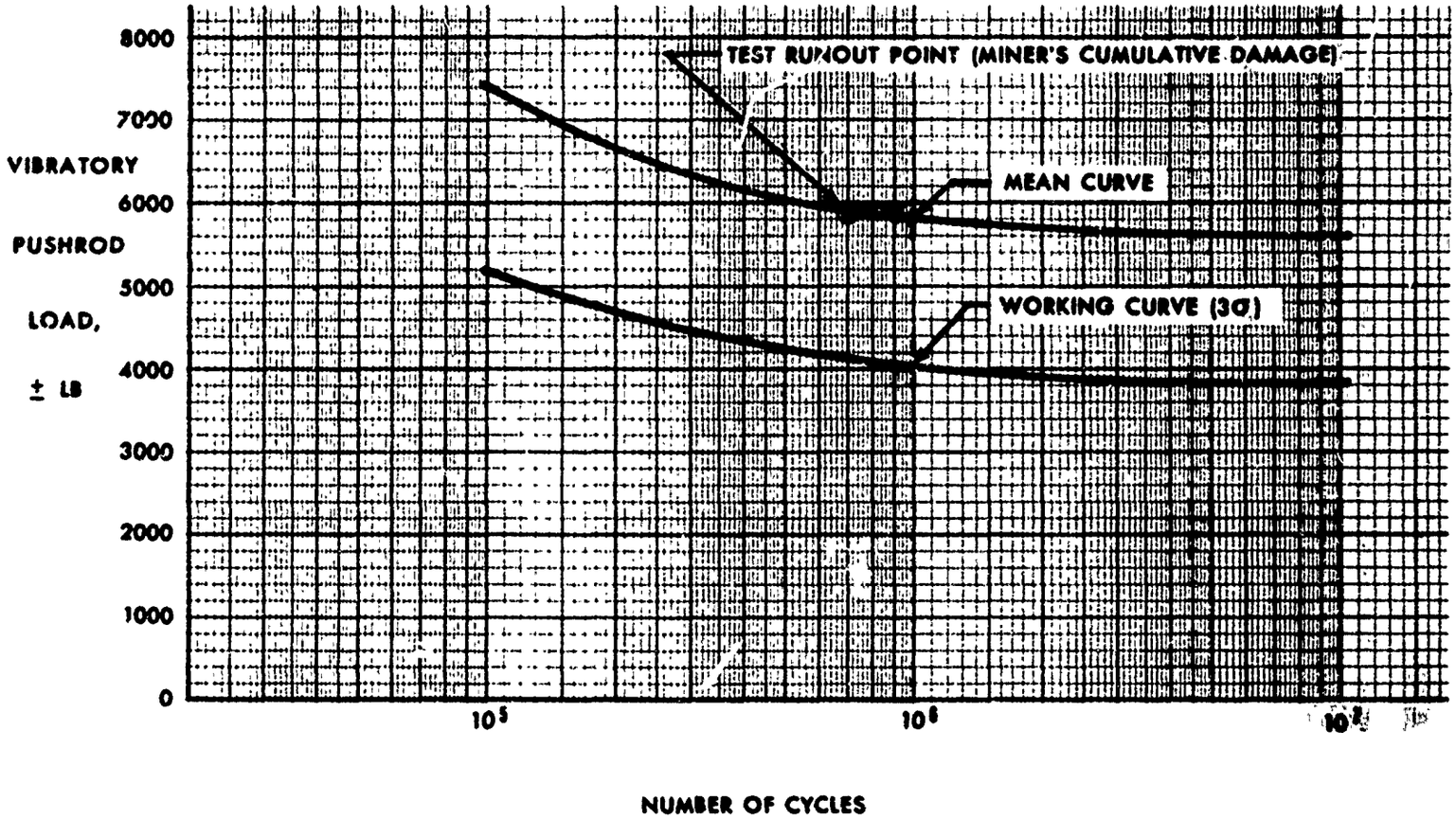

Figure 20. End Cap Weldment Fatique Test Results.

Conclusions

The above characteristics are considered acceptable, although the damping rate is higher than that found for the qualification unit. This can be attributed to the smaller accumulator setup used in these runs, which is more representative of the aircraft installation. These characteristics were used as one of the test cases in the aeroelastic analysis, and it was found to be a stable configuration.

No problems or abnormalities were found with the six spring-dampers in any of these tests.

Part 5 - Installed System Whirl Tests

The purposes of these tests were to:

- Examine the basic stability and safety of the stall flutter damper system.
- Obtain experience with the installation and with blade tracking.
- Determine if the system were stable following loss of precharge air or test fluid due to leakage.
- Determine the torsional natural frequency of the installed system.

Blade Balance

Prior to installation on the whirl tower, the six rotor blades to be used for flight test were subjected to dynamic blade balancing on the Sikorsky 4000 hp blade balance test stand. Each of the six flight blades was "balanced" against two "master" balance blades, using master blade tolerances. This procedure, which uses one-half the production blade tolerances, was conducted as a contingency measure due to the possible sensitivity of the spring-damper installation to rotor tracking problems. The dynamic pitching moments of the six blades were thereby closely equalized, reducing as much as possible any potential tracking problems. Further investigation would be required to determine whether or not production blade tolerances would be adequate.

Installation

The six flight blades, the six flight dampers and the three accumulators and associated hydraulic lines were installed on the test rotor head on the Sikorsky 10,000-hp main rotor whirl test stand. The installation is shown in Figures 21 and 22. Bleeding and precharge procedures were developed and the system checked for leakage. Instrumentation was installed to measure blade stress and motion, and spring-damper load, displacement, and pressure. In addition, the test facility systems to measure torque, power, shaft bending, vibratory side force, and blade track were checked out.

Rotor Tracking

With the spring-damper system in standard configuration and 55 psig air precharge, the test rotor was started and accelerated slowly to 185 rpm (normal operating speed). All parameters were normal, but the rotor was four inches out of track. After shutdown, pushrod length adjustments were made and the rotor was run again for a tracking check. A total of four tracking runs was required to reduce the total track spread to 1 inch, about the best that could be achieved with the spring-damper installation.

Standard Configuration Test

With the rotor tracked and the spring-damper system in standard configuration with 55 psig air precharge, each of the following test conditions was run at 185 rpm (normal operating speed) for at least 1 minute. The thrust and flapping values used are well in excess of those expected in the flight test.

- Low thrust, low flapping
- 55,000 lb thrust, low flapping
- 55,000 lb thrust, $\pm$ 4° flapping
- Low thrust, $\pm$ 8° flapping
- 55,000 lb thrust, $\pm$ 8° flapping

In addition, a run was made at 204 rpm (CH-54B rotor redline) at flat pitch for 1 minute.

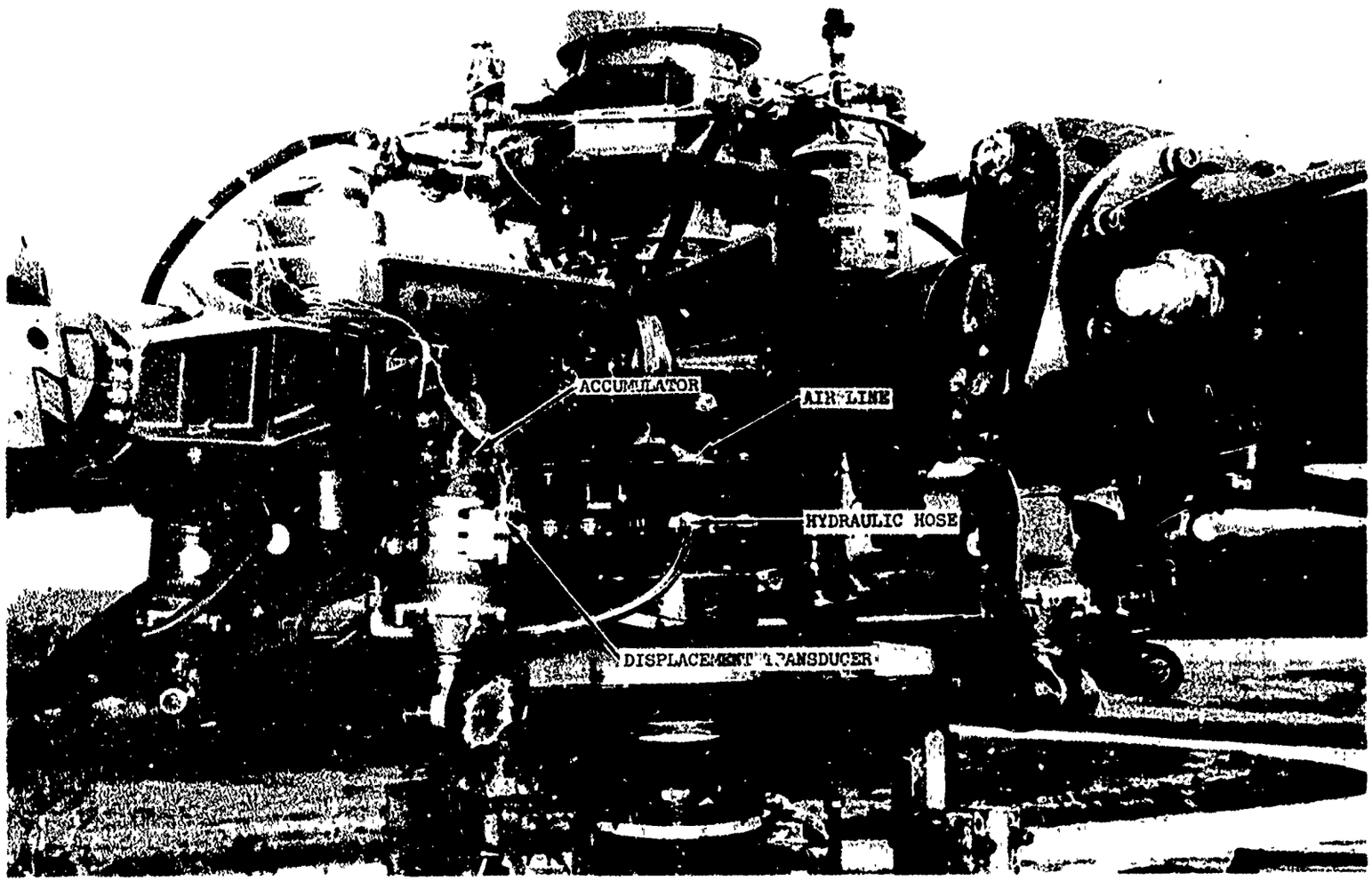

Figure 21. Spring-Damper System Installed on the Sikorsky 10,000 HP Whirl Test Tower.

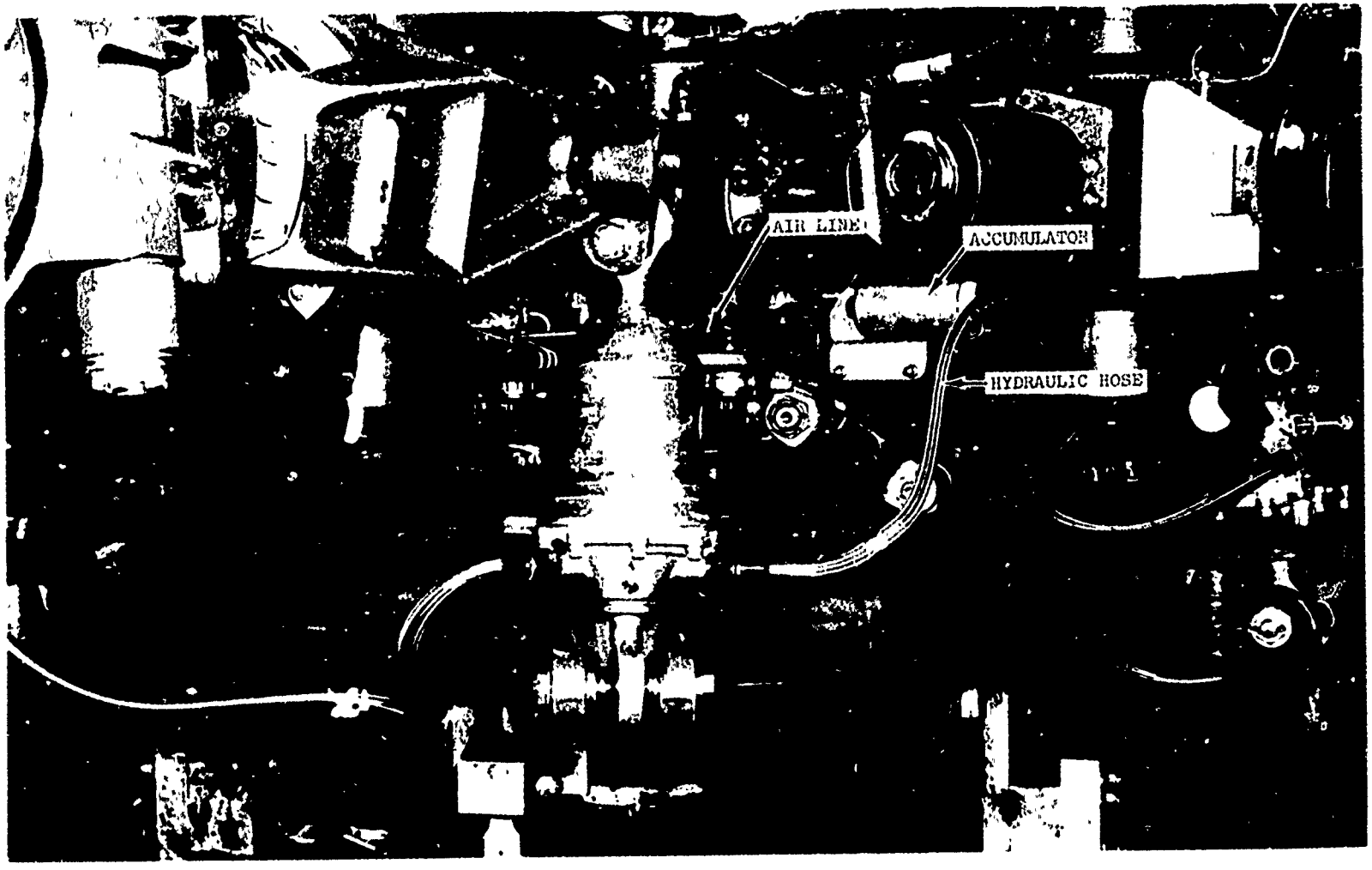

Figure 22. Spring-Damper Installed on Whirl Test Rotor Head.

No indication of instability, high blade stresses, or high control loads was observed in any of the above test conditions. In fact, stresses and loads were observed to be somewhat lower than the levels generally found in this type of test. Spring-damper displacements were also low, about 1/16 in., reflecting the low control loads.

Both the air and fluid pressures in the spring-damper hydraulic system were measured. These, of course, would have the same mean value (unless the accumulator pistons were bottomed), but the fluid pressure did show a much greater sensitivity to "vibratory" pressure changes. In view of this result, the air pressure measurement was considered unnecessary and was deleted from flight test measurements in order to conserve slip-ring channels. The fluid pressure alone is sufficient to determine system hydraulic performance and integrity.

The rotor track was found to have up to a 4-in. spread at the high thrust, high flapping condition; this is acceptable since values close to this level often occur with rigid pushrods at this condition.

"Failure Mode" Testing

Leakage on either the air or the fluid side of the stall-flutter damper hydraulic system can cause a loss in damping, although the pure spring rate is unaffected. Two whirl test runs were conducted, first with the air side vented and then with the fluid side vented. All of the test conditions run with the standard configurations were repeated for both the "loss of air" and "loss of fluid" configurations.

Again, no indication of instability, high blade stresses, or high control loads was observed in any of the test conditions. Changes in stresses, loads or damper displacement due to loss of fluid were negligible. Rotor track was as good as in the standard configuration.

Natural Frequency Determination

The Sikorsky main rotor test stand has the capability of applying vibratory control inputs to the test rotor head, thereby allowing determination of rotating natural frequency intercepts. The excitation is in the form of stationary swashplate vibratory tilting motions which result in vibratory blade angles. This blade-angle oscillation is sufficient to excite the torsional, edgewise, or flatwise modes of blade response. The frequency of excitation is synchronized to the rotor in terms of specific multiples of rotor speed. The natural frequency is then found by sweeping rotor speed through the area of interest while observing for a buildup in blade stress and/or control load. This normally indicates a natural frequency point, the mode being determined by which blade strain gage shows the buildup.

In the case of the stall-flutter damper installation, a torsional natural frequency of about 7 per rev at 185 was predicted by analysis, using the measured characteristics of the flight test spring-dampers. In order to generate this frequency of excitation in the rotating system, the stationary system excitation was set for 6 per rev (n-1).

A nominal condition of 3000, $\pm 3°$ of flapping was used during these shake runs. The rotor speed range used was 150 to 200 rpm and the amplitude of excitation was about $\pm .150$ in. at the damper-swashplate connection.

When these test conditions were applied, no buildup in blade stress or control load was observed in the torsional mode. Some small response was noted in spring-damper system fluid pressure and displacement indicating that the system responded at 7 per rev. In order to check for a lower harmonic response, the excitation was changed to 5 per rev and again no buildup of blade stress or control load occurred. Some small pressure and displacement response was noted at 6 per rev. It can therefore be concluded that the system torsional natural frequency is the predicted 6 to 7 per rev, since a lower natural frequency would have caused responses at 5 and 4 per rev in thest tests. Due to the lack of a blade stress buildup, no more quantitative conclusion can be reached.

FLIGHT TESTS

The performance of the stall-flutter spring-damper pushrod system installed on a CH-54B helicopter was evaluated in a series of flight tests consisting of: (1) base-line flights of the CH-54B helicopter in standard configuration, and (2) comparison flights with the spring-damper system installed. The flight program was successfully completed and control loads in deep stall were significantly reduced as a result of the spring-damper installation.

The flight test of five hours was necessarily limited in scope. The investigation was limited to the feasibility of the damper and did not extend to an extensive evaluation of the overall effect on the CH-54B operating envelope. The limited tests that were made to measure vehicle performance and stability were performed to insure that no problems which made the damper totally unacceptable were overlooked.

Part 1 - Base-Line Flights

The purposes of the base-line flights were to:

- Obtain base-line performance data on control and rotor head loads during deep stall for comparison with later data.
- Check out the aircraft and systems after a long period of inactivity.
- Refamiliarize the program's personnel with the stall-flutter phenomenon.

Description of Aircraft

The aircraft used in this program was a bailed Army CH-54B, which is described generally below:

Helicopter Type:	S64F/CH-54B
Aircraft Number:	18462
Engine Manufacturer:	Pratt and Whitney Aircraft
Engine Type (2):	JFTD-12A-5A
T.O. & 30 Min. O.E.I.	4800 hp
Maximum Continuous	4430 hp
Number of Main Rotor Blades:	6
Main Rotor Speed	185 RPM
Blade Type:	Constant Chord, NACA 0011 Mod.
Rotor Radius:	36 feet
Blade Twist(theoretical):	Nonlinear, 10.46°
Blade Chord:	26.0 inches

Number of Tail Rotor Blades:	4
Tail Rotor Speed	850 RPM
Blade Type:	Constant Chord, NACA 0012
Blade Chord:	15.4 inches
Tail Rotor Diameter:	16 feet
Stabilizer Type:	NACA 0012
Stabilizer Chord:	56.0 inches
Span:	103.0 inches
Area:	40.0 square feet
Angle of Incidence:	0 degrees
Gross Weight:	47,000 pounds

Gross weight changes were accomplished using a water ballast pallet.

Measurements

The following parameters were measured and recorded on an on-board magnetic tape data acquisition system. An asterisk indicates that one of those parameters was also telemetered to the Sikorsky ground station for real-time monitoring of the aircraft's performance.

* * Pushrod Load (2)
* * Stationary Star Loads (2)
* * Rotating Scissors Load
  * Stationary Scissors Load
* * Main Rotor Blade Stresses (5 edgewise and 5 flatwise)
  * Main Rotor Blade Flapping (2)
* * Main Rotor Blade Pitch (2)
  * Main Rotor Blade Hunting (2)
  * Pitch, Roll, and Yaw Rate
  * Pitch, Roll, and Yaw Acceleration
  * Collective, Lateral, and Longitudinal* Stick Positions
  * Vertical Vibration at Pilot's and Copilot's Stations
* * Vertical Vibration at the Main Gearbox
  * Lateral Vibration at the Pilot's Station
* * Load Factor at C.G.
  * Rotor Head Camera

Base-Line Flight Results

Four flights, all at 47,000 lb gross weight, were required to meet all test requirements. Aircraft and instrumentation problems, as well as turbulent air

conditions precluding accurate setup of the required flight conditions, increased the number of flights required. The data obtained on these flights were used as base-line points and are summarized, with pertinent flight data, in Tables IV and V.

Of the conditions flown, the 115 kt, 96% rotor speed, level flight point was the best stall condition from the standpoint of uniformity and repeatability. The maximum pushrod vibratory load observed was about ±2100 lb. This is lower than some stall results observed in the past on this aircraft, but the typical stall-flutter characteristic was observed in the pushrod time histories and was therefore adequate for base-line purposes. Analysis of these conditions appears in the next section.

Part 2 - Stall-Flutter Damper Flights

The purposes of the stall-flutter damper flights were to:

- Buildup to the required test conditions through several steps in gross weight, airspeed, and altitude.
- Obtain spring-damper pushrod and aircraft performance data at 47,000 lb gross weight and 2000 ft density altitude.
- Repeat the test conditions run in the baseline flight.

Installation of the Stall-Flutter Damper System

Each damper was installed with the same rotor blade and on the same relative spindle as on the whirl test. Hoses and accumulators were installed as on the whirl test with some improvement in the securing of lines and fittings. The installation is shown in Figures 23 and 24.

The damper lengths were adjusted to suit the aircraft rigging requirements, which include a 3-inch split-track (three alternate blades tracked 3 inches higher than the other three). The subsequent tracking run showed an out-of-track condition which was corrected using electronic blade tracker data. Two additional runs were required to reduce the out-of-track condition to about 1 inch, which is acceptable.

TABLE IV. FLIGHT TEST CONDITIONS

Flt. No.	Aircraft Config	Initial GW (lb)	Data Point	Nominal Airspeed (kt)	Rotor Speed (%)	Flight Regime
1	Standard	48,000	1	0	100	Hover
			2	90	100	Level Flight
			3	90	100	30° Right AOB
			4	90	100	30° Right AOB
			5	100	100	Level Flight
			6	100	100	30° Right AOB
			7	100	100	30° Right AOB
			8	15	100	600 fpm Descent
2	Standard	48,000	1	90	100	Level Flight
			2	100	100	Level Flight
			3	90	100	30° Right AOB
			4	90	100	30° Left AOB
			5	20	100	800 fpm Auto.
3	Standard	48,000	1	0	100	Hover
			2	90	100	Level Flight
			3	100	100	Level Flight
			4	110	100	Level Flight
			5	110	100	Level Flight
			6	115	100	Level Flight
			7	100	96	Level Flight
			8	110	96	Level Flight
			9	115	96	Level Flight
4	Standard	48,000	1	0	100	Hover
			2	110	96	Level Flight
			3	115	96	Level Flight
			4	90	100	30° Right AOB
			5	90	100	30° Right AOB
			6	100	100	30° Right AOB
			7	110	100	30° Right AOB
			8	110	100	30° Right AOB
			9	110	100	30° Right AOB
			10	115	96	Level Flight

TABLE IV - Continued

Flt. No.	Aircraft Config	Initial GW (lb)	Data Point	Nominal Airspeed (kt)	Rotor Speed (%)	Flight Regime
5	Spring-Damper System Installed	37,000	1	0	--	Rotor Engagement
			2	0	94	Ground Run
			3	0	96	Ground Run
			4	0	98	Ground Run
			5	0	100	Ground Run
			6	0	100	Taxi
			7	0	105.5	Overspeed
			8	0	100+	Accel
			9	0	100+	Accel, Decel
			10	0	100	Long. Reversal
			11	0	100	Lat. Reversal
			12	0	100	Coll. Reversal
			13	[illegible]	100	Lift-off
			14	0	100	Hover
			15	0	105	Hover
			16	0	95	Hover
			17	0	100	Long. Reversal
			18	20	100	Right Sideward Flt
			19	20	100	Left Sideward Flt.
			20	30	100	Rearward Flt.
			21	0	100	Collective Pulse
			22	40	100	Across Field
			23	45	100	Across Field
			24	100	100	Pattern Circuit
6	Spring-Damper System Installed	40,000	1	0	100	Hover
			2	0	100	Long. Reversal
			3	0	105	Hover
			4	0	95	Hover
			5	45	100	Across Field
			6	60	100	Level Flight
			7	80	100	Level Flight
			8	100	100	Level Flight
			9	70	100	Approach

TABLE IV - Continued

Flt. No.	Aircraft Config	Initial GW (lb)	Data Point	Nominal Airspeed (kt)	Rotor Speed (%)	Flight Regime
7	Spring-Damper System Installed	48,000	1	0	100	Hover
			2	0	100	Long. Reversal
			3	0	105	Hover
			4	0	96	Hover
			5	0	96	Long. Reversal
			6	40	100	Across Field
			7	40	100	Climb
			8	60	100	Level Flight
			9	70	100	Level Flight
			10	80	100	Level Flight
			11	90	100	Level Flight
			12	100	100	Level Flight
			13	110	100	Level Flight
			14	115	100	Level Flight
			15	60	104	Level Flight
			16	90	104	Level Flight
			17	60	96	Level Flight
			18	70	96	Level Flight
			19	80	96	Level Flight
			20	90	96	Level Flight
			21	100	96	Level Flight
			22	110	96	Level Flight
			23	115	96	Level Flight
			24	70	100	Long. Reversal
			25	0	100	Hover
8	Spring-Damper System Installed	48,000	1	0	100	Hover
			2	100	100	Level Flight
			3	0	100	Grd. Res. Flat Pitch
			4	0	100	Grd. Res. 20% Torque
			5	0	100	Grd. Res. 30% Torque
			6	0	100	Grd. Res. 35% Torque
			7	0	100	Grd. Res. 40% Torque

TABLE IV - Continued

Flt. No.	Aircraft Config	Initial GW (lb)	Data Point	Nominal Airspeed (kt)	Rotor Speed (%)	Flight Regime
9	Spring-Damper System Installed	48,000	1	0	100	Hover
			2	100	100	Level Flight
			3	110	100	Level Flight
			4	115	100	Level Flight
			5	90	96	Level Flight
			6	100	96	Level Flight
			7	110	96	Level Flight
			8	115	96	Level Flight
			9	90	100	30° Right AOB
			10	100	100	30° Right AOB
			11	110	100	30° Right AOB
			12	115	96	Level Flight
			13	115	96	Level Flight
			14	70	100	Long. Reversal
			15	90	100	Long. Reversal
			16	100	100	Long. Reversal
			17	110	100	Long. Reversal
			18	100	100	Fwd. Pulse
			19	100	100	Aft. Pulse
			20	100	100	Left Pulse
			21	100	100	Right Pulse
			22	110	100	Fwd. Pulse
			23	110	96	Fwd. Pulse
			24	110	96	Fwd. Pulse
			25	115	96	Fwd. Pulse
			26	110	100	30° Rt. AOB, Fwd Pulse
			27	60	104	Level Flight
			28	90	104	Level Flight
			29	60	96	Level Flight

Condition	Flight No.	Run No.	OAT (°C)	Alt. (ft)	RPM (%)	CAS (kt)	Density Altitude (ft)	Weight (lb)
	3	8	+3	2580	101	88	1700	47340
		9	+4	2670	101	95	1950	47230
		10	+4	2680	101	105	1950	47140
Base-Line Flight		11	+4	2540	101	103	1800	46900
		12	+4	2580	101	107	1850	46810
		13	+4	2520	96	96	1750	46630
		14	+4	2460	96	105	1700	46560
		14	+3	2440	97	105	1600	46560
	4	21	+4	2800	97	103	2100	47420
Base-Line Flight		21	+3	2800	97	106	2000	47420
		22	+4	2220	97	106	1400	47370
		29	+3	2400	96½	110	1500	46380
	9	8	-8	3860	100	94	1800	47410
		9	-8	3850	100	104	1800	47360
		10	-8	3850	100	111	1800	47280
		11	-9	3810	100	111	1750	47140
		12	-9	3820	96	86	1760	46960
		13	-9	3820	96	97	1760	46910
		14	-9	3810	96	106	1750	46870
		15	-9	3770	96	112	1700	46670
Spring-Damper Flight		19	-9	3980	96	112	2000	46440
		20	-9	4020	96	108	2040	45990
		34	-9	4120	104	60	2100	45720
		35	-9	4130	104	88	2110	45680
		36	-10	4070	100	62	1950	45620
		37	-10	4060	100	73	1940	45590
		38	-10	4070	100	79	1950	45570
		39	-9	4040	100	87	2050	45550
		40	-11	4020	96	63	1800	45520

TABLE V. FLIGHT TEST DATA SUMMARY

S (kt)	Density Altitude (ft)	Weight (lb)	Load Factor	ERITS (37,500)	Vibratory Pushrod Load (lb)	Vibratory RLSS (lb)	Vibratory Blade Stress (psi) NB-6	Vibratory Blade Stress (psi) L-6	Vi
88	1700	47340	1.00	285	900	500	2300	2400	
95	1950	47230	1.00	278	1000	550	2500	2600	
05	1950	47140	1.01	268	1200	700	2900	3000	
03	1800	46900	1.01	271	1200	400	2700	2700	
07	1850	46810	1.00	268	1300	500	2700	3000	
06	1750	46630	1.02	259	1600	1700	2900	3000	
05	1700	46560	.98	256	1500	1700	2600	2500	
05	1800	46560	1.05	252	2000	2800	2800	3300	
03	2100	47420	.95	268	1000	700	2500	3200	
06	2000	47420	1.00	255	1300	1600	2700	3300	
06	1400	47370	1.02	254	2100	3400	2800	3100	
10	150	46380	1.02	248	2050	3700	2700	3300	
04	1800	47410	.99	277	800	600	2500	2500	
04	1800	47360	1.00	267	1000	800	2300	3000	
1	1800	47080	1.00	26[illegible]	1300	1300	2900	3300	
11	1750	47140	1.01	269	1400	1300	3000	3300	
06	1760	46960	1.00	269	900	800	2500	2700	
07	1760	46910	.99	261	1200	1500	2500	3000	
06	1750	46870	.99	254	1500	2100	2800	3300	
12	1700	46670	1.00	247	1800	2300	2900	3100	
12	2000	46440	.97	251	1500	2100	2900	2900	
08	2050	45990	1.00	249	1600	2300	2800	2950	
50	2100	45720	1.00	324	500	400	2200	2200	
08	2110	45680	1.01	297	800	400	2400	2000	
02	1950	45620	.98	312	500	500	2000	2600	
03	1940	45590	1.01	296	600	500	2500	2500	
09	1950	45570	1.02	292	700	500	2500	2300	
07	2050	45550	.98	299	700	400	2500	2300	
03	1800	45520	1.00	294	600	600	2400	3150	

Vibratory Disp.	Vibratory Blade Stress (psi)		Vibratory Pushrod Displacement (in.)	Control Positions (%)		Vibration at Pilot's Station (in/sec)	
	NB-6	L-6		Long.	Lateral	Vertical	Lateral
00	2300	2400	-	66	53	0.5	0.7
50	2500	2600	-	67	52	0.8	0.8
00	2900	3000	-	72	52	0.8	0.8
00	2700	2700	-	70	53	0.8	0.8
00	2700	3000	-	72	52	0.8	0.8
00	2900	3000	-	72	50	0.7	0.8
00	2600	2500	-	75	50	0.7	0.6
00	2800	3300	-	76	48	0.9	0.6
00	2500	3200	-	72	48	0.4	0.4
00	2700	3300	-	73	49	0.4	0.4
00	2800	3100	-	78	47	0.7	0.4
00	2700	3300	-	78	48	0.7	0.4
00	2500	2500	.102	68	52	0.7	0.7
00	2300	3000	.123	73	55	0.6	0.7
00	2900	3300	.157	80	57	0.7	0.6
00	3000	3300	.160	78	58	0.7	0.7
00	2500	2700	.105	70	52	0.3	0.5
00	2500	3000	.138	77	52	0.7	0.6
00	2800	3300	.185	84	52	0.7	0.5
00	2900	3100	.208	86	58	1.2	0.7
00	2900	2900	.187	86	52	1.0	0.6
00	2800	2950	.195	86	50	1.0	0.5
00	2200	2200	.070	62	50	0.6	0.3
00	2400	2000	.093	61	54	0.4	0.6
00	2000	2600	.060	63	50	0.3	0.4
00	2500	2500	.060	62	47	0.6	0.4
00	2500	2300	.077	61	53	0.7	0.3
00	2500	2300	.087	66	54	0.4	0.6
00	2400	3150	.070	63	45	0.3	0.3

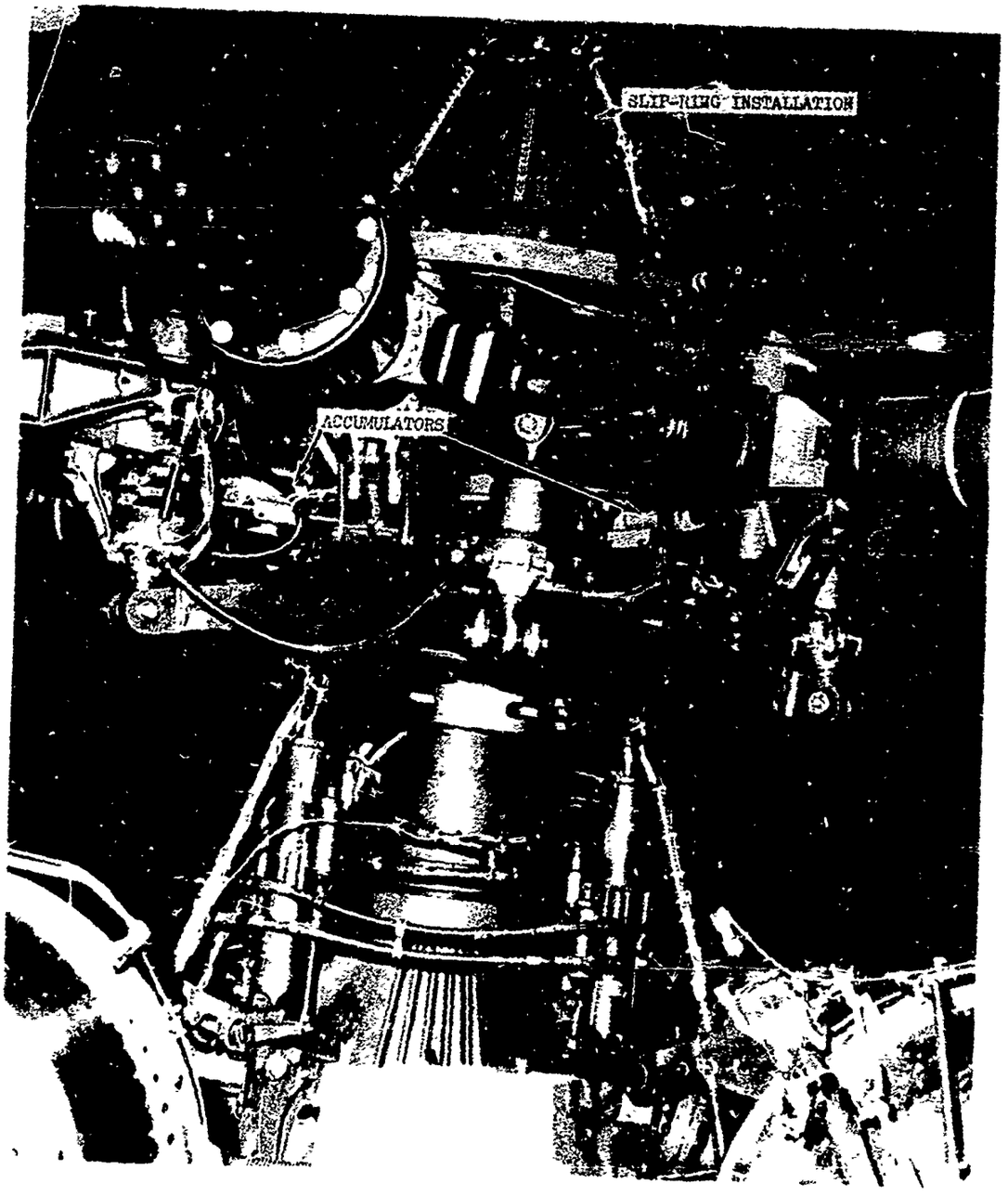

Figure 23. Spring-Damper System Flight Aircraft Installation.

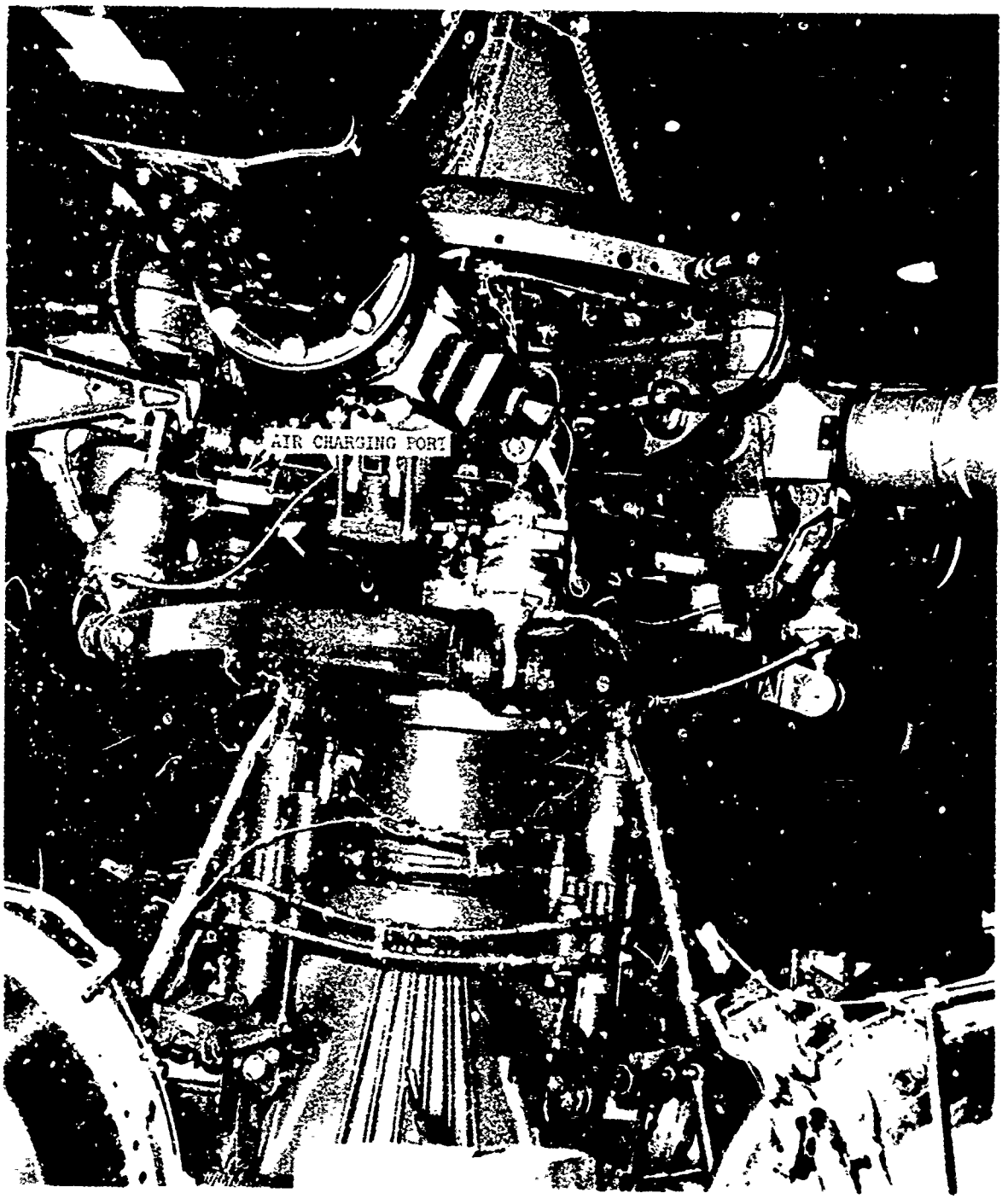

Figure 24. Spring-Damper System Flight Aircraft Installation.

Measurements

In addition to the measurements listed for the base-line flights, the following parameters were recorded and telemetered:

Stall-Flutter Damper Displacement (2)
Stall-Flutter Damper Temperature
Damper System Fluid Pressure

Stall-Flutter Damper Flight Test Results

A total of five flights was required to meet all the test objectives.

The first flight was flown at the light gross weight of 37,000 lb and consisted of yard and pattern work (see Figure 25). Flight characteristics were normal and all loads and displacements were low. A second buildup flight was conducted at 42,000 lb with similar results.

The third flight was conducted at 47,000 lb, but weather and instrumentation problems precluded acquisition of final data. Flight characteristics were normal and loads and displacements were again low. The fourth flight was also aborted due to turbulence, and test results were similar.

Conditions were good for the fifth damper flight (Flight 9 of the program) and all the required data was obtained. The conditions flown and the pertinent flight parameters are shown in Tables IV and V. The pilots reported that the aircraft behaved normally in all regimes of flight, and the vibration in stall was about the same. Analysis of the data, however, showed that significant reductions in control loads did occur, as shown in the next section.

Figure 25. First Flight of the Spring-Damper System, February 6, 1973.

ANALYSIS OF PERFORMANCE

Comparative analysis of base-line and damper flight test data indicates the following major results:

- There is no control load evidence of stall-flutter with the spring-dampers installed.
- High-frequency rotating pushrod loads are reduced by almost 50%, although peak-to-peak loads are only slightly reduced, due to some increase in the lower frequency harmonics.
- Stationary control loads are reduced by more than 40% overall.
- The effects of blade stall on the CH-54B helicopter equipped with the stall-flutter spring-dampers are otherwise the same. Blade stresses, performance, handling, and vibration are unchanged.

ERITS Comparison

The ERITS parameter (Equivalent Retreating Indicated Tip Speed) is used as the basis for comparing specific data bursts from the base-line and damper flights. ERITS is a normalized retreating blade tip speed which takes into account the aircraft gross weight and the density altitude at the moment of the data burst. All ERITS data in this report is normalized to a gross weight of 37,500 lb, which was used as the standard in the CH-54B structural substantiation work. The ERITS relation is therefore

$$\text{ERITS} = \frac{(\text{Rotating Tip Speed} \times \sqrt{\text{Air Density Ratio}}) - \text{CAS}}{\sqrt{\frac{\text{Load Factor} \times \text{Gross Weight}}{37{,}500}}}$$

Two flight test conditions are chosen for point to point comparisons: 110 kt and 115 kt airspeeds at 96% rotor speed, 47,000 lb gross weight and 2000 feet density altitude (nominal conditions). Referring to Table V, the nominal 110 kt comparison is between run 21 of flight 4 (ERITS = 255 kt) and run 14 of flight 9 (ERITS = 254 kt). The 115 kt comparison is between run 29 of flight 4 (ERITS = 248) and run 15 of flight 9 (ERITS = 247). In each case, typical measured time histories were chosen from data bursts with rigid pushrods (flight 4) and with spring-dampers installed (flight 9).

Comparison of Rotating Pushrod Loads

Flight test time-histories of rotating pushrod load for rigid pushrods and for the spring-damper pushrods are shown below in Figures 26 and 27.

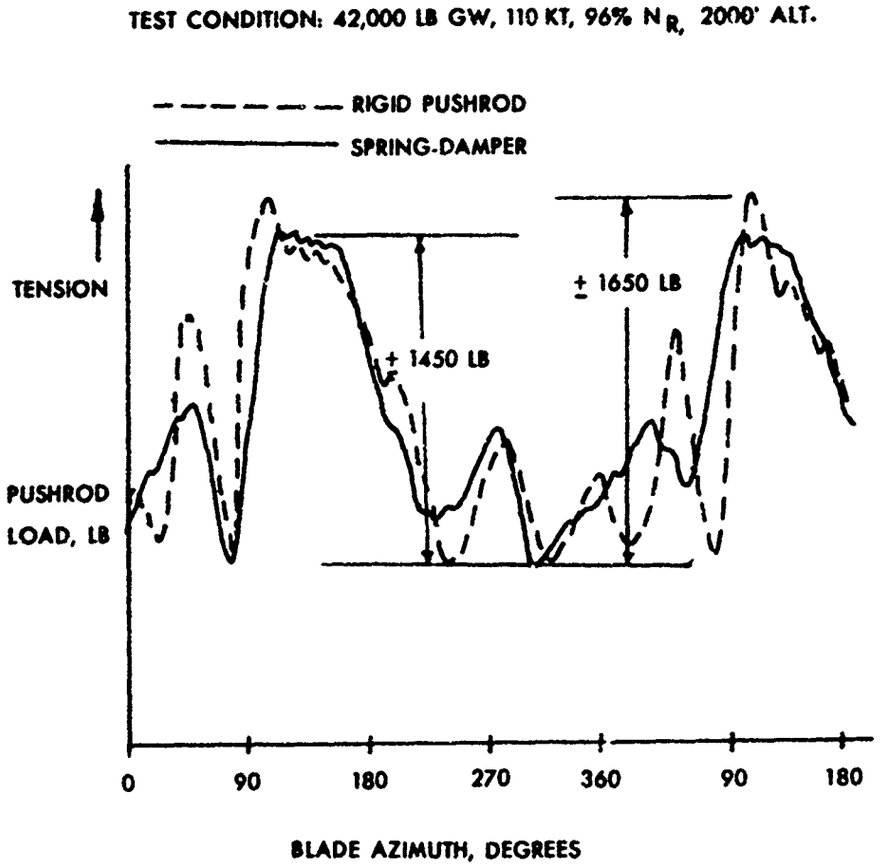

Figure 26. Rotating Pushrod Load Comparison, 110 Kt.

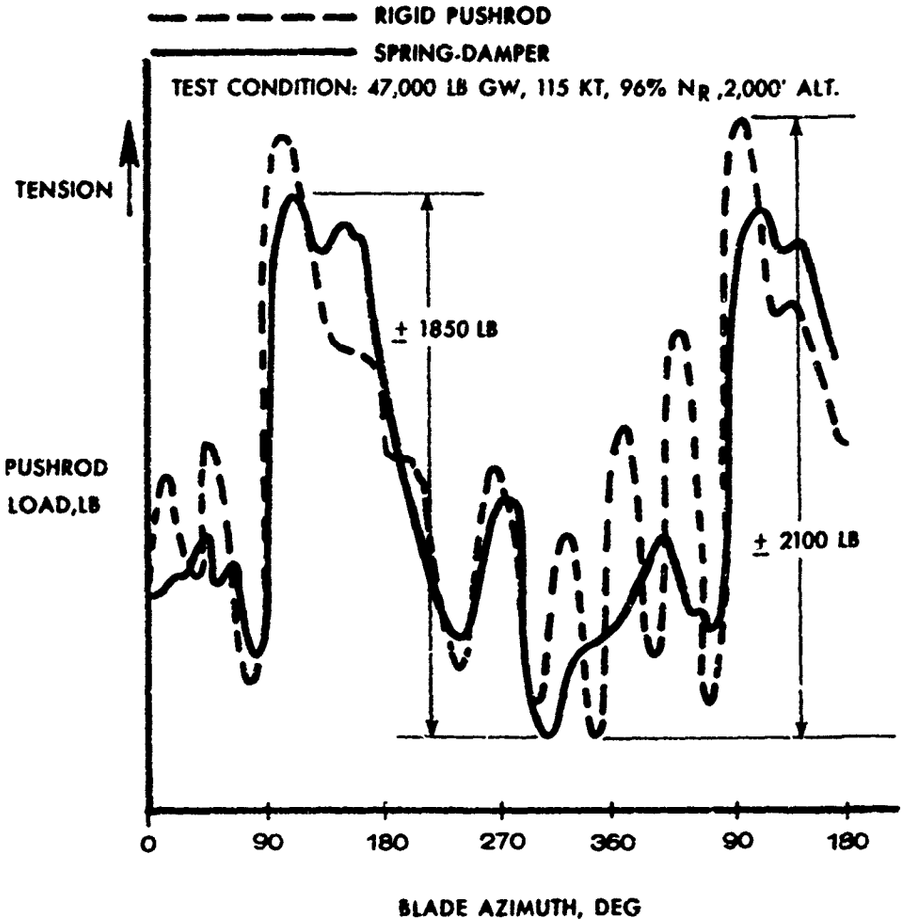

Figure 27. Rotating Pushrod Load Comparisor, 115 Kt.

The rigid pushrod record exhibits the high-frequency oscillation beginning on the retreating side which is characteristic of the stall-flutter phenomenon. This frequency can be seen to be 7 or 8 per rev and compares well with the calculated system "torsional" natural frequency of 7.4 per rev. A spectral analysis of the data burst which contains this cycle was conducted and the result is shown in Figure 28. The data burst did not contain sufficient stall-flutter cycles to identify the torsional frequency; however, the predominance of several higher harmonices is seen.

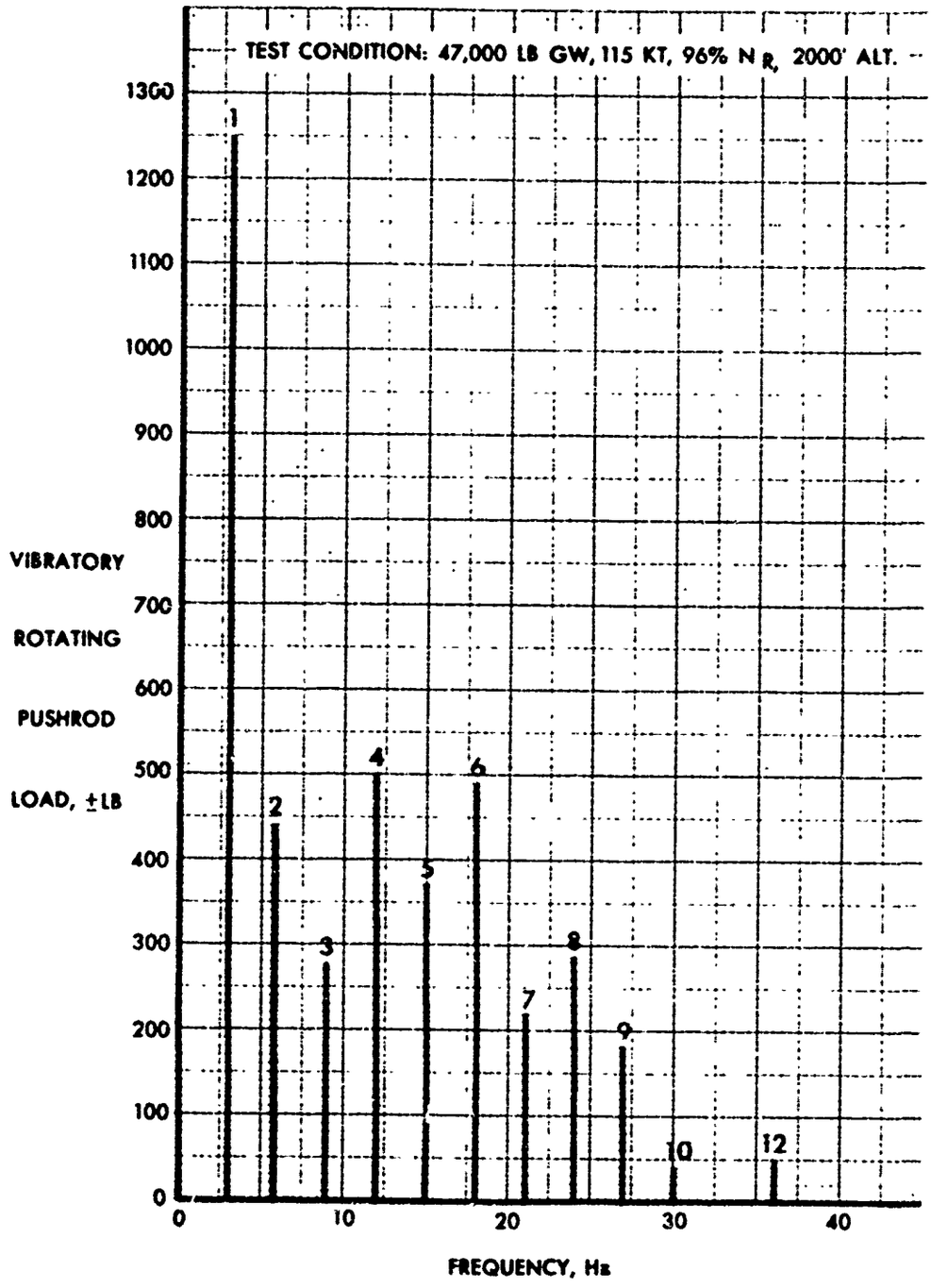

Figure 28. Spectral Analysis, Rigid Pushrod Load.

The spring-damper pushrod record shows a sharp attenuation of the higher harmonics, and for these cycles, shows a reduction in the overall load. The spectral analysis for this case is shown in Figure 29.

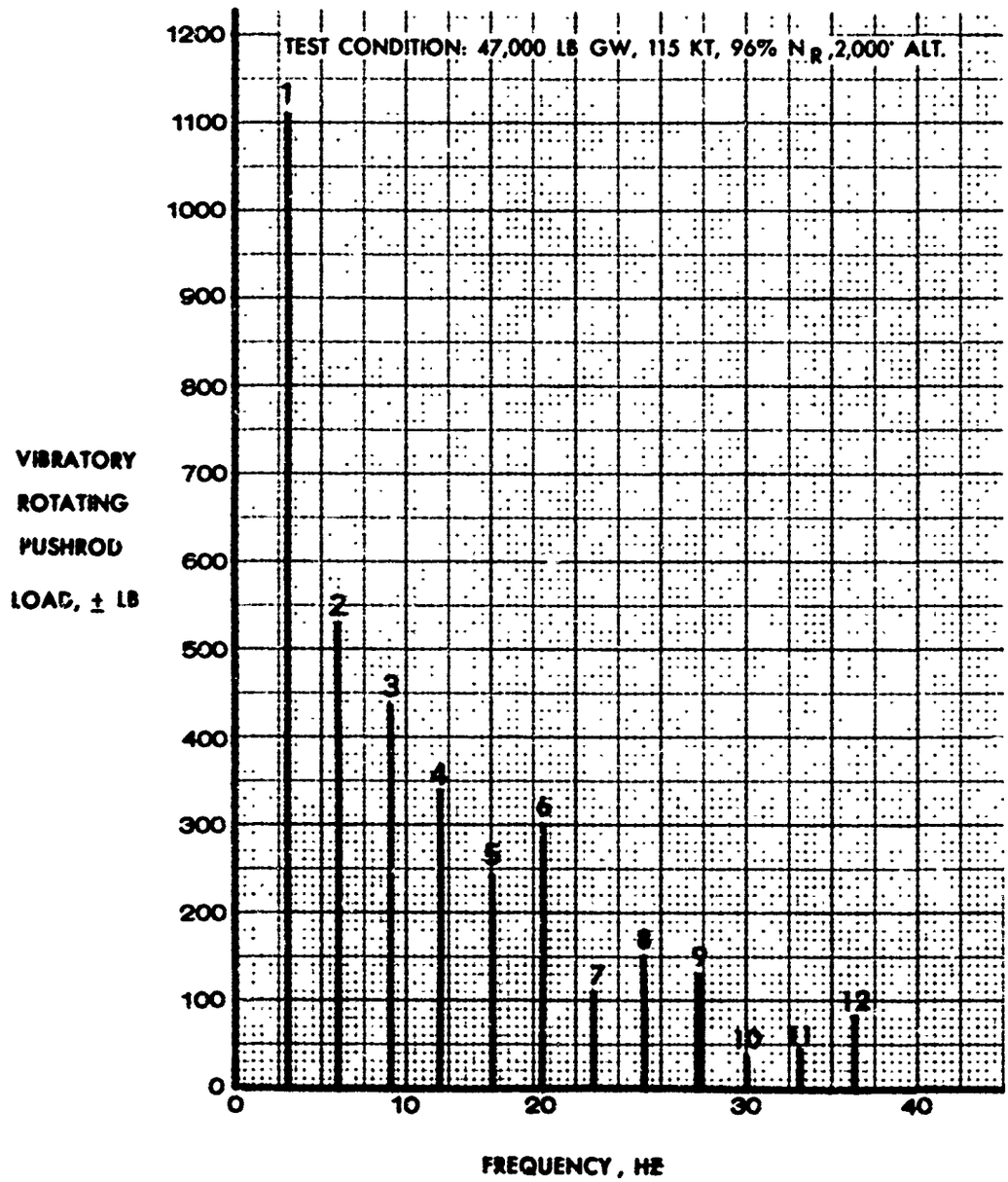

Figure 29. Spectral Analysis, Spring-Damper Load.

The harmonic contents can be compared by plotting the ratio of damper load to pushrod load against frequency for the same flight condition. This plot is shown as Figure 30, where frequencies above 4 per rev are seen to be attenuated by as much as 47%. An increase in the less-damaging 2 and 3 per rev harmonics is also seen, cancelling in part the reduction in overall load due to the lowering of the higher harmonics.

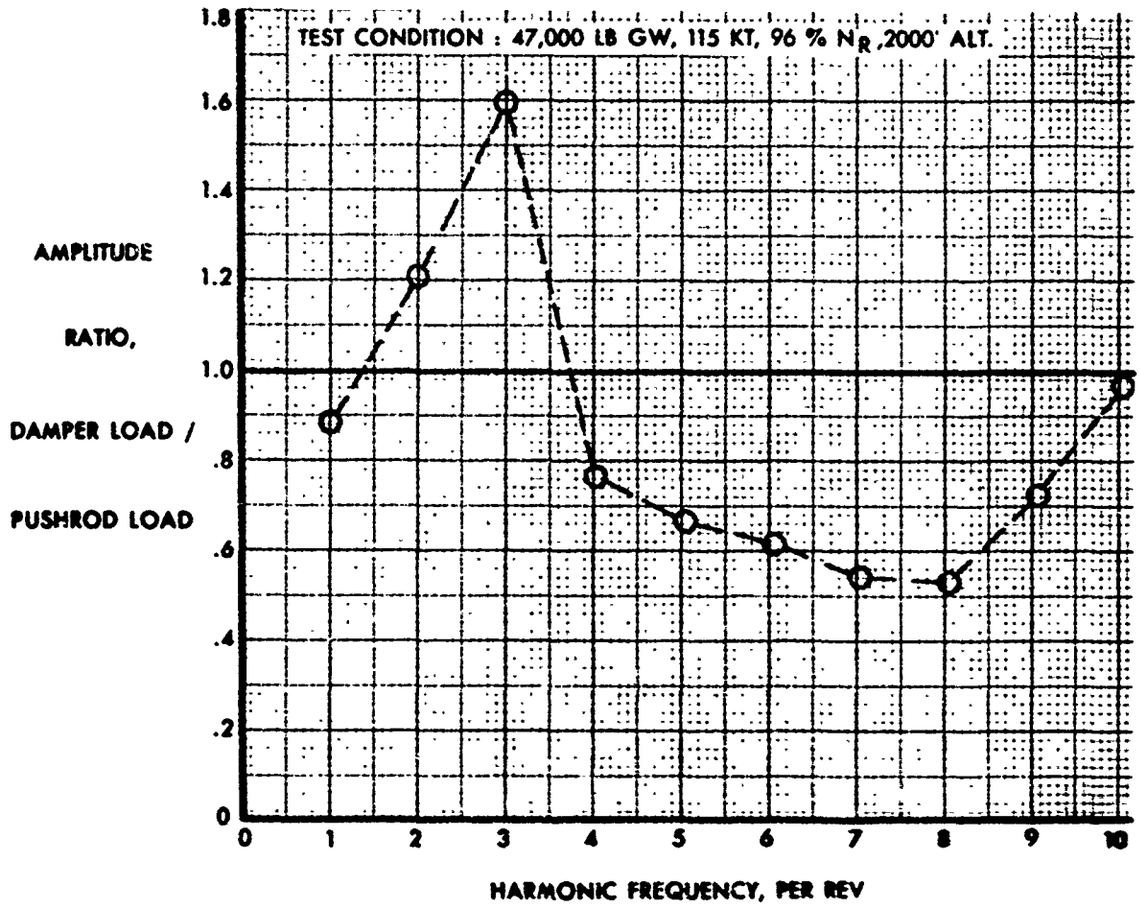

Figure 30. Rotating Control Load Harmonics Reduction.

A plot of rotating pushrod load against ERITS is shown as Figure 31. The solid line represents the large number of data points obtained in the CH-54B structural substantiation flight test program, obtained by automatic data processing. It has been recognized that this method produces conservative results due to its treatment of load factor. Manually read points are generally lower, as indicated by the base-line test points in Figure 31. The spring-damper points show a trend that is generally lower than base-line points, but no firm quantitative conclusion can be made.

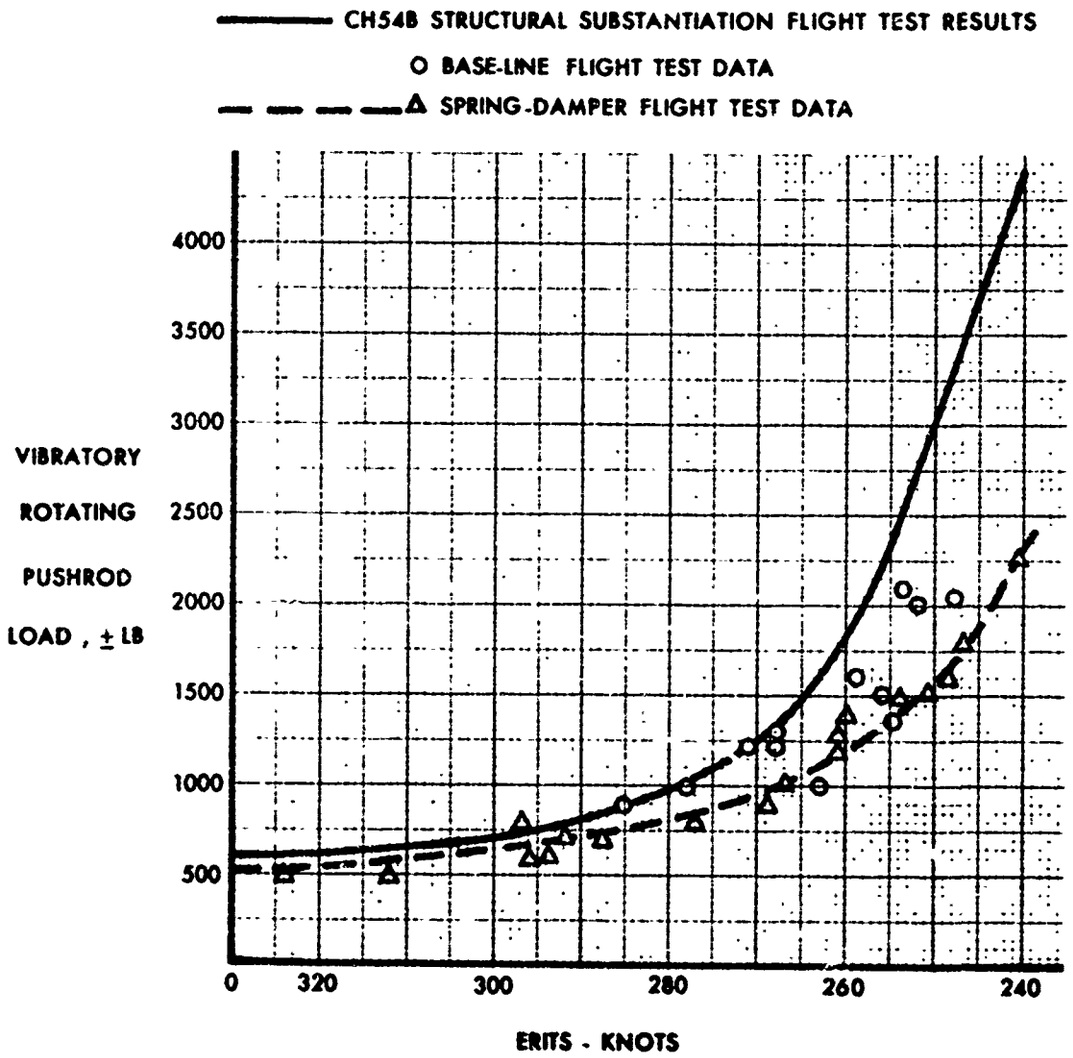

Figure 31. Pushrod Load Against ERITS.

Comparison of Stationary Control Loads

Flight test time-histories of right lateral stationary star load for rigid pushrods and for spring-damper pushrods are shown in Figure 32. These records show the dominance of the 6 per rev response in a 6-bladed rotor when rotating control loads provide a 5, 6, and/or 7 per rev excitation.

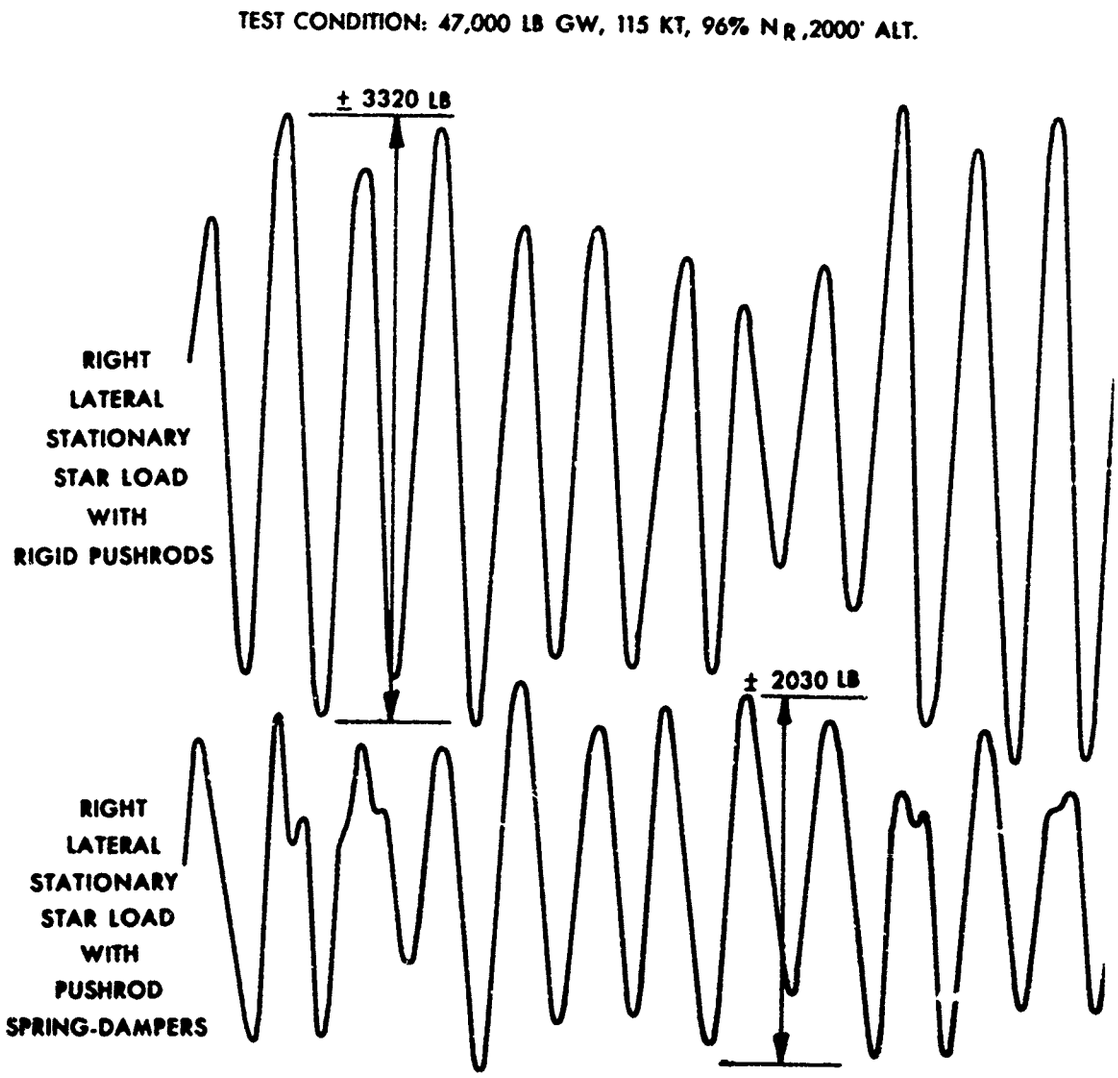

Figure 32. Comparison of Stationary Control Loads.

The spectral analyses for these are shown in Figures 33 and 34.

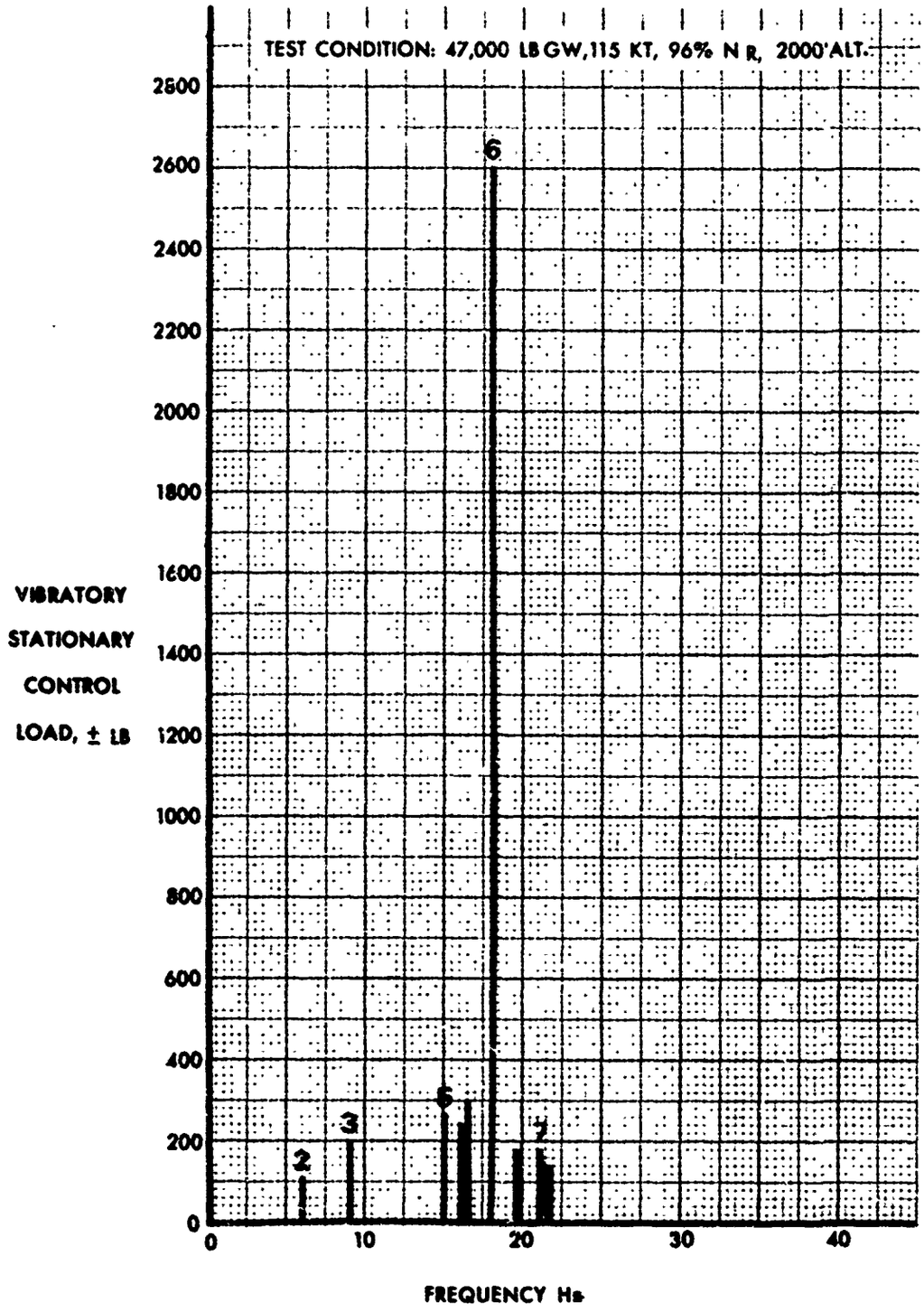

Figure 33. Spectral Analysis, Stationary Control Load With Rigid Pushrods.

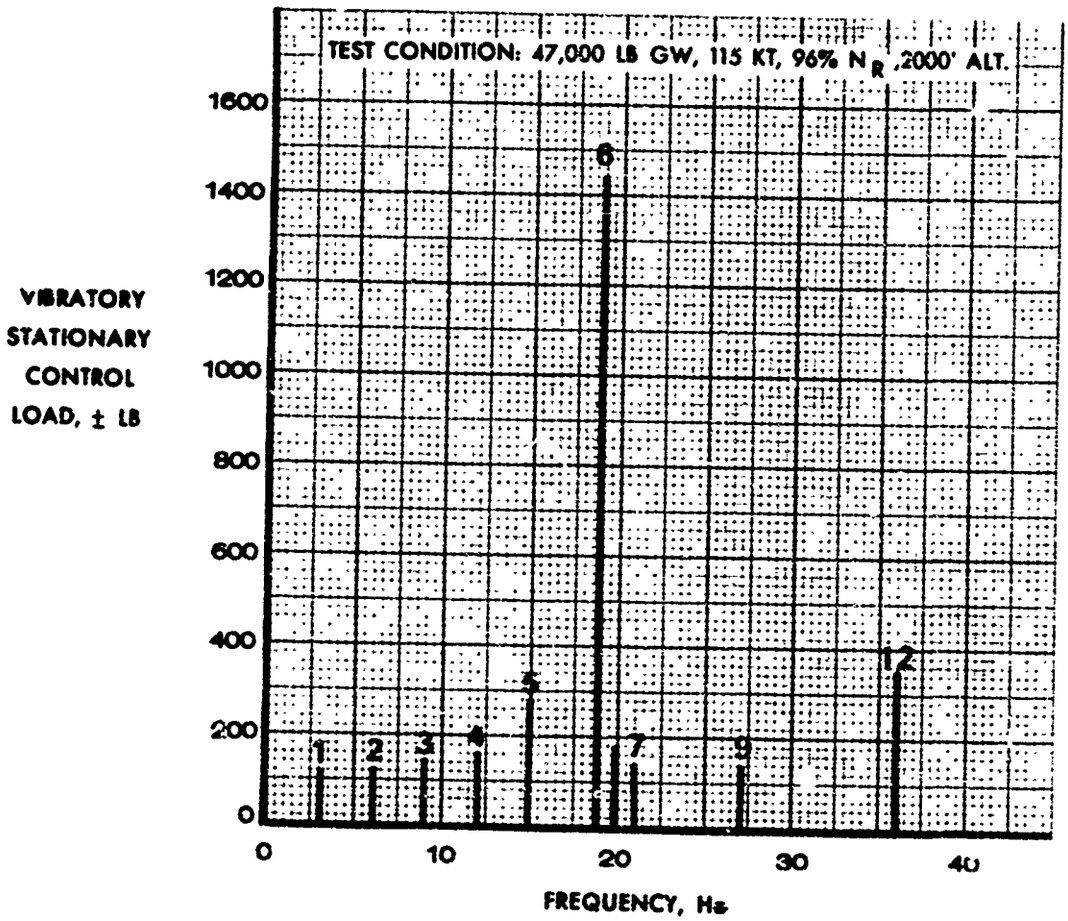

Figure 34. Spectral Analysis, Stationary Control Load With Spring-Damper Pushrods.

The reduction in the stationary 6 per rev with the dampers installed is seen to be 45%, and can be attributed to the sharp reduction in the 5, 6, and 7 per rev in the rotating system.

A plot of stationary control load against ERITS is shown as Figure 35. The sharp knee, characteristic of this plot, is seen to be unchanged by the damper installation, but as the aircraft goes deeper into the stall region, the frequency changes occur and the loads are reduced.

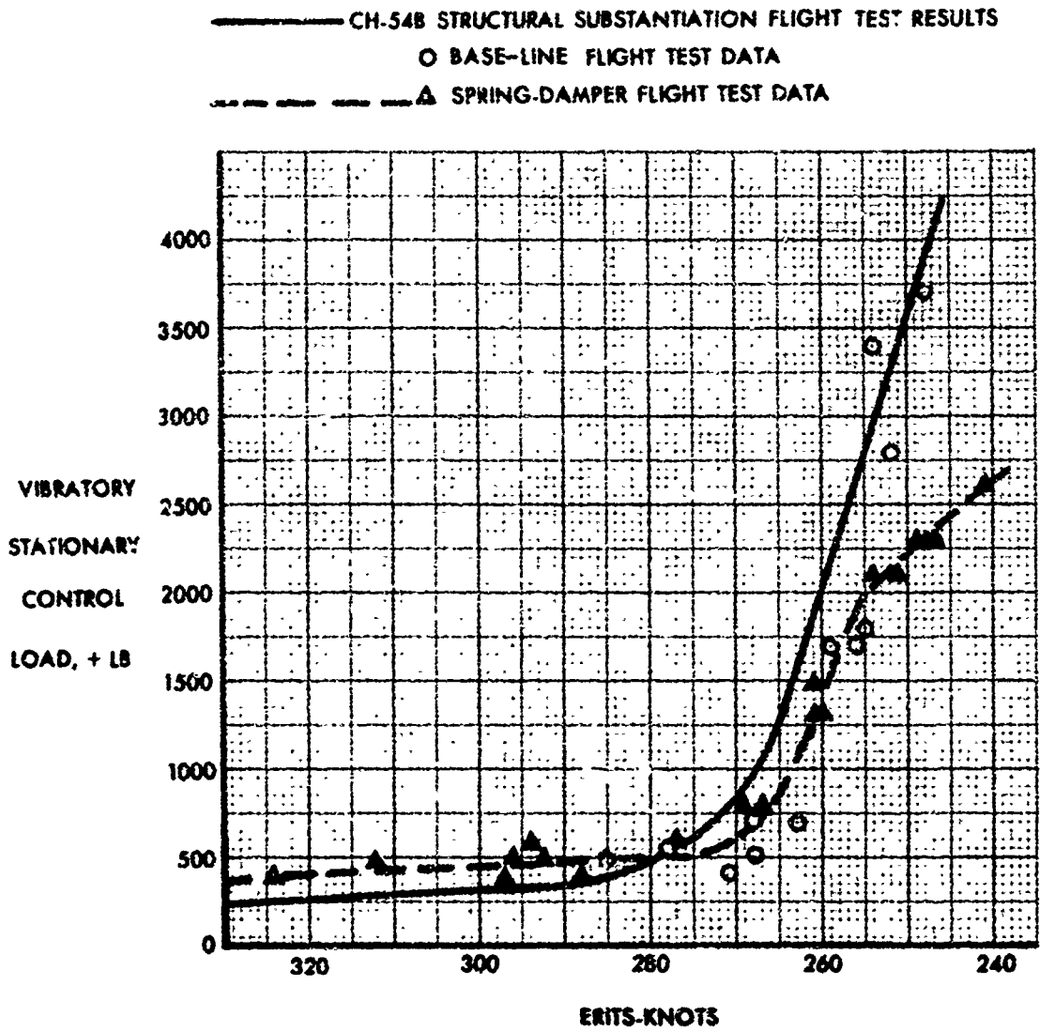

Figure 35. Stationary Control Load Against ERITS.

Analysis of Spring-Damper Characteristics

In order to make a valid evaluation of the stall-flutter spring-damper concept, an estimate of the actual spring and damping characteristics occurring in flight must be made. A typical flight test spring-damper relative displacement time history, along with the corresponding load history, is shown in Figure 36.

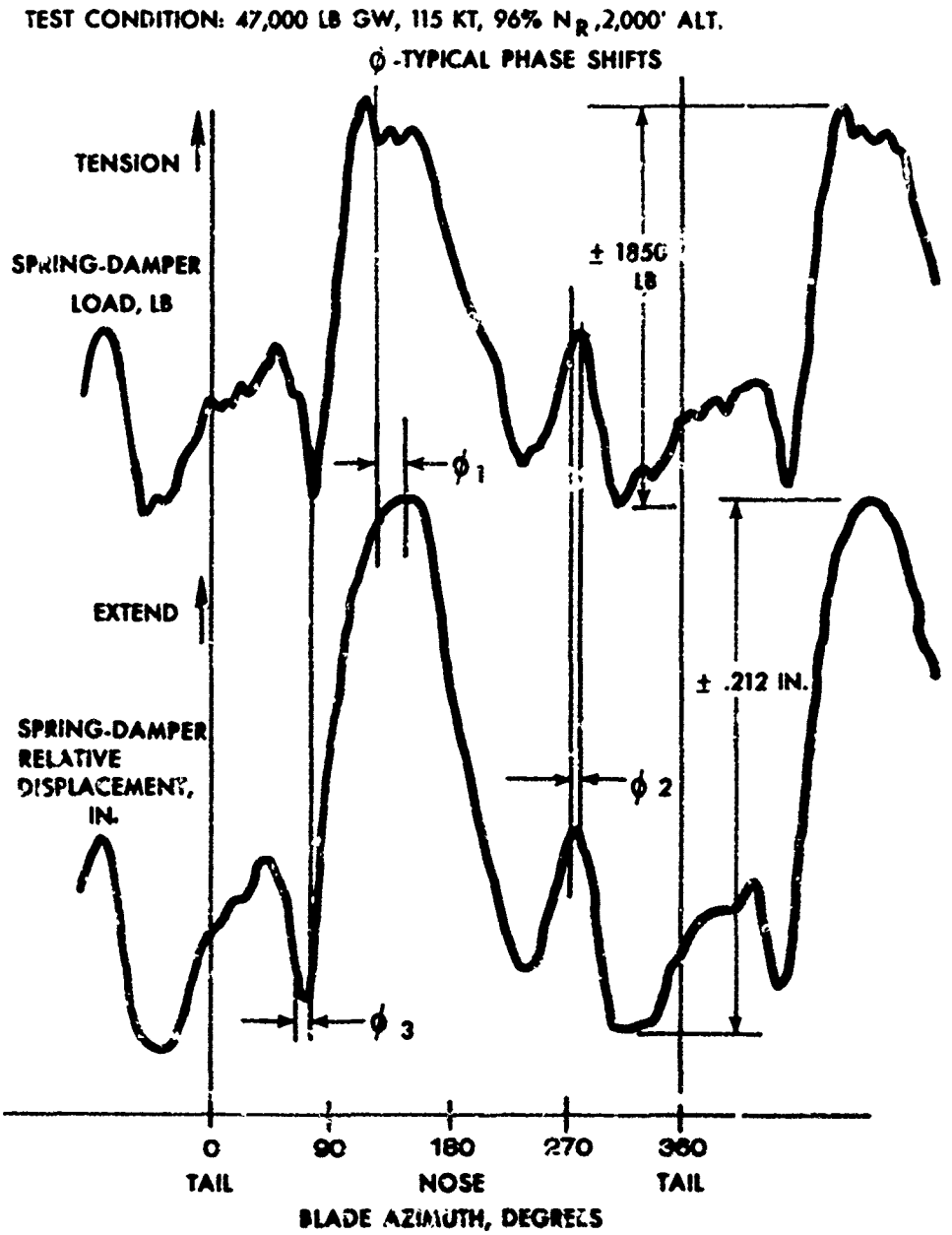

Figure 36. Spring-Damper Displacement and Load.

This data may be used to determine spring and damper characteristics, but due to the complex excitation and the frequency-sensitive nature of the spring-damper, the following results must be considered as only an estimate.

The spring-damper impedance is found by simply dividing peak-to-peak load by peak-to-peak displacement. For the overall cycle, the impedance is 8700 lb/in. and varies up to 14,000 lb/in. for the higher frequency component cycles. An impedance of about 10,000 lb/in. was found in several cases near 18Hz, and this compares well with lab test data.

A typical phase shift for the higher frequency component cycles is 40°, which results in damping rates between 70 and 100 lb-sec/in. The phase shift for the one per rev component is 6°, yielding a damping rate of 40 lb-sec/in. Again, these figures are consistent with lab test data.

Comparison of Aircraft Handling Qualities

In general, the handling qualities of the aircraft were unchanged. Pilot's reports indicate that the aircraft exhibited the characteristic increase in vibration, difficulty in maintaining airspeed, and forward control motion required when approaching a stall condition in both the base-line and spring-damper flights. The stalled condition of the rotor appears unaffected by the installation of the spring-damper. Blade stresses and blade motions (except for the stall-flutter torsional oscillation) are virtually the same in each case. Analysis of the flight test data also indicates that cockpit vibration levels are unchanged, as shown in Figure 37.

The effect of damper motion on the control system can be seen in the plots of control positions against airspeed (Figure 38). The lateral control is seen to be unaffected, but as much as 10% more forward longitudinal control is required when flying at the 115 kt, 96% N_R reference stall condition. The use of up to 90% of the available control motion in a level flight condition would be unacceptable if it were within the normal flight envelope of the aircraft.

A correlation between the observed damper motion and the required control position may be shown as follows. The observed damper motion of ±0.208 inch is made up of damper extension when on the rotor's advancing side (90° azimuth) and damper compression on the retreating side (270° azimuth). Since identical one-per-rev blade pitch motions are required to produce identical flight conditions, the swashplate position must be changed to compensate exactly for the damper motion. Working in terms of blade angle, the ±0.208-in. motion on an 8-in. arm would produce a ±1.5° blade angle

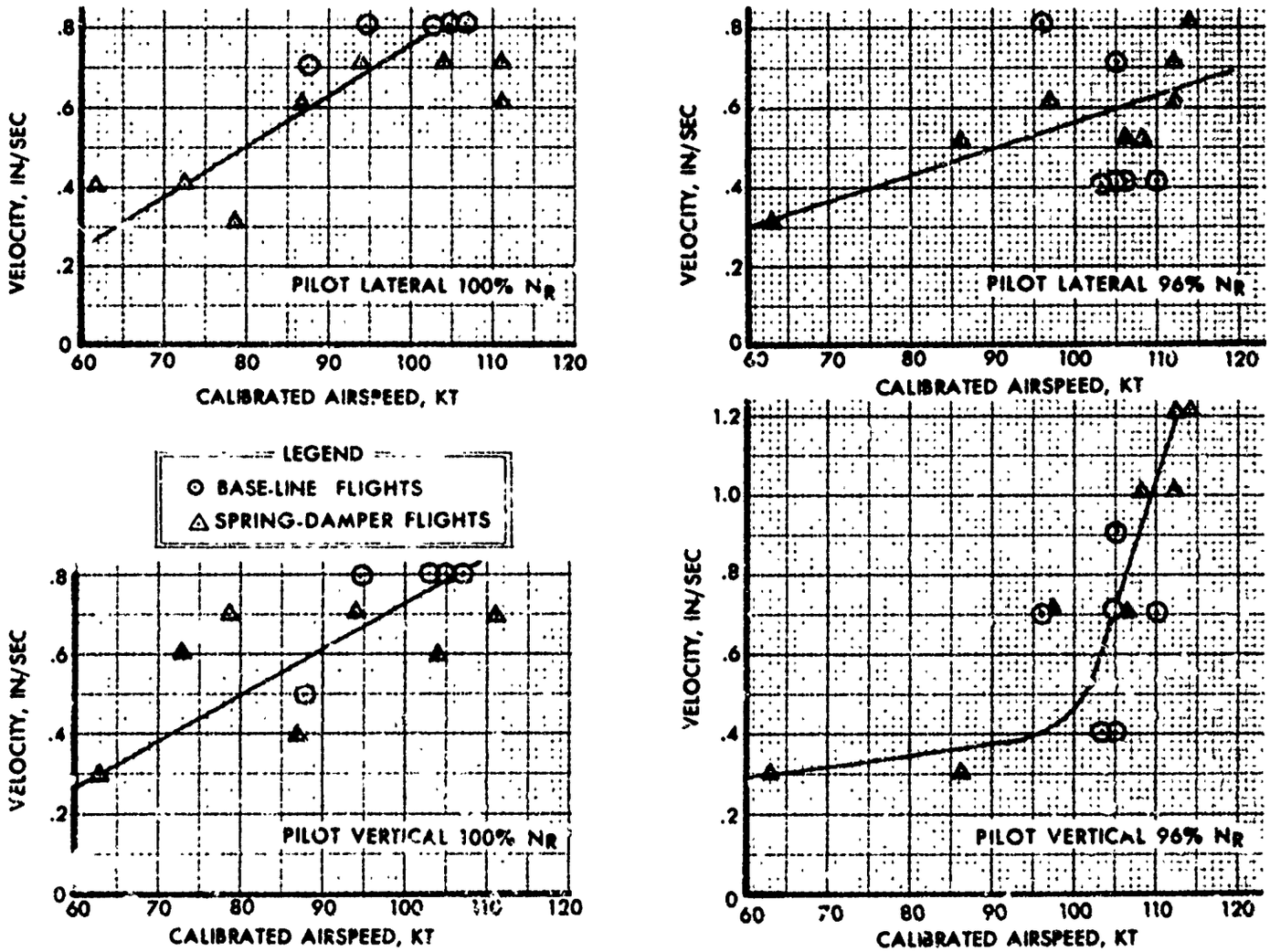

Figure 37. Comparison of Cockpit Vibration Levels.

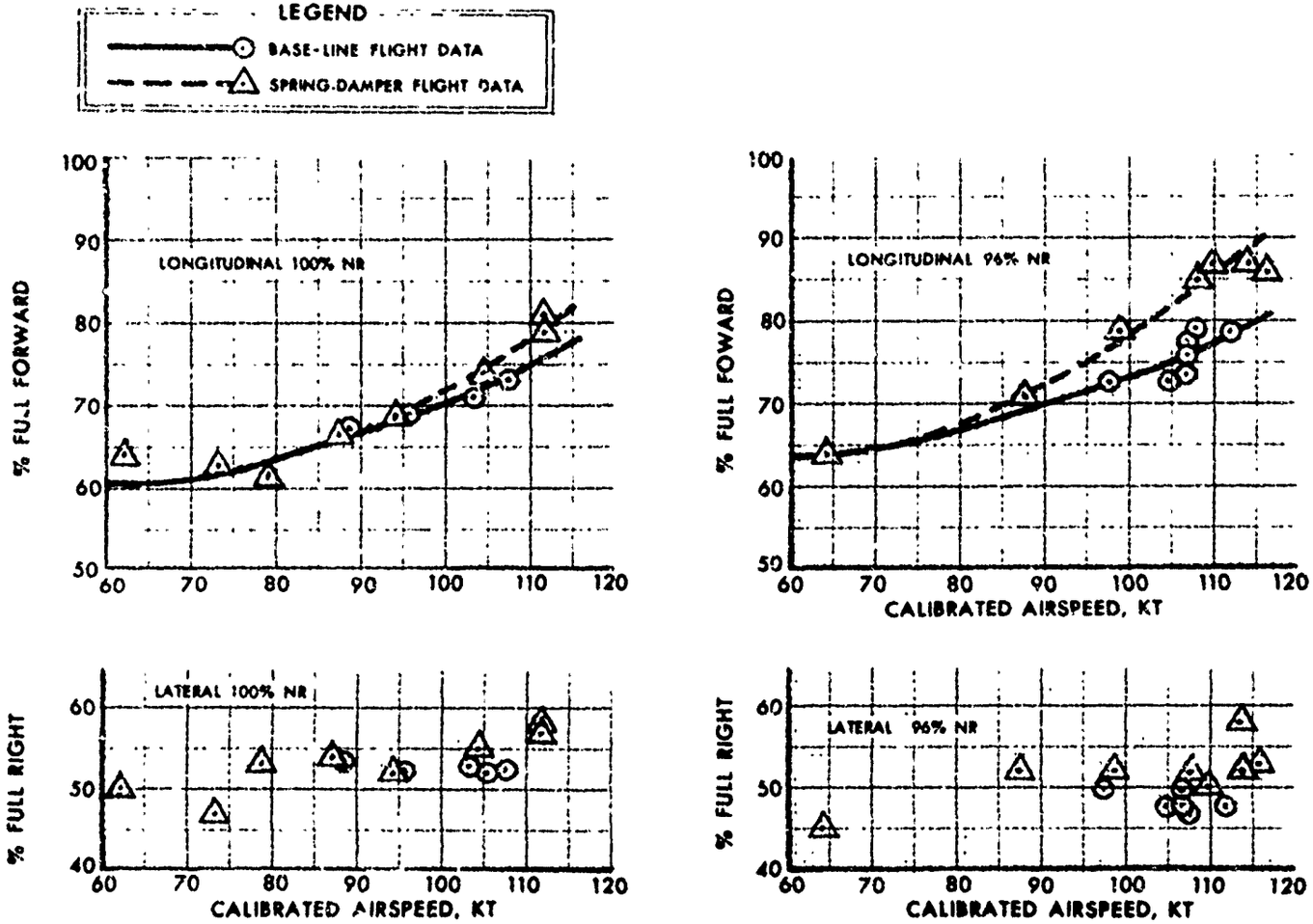

Figure 38. Longitudinal and Lateral Control Positions.

change. This correlates with the control system rigging on the CH-54B, where a 10% longitudinal control change produces about 2.7° of blade angle change, or ±1.35°. The control correction required is longitudinal since the effect of a blade pitch-change input is felt 90° later in azimuth, whether it is the spring-damper motion or the control system motion.

Aeroelastic Analysis of Flight Test Data

Three additional computer analysis conditions were run, using test conditions actually observed in the flight tests. The methods used are the same as described in the Analytical Design section (which are based on the work of Reference 9), with the exception that a calculated lift higher than the gross weight actually flown is used. The amplitudes of pushrod load predicted were much lower than observed using the correct lift, and since the comparison with and without the spring dampers was of primary interest, the calculated lift was increased to produce agreement.

Figure 39 shows pushrod load vs azimuth for the 115 kt, 96% N_R reference condition for conventional pushrods as generated by the aeroelastic analysis and as observed in the base-line flight. The analysis again shows a good correlation in wave shape with test result. Using this as a basis for comparison, two sets of damper characteristics were run: a spring rate of 5000 lb/in. with damping rates of 70 and 40 lb-sec/in. These values had been determined as likely levels of these parameters in the flight tests.

Figure 40 compares the 70 lb-sec/in. damping case with test results, and Figure 41 compares the 40 lb-sec/in. damping case with the same test result. A good correlation in wave shape is obtained in both cases, with the lower damping case perhaps being slightly better. The sharp reduction in amplitude over the rigid pushrod case as predicted by the aeroelastic analysis however, is again not achieved in practice. It should be noted that the aeroelastic analysis assumes that all blades and spring-dampers are identical, which is known not to be the case. Difference among spring-dampers would at least contribute to the one-per-rev component and perhaps the harmonics as well.

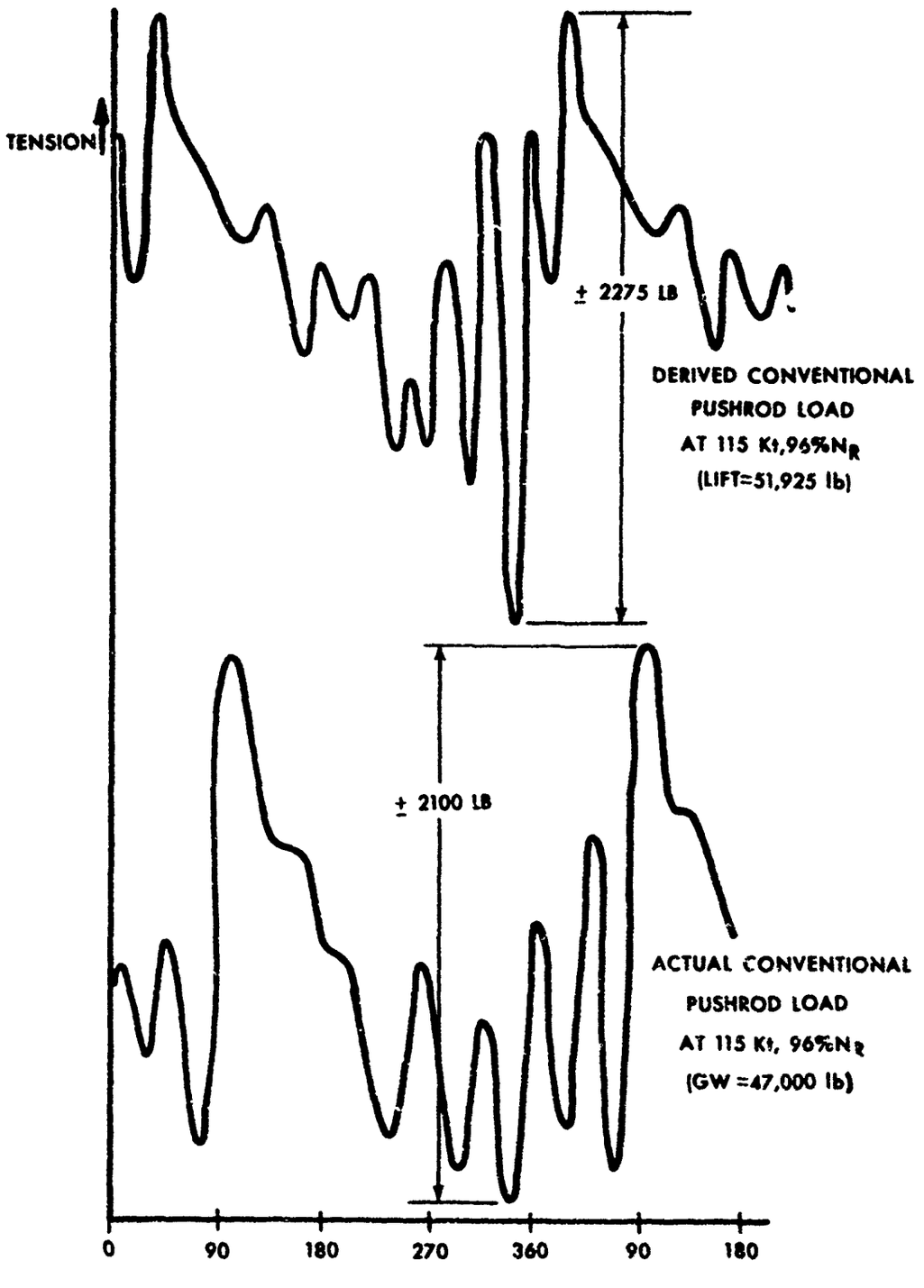

Figure 39. Comparison of Actual and Derived Conventional Pushrod Loads.

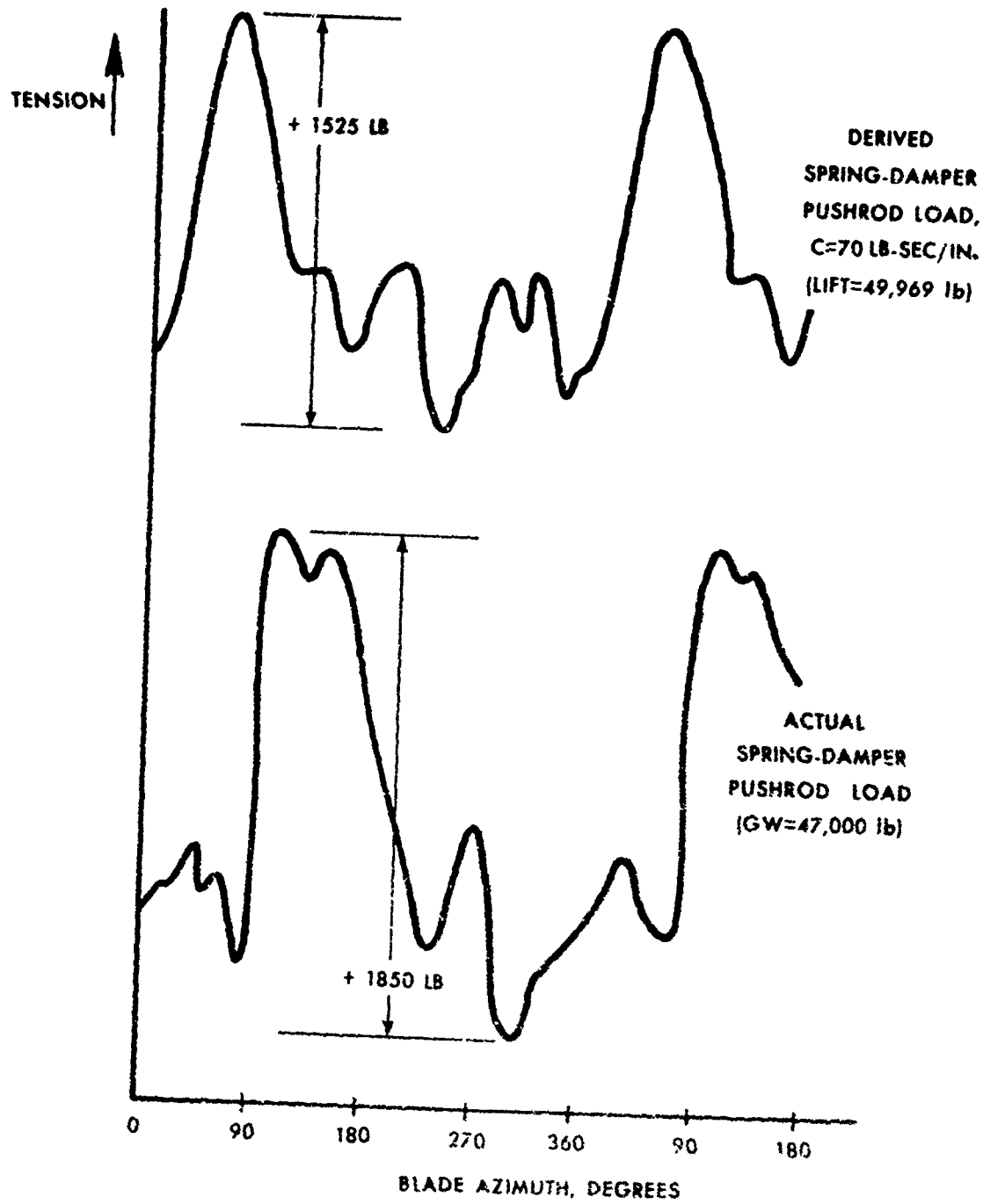

Figure 40. Comparison of Actual and Derived Spring-Damper Pushrod Loads, C = 70.

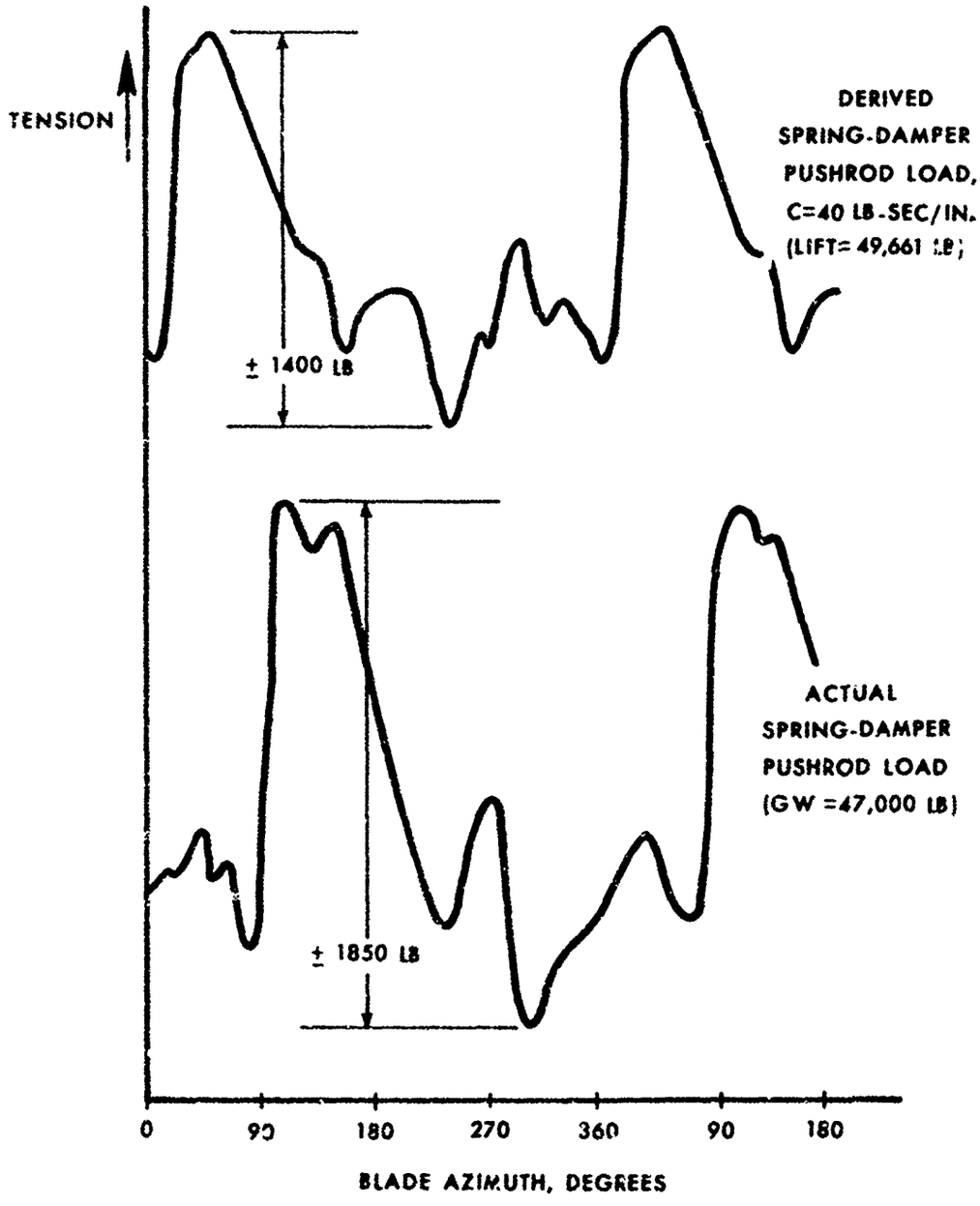

Figure 41. Comparison of Actual and Derived Spring-Damper Pushrod Loads, C = 40 .

CONCLUSIONS

It is concluded that:

1. Stall-flutter spring-damper pushrods located in the rotating control system effectively reduce stall-induced high-frequency rotating control loads by almost 50% and overall stationary control loads by more than 40%.

2. Based upon measured data as well as pilots' observations, the spring-damper pushrod system does not significantly alter the performance or handling qualities of the CH-54B helicopter.

3. The flight envelopes of some types of helicopters (specifically, maneuverable and/or high-speed helicopters whose primary envelope limitations are fixed by control load limits) can be expanded by the installation of stall-flutter spring-damper pushrods.

RECOMMENDATIONS

It is recommended that:

1. The stall-flutter spring-damper pushrod concept be evaluated in a production configuration.

2. The application of the spring-damper pushrod concept to high-speed helicopters, with the intent of reducing control system weight and expanding flight envelopes, be investigated.

LITERATURE CITED

1. Harris, F. D.,and Pruyn, R. R., BLADE STALL - HALF FACT, HALF FICTION, American Helicopter Society, 23rd Annual National Forum Proceedings, AHS Preprint No. 101, May 1967.

2. Ham, N. D., and Garelick, M. S., DYNAMIC STALL CONSIDERATIONS IN HELICOPTER ROTORS, Journal of the American Helicopter Society, Vol. 13, No. 2, April 1968, pp. 49-55.

3. Ham, N. D., AERODYNAMIC LOADING ON A TWO-DIMENSIONAL AIRFOIL DURING DYNAMIC STALL, AIAA Journal, Vol. 6, No. 10, October 1968, pp. 1927-1934.

4. Liiva, J., et al., TWO-DIMENSIONAL TESTS OF AIRFOILS OSCILLATING NEAR STALL, Vol. I, Summary and Evaluation of Results, The Boeing Company, Vertol Division; USAAVLABS TR 68-13A, U. S. Army Aviation Materiel Laboratories, Fort Eustis, Virginia, April 1968, AD 670957.

5. Carta, F. O., et al., ANALYTICAL STUDY OF HELICOPTER ROTOR STALL FLUTTER, American Helicopter Society, 26th Annual National Forum, AHS Preprint No. 413, June 1970.

6. Arcidiacono, P. J., et al., INVESTIGATION OF HELICOPTER CONTROL LOADS INDUCED BY STALL FLUTTER, United Aircraft Corporation, Sikorsky Aircraft Division; USAAVLABS Technical Report 70-2, U. S. Army Aviation Materiel Laboratories, Fort Eustis, Virginia, March 1970, AD 869823.

7. Carta, F. O., and Niebanck, C. F., PREDICTION OF ROTOR INSTABILITY AT HIGH FORWARD SPEEDS, Vol. III, Stall Flutter, United Aircraft Corporation, Sikorsky Aircraft Division; USAAVLABS Technical Report 68-18C, U. S. Army Aviation Materiel Laboratories, Fort Eustis, Virginia, February 1969, AD 687322.

8. Arcidiacono, P. J., STEADY FLIGHT DIFFERENTIAL EQUATIONS OF MOTION FOR A FLEXIBLE HELICOPTER BLADE WITH CHORDWISE MASS UNBLANCE, USAAVLABS TR-68-18A, February 1969, AD 685360.

9. Carta, F. O., et al., INVESTIGATION OF AIRFOIL DYNAMIC STALL AND ITS INFLUENCE ON HELICOPTER CONTROL LOADS, USAAVLABS TR72-51, Eustis Directorate, U. S. Army Air Mobility Research and Development Laboratory, Fort Eustis, Virginia, September 1972, AD 752917.

10. Degnan, William D., FATIGUE PROPERTIES AND ANALYSIS, Sikorsky Engineering Report No. SER 50586, Sikorsky Aircraft, April 1969.

12. Roark, R. J., FORMULAS FOR STRESS AND STRAIN, New York, McGraw-Hill, 1954.

13. Sikorsky Structures Manual, Sikorsky Aircraft, 1964.

APPENDIX
STRUCTURAL ANALYSIS

The following discussion outlines the structural analysis of metal components used in the CH-54B stall-flutter spring-damper pushrod. The analytical fatigue and static strength of these components is equal to or greater than the substantiated strength of the existing CH-54B rotating pushrod.

The fatigue allowable stresses used are derived from Sikorsky Engineering Report No. SER 50586, "Fatigue Properties and Analysis" (Reference 10), which was used to derive allowables for the CH-54B rotor system structural substantiation. The analysis is conservative, as it does not take into account the expected reduction in control load.

Preliminary analysis indicates that the following parameters are similar for all components, and are assumed constant.

- Size Effect Factor, $f_S = 0.70$
- Surface Finish Factor, $f_{SF} = 0.80$
- Reliability Factor, 3σ, $f_R = 0.70$
- Small Specimen Endurance Limit, E = 70,000

All structural components are machined "hog-outs" of 4340 steel, heat treat - 150,000 psi, except for the orifice plate (aluminum). Cracking of this component will only result in some loss of damping without reducing the structural integrity of the spring-damper. In addition, since the size of the orifice plate is dictated primarily by the size and location of the orifices and check valves, stress levels due to pressure differentials are low. The structural analysis of this component is therefore not included.

All parts considered in this appendix are identified by their Sikorsky part number or by military part number.

COMPARISON OF EWR 33111-043 ROD END
AND
PRODUCTION CH-54B ROD END P/N 64107-11006

EWR 33111-043

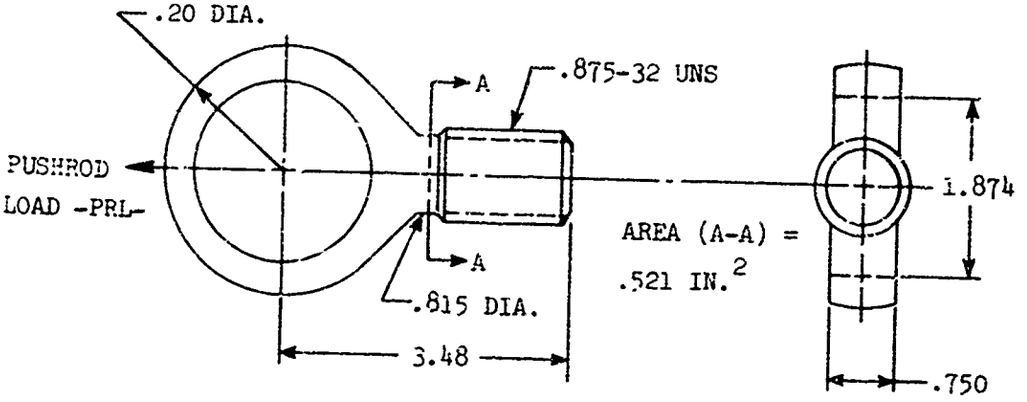

P/N 64107-11006

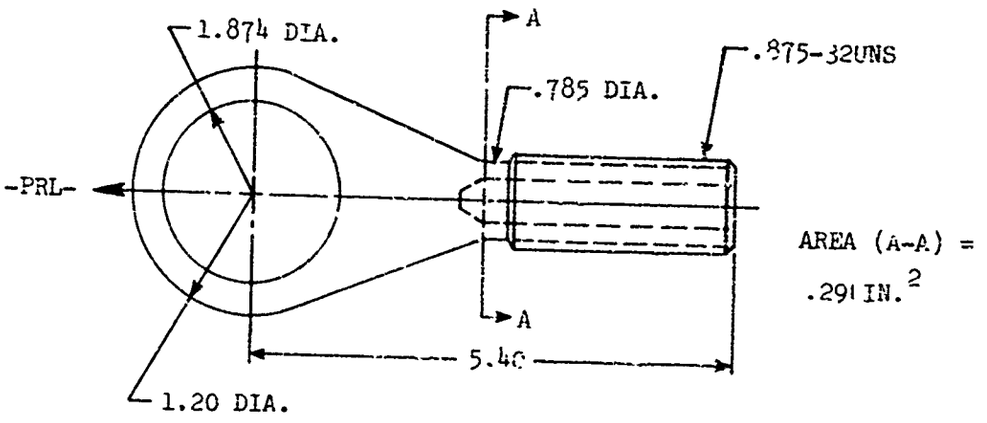

MATERIAL = 4340 STEEL HT = 150,000 PSI

Figure 42. Rod End Structural Analysis.

Based on previous fatigue test results, section A-A is critical.

- Production Rod End

  $A_{AA} = 0.291$ in.^{2}

  $f_{AA} = 3.436$ PRL

- Spring-Damper Rod End

  $A_{AA} = 0.521$ in.^{2}

  $f_{AA} = 1.919$ PRL

- Increase in Strength:

  $(3.436/1.919) - 1 = 80\%$

INNER SHAFT, EWR 31449-101

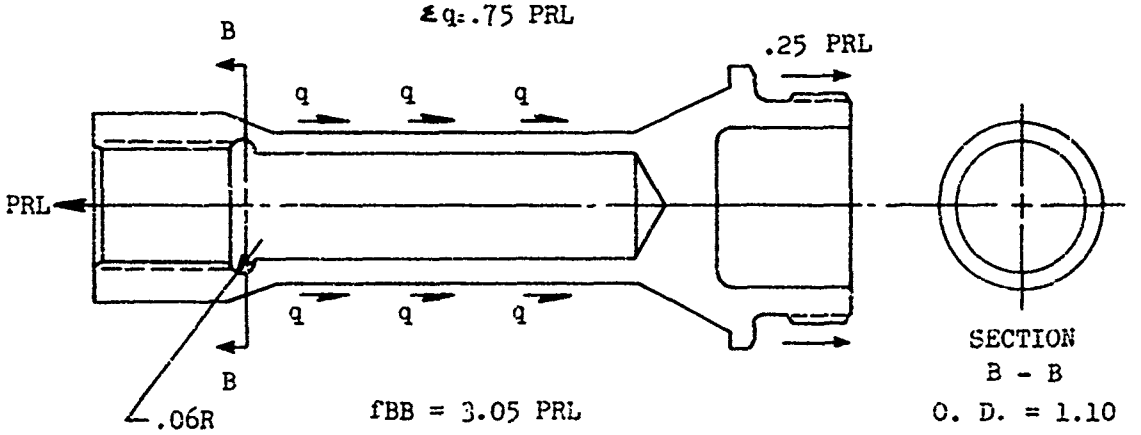

MATERIAL, 4340 STEEL
FTU = 150,000 PSI

Figure 43. Inner Shaft Structural Analysis.

- Stress Concentration Factor, K_T

  K_T = 3.0 (Reference 11)

- Notch Sensitivity, K_f

  K_f = 2.3 at 10^7 cycles (Reference 10)

Therefore, the working endurance limit, PRL (3σ) is:

$$PRL\ (3\sigma) = [E \times f_{SF} \times f_S \times f_R \times (1/K_f)]/3.05$$

or PRL (3σ) = $\pm$ 3910 lb

MIDDLE CYLINDER - BNR 31449-104

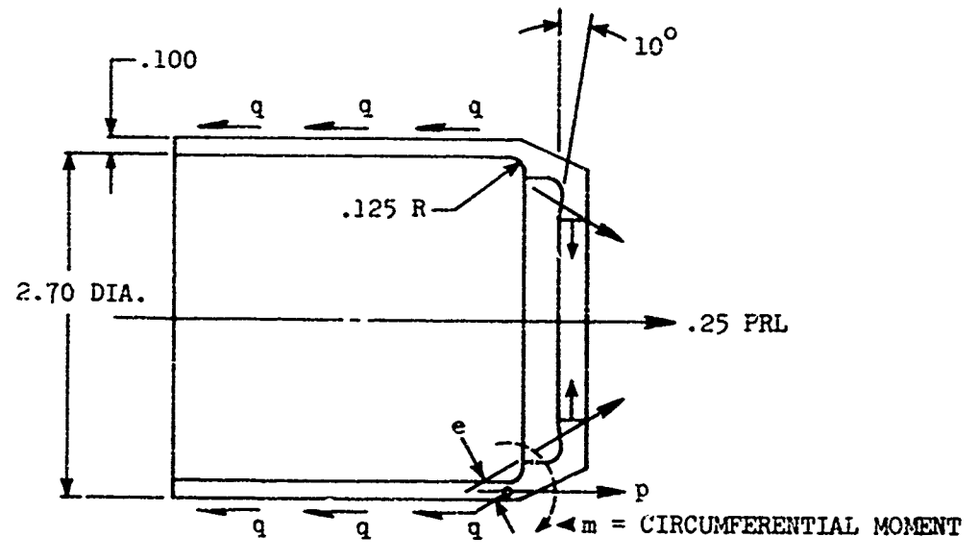

q = CIRCUMFERENTIAL SHEAR

Σ q = .25 PRL

MATERIAL 4340 STEEL
FTU = 150,000 PSI

$\mathcal{Z}$ = .0016 IN.^{3}

$f_b = mR/\ = 5.05$ PRL

$f_a = p/t = .29$ PRL

$f_{total} = f_b + f_a = 5.34$ PRL

e = .20 IN.
p = .25 PRL/(π x 2.70)
p = .029 PRL/IN.
m = pe = .006 PRL IN.LB/IN.
t = .100 IN.
R = 2.7/2 = 1.35 IN.

Figure 44. Middle Cylinder Structural Analysis.

Assume ring under uniform rolling moments (Reference 12).

- Stress Concentration, K_T

  K_T = 2.0 (Reference 11)

- Notch Sensitivity, K_f

  K_f = 1.6 at 10^7 cycles (Reference 10)

Therefore the working endurance limit, PRL (3σ) is:

PRL (3σ) = [E X f_S X f_{SF} X f_R X(1/K_f)]/5.34

or PRL (3σ) = ± 3220 lb

MAIN HOUSING -

EWR 33111-111

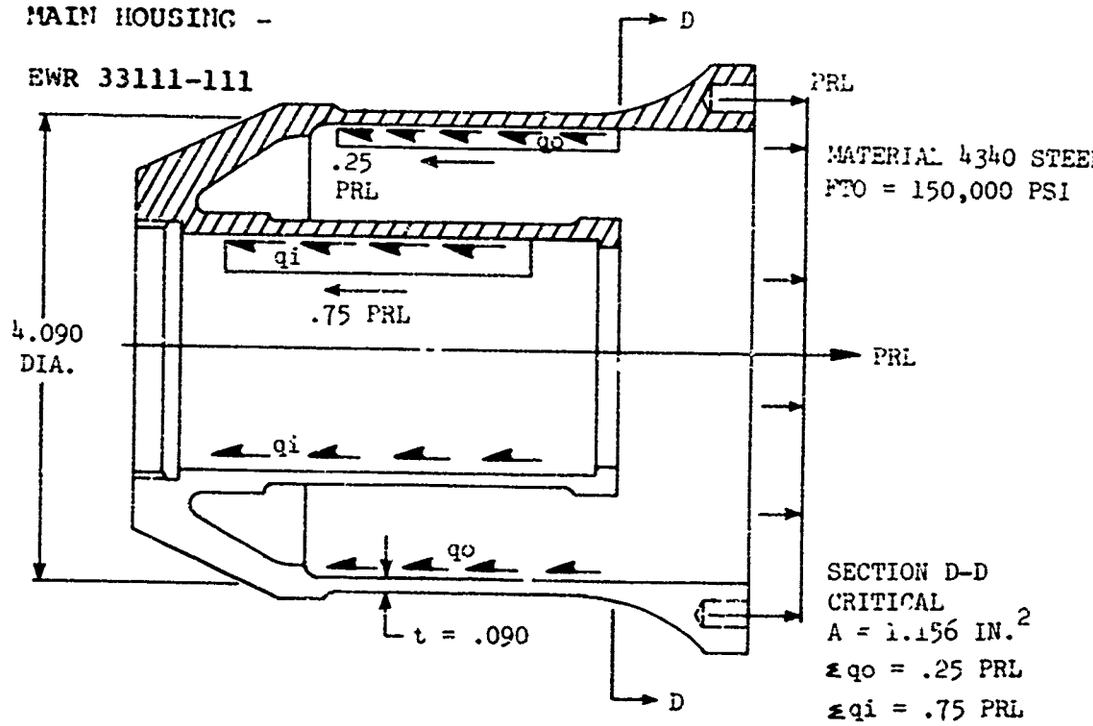

$$PRL = \frac{FRC}{(4.090)\pi} = .078 \text{ PRL/INCH OF CIRCUMFERENCE}$$

$$foo = \frac{PRL}{t} = \frac{.078\ PRL}{.090} = \frac{.87\ PRL}{} \quad \text{AXIAL}$$

NOTE:
ASSUME ECCENTRICITY INDUCED BENDING MOMENTS AT SECTION D-D ARE REACTED BY "O" RING LIP OF ALUMINUM ORIFICE HOUSING

Figure 45. Main Housing Structural Analysis.

- Stress Concentration Factor, K_T

  K_T = 1.5, due to flange transition (Reference 11)

- Notch Sensitivity Factor, K_f

  K_f = 1.3 (Reference 10)

Therefore the working endurance limit, PRL (3σ) is:

$$PRL\ (3\sigma) = [E \times f_S \times f_{SF} \times f_R \times (1/K_f)]/0.87$$

or PRL (3σ) = $\pm$ 24,250 lb

CONE/FLANGE ATTACHMENT BOLTS (8) - NAS-624H-8 (½-28)

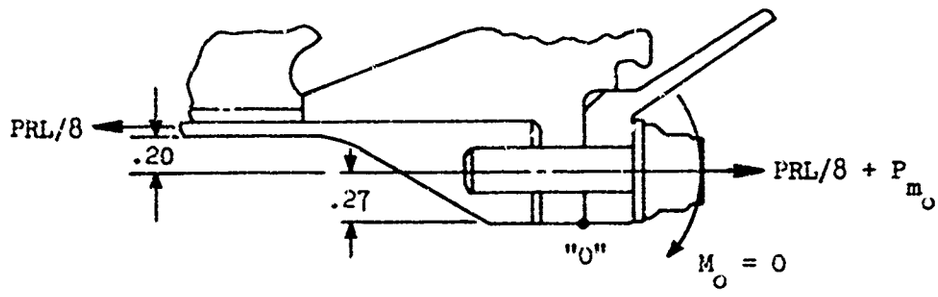

BOLT MINOR DIA. = .2062 IN.

AREA = .0334 IN.^{2}

BOLT LOAD = PRL/8 = .125 PRL + P_{m_o}

P_{m_o} = .125 PRL $(\frac{.47}{.27})$ = .212 PRL

BOLT LOAD = .336 PRL

$f_{BOLT} = \frac{.336\ PRL}{.0334}$ = 10.0 PRL (TENSION ONLY)

Figure 46. Cone/Flange Attachment Bolts Structural Analysis.

- Stress Concentration Factor, K_T

  K_T = 4.5, thread root radius (Reference 11)

- Notch Sensitivity Factor, K_f

  K_f = 2.0 for R=0 (Reference 10)

Therefore the working endurance limit, PRL (3σ), is:

$$PRL\ (3\sigma) = [E \times f_S \times f_{SF} \times f_R \times (1/K_f)]/10.0$$

or PRL (3σ) = ± 1500 lb

Since the bolts react only tensile control loads, the actual loading is a steady plus and minus an equal vibratory load. Since the allowable vibratory is 1500 lb, a peak tensile load of 3000 lb is allowed. Since the strength in compression is at least 3000 lb, the strength of the joint is expressed as ± 3000 lb.

CONE ANALYSIS

To accommodate the external accumulator setup, the -109 end cap is modified as follows:

- Two 3/8-in. holes are drilled into the basic 0.100-in. thick cone.
- Two steel hydraulic fittings are T.I.G. (Tungston-Inert-Gas) welded to the cone, inside and out, concentric with the 3/8-in. holes.
- The assembly is re-heat-treated to 150,000 psi ultimate and then shot-peened.

In order to accurately determine the bending stresses adjacent to the weld end hole, a computer program for the analysis of shells of revolution was utilized. The end cap geometry was identified as shown below.

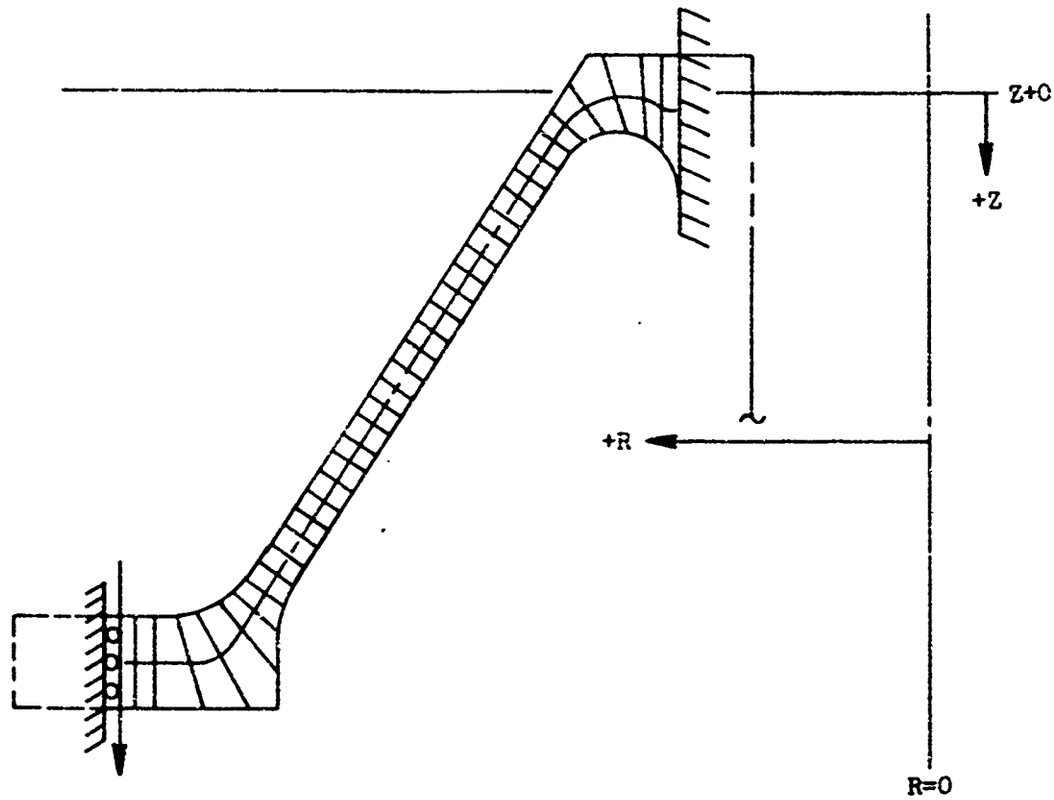

Figure 47. Cone Analysis Geometry.

The direct result of the analysis is shown below:

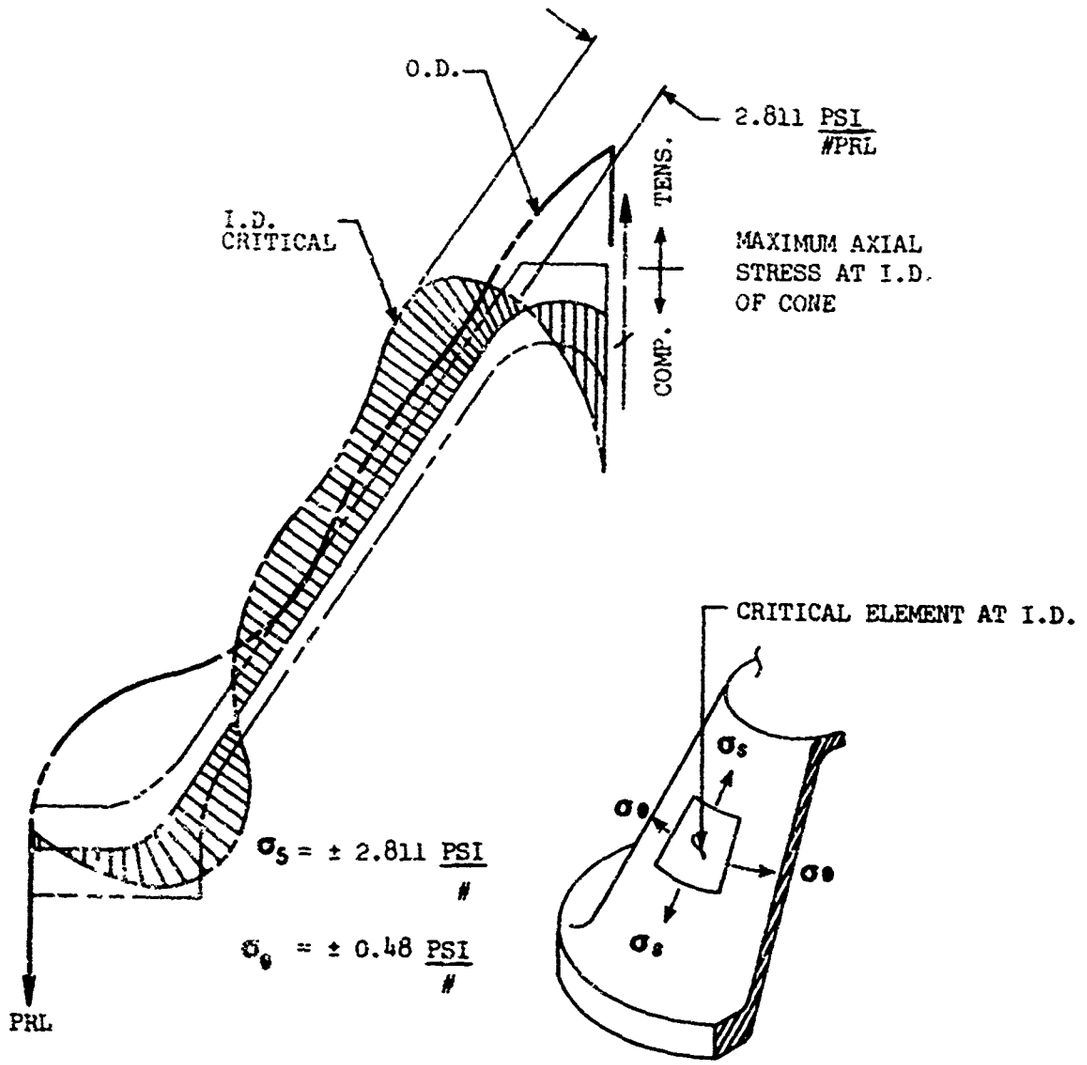

Figure 48. Cone Analysis Axial Stress Summary.

Based on the analytical "shell of revolution" program, the maximum stress at the I.D. is $\pm$ 2.811 PRL (with no holes or welds).

The stress concentration factor, K_T, is determined as follows: assume the stress concentration of the 3/8-in.-diameter hole in the cone is identical to a 3/8-in.-diameter radial hole in a thin wall cylinder.

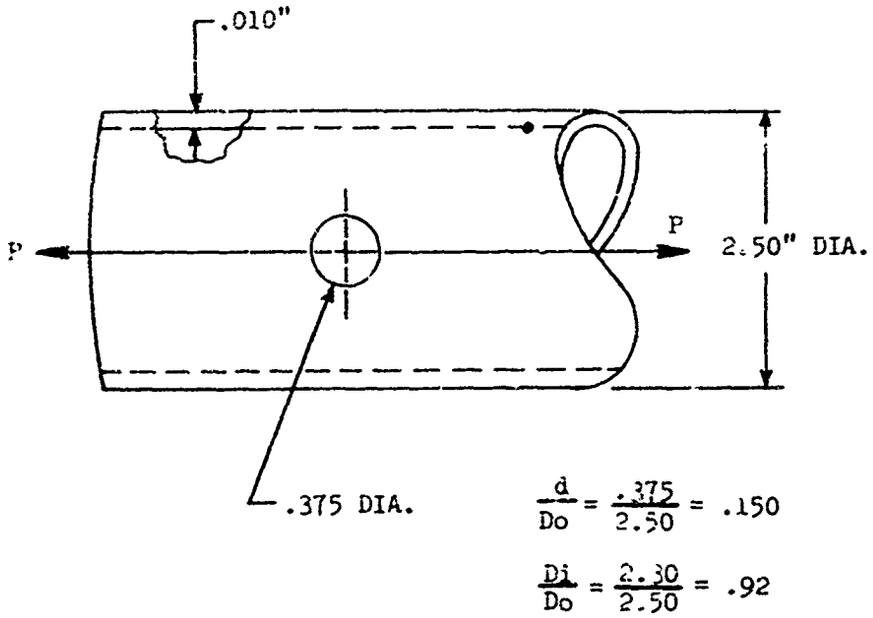

Figure 49. Determination of Cone Stress Concentration Factor.

From Reference 11, $K_T = 4.0$. Therefore, from Reference 10, K_f at 10^8 cycles is 3.0.

In addition to the factors previously used, a reduction is required due to the weld. A weld factor of 2/3 has been found to be appropriate in recent Sikorsky experience for this type of welded structural joint.

The working endurance limit, PRL (3σ), is:

$$PRL\ (3\sigma) = [E \times f_S \times f_{SF} \times f_R \times f_W \times (1/K_f)]/2.81$$

or PRL (3σ) = ± 2200 lb